Experiments and Simulation of Transverse Cooling and Heating in Ion Channeling

Dissertation
an der Fakultät für Physik der
Ludwig-Maximilians-Universität München

vorgelegt von
Florian Grüner
aus München

September 2003

1. Gutachter: Univ. Prof. Dr. F. Bell
2. Gutachter: Univ. Prof. Dr. D. Habs
Vorsitzender: Univ. Prof. Dr. J. v. Delft
Beisitzer: Univ. Prof. Dr. H. Gaub

Tag der mündlichen Prüfung: 18. Dezember 2003

For Kerstin and Paul

Summary

According to the present theory of ion channeling no flux redistributions after transmission of an isotropic ion beam through a crystal are expected. This is in clear contrast to measurements of our group, which show, depending on experimental conditions, strong flux enhancements along axial or planar crystal directions as well as flux reductions. An ion is said to be channeled, if it enters the crystal along a lattice direction under an angle smaller than a certain critical angle. In such a case the ion experiences a guidance along the crystallographic directions due to correlated small-angle scattering. In channeling, the ion is confined to such impact parameters which prevent any large-angle scattering above the critical angle. However, due to multiple scattering on target electrons or on thermally vibrating target nuclei a channeled ion can become dechanneled. On the other hand, the same scattering processes apply for non-channeled, or random, ions. Thus, a random ion can be scattered into a channeling motion, and this event is called rechanneling in contrast to dechanneling. The so-called "Rule of Reversibility", developed within the theory of channeling, predicts that for an initially isotropic ion beam both de- and rechanneling occur with the same rates, and, therefore, the initially isotropic flux distribution should be conserved - in contrast to our experiments. It is thus concluded that our findings show clear violations of this reversibility. In order to directly compare the channeled and random ion flux we have used an ion beam which was quasi-isotropic within the acceptance angle of our position sensitive detectors behind the crystals. Since the initial beam was isotropic, a flux redistribution in terms of an enhancement along crystal directions means that the corresponding ions must have lost their transverse momentum in respect to the observed lattice directions. This loss of transverse momentum was denoted as "transverse cooling", as these ions become "cooled down" into the channels. By analogy, a flux reduction means a gain of transverse momentum, which is hence called "transverse heating".
The experimental part of this work was a systematic study of the dependencies of this effect of transverse cooling and heating. The most prominent and puzzling result was the transition from cooling to heating, when the ion energy is decreased below a certain transition energy. Equally remarkable was the fact that this transition disappears, if the projectile nuclear charge is somewhat lower than the crystal target nuclear charge. In case of Pt crystals, there was no heating found for all measured ions, even up to the heaviest observed Th ions. A further puzzling feature about the transition was its rapidness: within a relative ion velocity change of only 15 % the transition is clearly visible. Systemic measurements for the energy dependence revealed that the cooling

effect disappears, when the ion becomes fully stripped. Therefore, in such a case the rule of reversibility is strictly fulfilled.
In order to find the responsible mechanism for transverse cooling and heating, charge exchange was considered a possible candidate from the very beginning. However, due to the lack of available theories for impact parameter dependent electron capture and loss within the regime of strong target perturbations, first estimates were rather qualitative and failed in correctly describing the transition behavior. Quantum mechanical, first-principle theories are practically impossible due to the situation of a many-body problem with strong perturbation and non-stationary ion-atom potentials. The only possible way then seems to be a classical approach in terms of a detailed computer simulation that takes all involved particles into account, that is, the projectile and target nuclei as well as all electrons. The computer simulation developed and applied in this work was based upon the long-known so-called "Classical Trajectory Monte-Carlo" (CTMC) method, which has already successfully reproduced *single* ion-atom collisions in dilute gases. Thus, in this work, CTMC was further extended to the ion transmission through a crystal, where the ion interacts *simultaneously* with *several* atoms. These simulations could not only reproduce measured charge states of channeled vs. non-channeled ions, but also clear signatures of cooling and heating, and yielded also a detailed study of the underlying mechanism for cooling and heating in terms of a "hysteresis" behavior of the channeling charge states. It was found that in cooling the ion approaches the strings of crystal atoms with a higher charge state and leaves them with a lower charge state, which thus leads to the required irreversible loss of transverse energy in order to violate the rule of reversibility. In case of heating this hysteresis is reversed. The explanation for this reversal is given in terms of energy dependent different impact parameter regions for effective electron capture.

Contents

Chapter 1

Introduction

Despite over four decades of studying channeling, both experimentally and theoretically, a new effect has been discovered which lacks any explanation within the context of the present channeling theory. Channeling phenomena occur if ions enter a crystal with entrance angles very close to crystallographic directions [1]. If ions move with an angle relative to such directions being smaller than a certain critical angle, they experience correlated small-angle scattering. Due to this guidance along crystal directions the ions are kept away from the lattice strings or planes, that is, they are confined to larger impact parameters preventing large-angle scattering. Ions moving with larger angles then the critical ones traverse the crystal as if it were an amorphous solid, that is, there is no correlated scattering any more. Channeled ions can become dechanneled due to multiple scattering on target electrons and thermally vibrating atomic nuclei, which is called dechanneling. On the other hand, non-channeled ions suffer the same scattering events and can hence become channeled, which is named rechanneling as opposed to dechanneling. A central point of channeling theory is the so-called rule of reversibility, from which it follows that the two probabilities for de- and rechanneling are equal, if energy loss can be neglected. This prediction was verified in experiments with GeV protons where the condition of negligible energy loss is satisfied [2].
All previous channeling experiments were performed by using well collimated beams with a divergence significantly smaller than the corresponding critical angles. Under such circumstances it is hardly possible to measure any redistribution of the channeled vs. the non-channeled flux. But our group has found very strong angular flux redistributions when using ion beams that were initially nearly *isotropic* within the acceptance angle of the detectors [3].

These results were soon understood as a clear evidence for a strong violation of the rule of reversibility, whereas violations simply due to presence of energy loss can be estimated to be rather weak. This violation of reversibility must be clearly distinguished from earlier measurements by other groups, which also showed flux enhancement or reductions, but these could be exhaustively explained by the present channeling theory. A typical example is a measurement of the transmitted flux of He ions with a mean range in the order of the crystal thickness [4]. It is confirmed by measurements that

channeled ions suffer less energy loss due to a reduction of the ion-crystal interaction strength because of their restriction to larger impact parameters. Therefore, the channeled He ions in this experiment had a larger range and could traverse the entire crystal, while the non-channeled He ions were stopped inside. Such a selection then pretends a flux redistribution towards enhancement of the channeled flux. Another typical example of selection were experiments that used photo plates for particle detection that were energy sensitive. Again, since channeled ions exit a crystal with higher energy, they caused a stronger blackening of the developed films, thus also falsely pretending a flux enhancement along crystal directions. In other experiments, collimated proton beams along a crystal axis exhibited so-called "star patterns", that is, apparent flux enhancements along planar directions, which turn into flux reductions at relatively large angles away from the incident direction [5]. However, these patterns are not to be confused with the redistribution of an initially isotropic flux as measured by our group, because the star patterns could be explained in terms of the angular spread of ions dechanneled from the incident collimated beam by multiple scattering on target electrons and nuclei. Their angular spread is much stronger than for channeled ions, which only suffer multiple electron scattering. Thus, dechanneled ions were spread out more then channeled ones, resulting in an apparent flux enhancement of channeled ions as compared to the dechanneled ions. At the larger angles, where the apparent flux enhancements turned into flux reductions, the so-called blocking effect occurred. Blocking is the complementary effect to channeling, whereby an ion starts from or at a very small impact parameter to a lattice atom. Thus, blocking has to do with large-angle scattering in contrast to channeling with its correlated small-angle scattering. In blocking, the ion is scattered away, or "blocked", respectively, from the corresponding lattice direction. Thus, there appears a flux reduction within the star patterns at large enough angles for blocking.

It was about ten years ago when S. Karamian discovered flux redistributions over and above simple selection effects [6]. He has observed that ions from a larger depth inside a crystal showed another flux distribution behind the crystal than ions from nearby the surface. However, due to the lack of a definite scattering geometry it was still possible that these measured differences may have been caused by a selection of ions inside the crystal, because it was not possible to uniquely associate the starting depth of the ion to its exit energy.

In contrast to all these mentioned *selective* experiments, the scattering geometry as applied in this work avoids any such selection effects, precisely because all ions entering the crystal are detected independent on their energies. In the beginning of this discovery it appeared a bit odd to the channeling community that one would use isotropic beams, in contrast to the great overall efforts of preparing collimated beams as divergence-free as possible. But it is this very isotropic initial flux which probes best the question of possible redistributions. Due to the equal population of channeled vs. non-channeled ion states by the initially isotropic beam, angular flux redistributions after transmission clearly point to a strong violation of the rule of reversibility, which predicts the conservation of an isotropic flux. Since the initial flux is isotropic,

a flux enhancement along crystal directions means that the corresponding ions must have lost transverse momentum relative to these directions, and this momentum *loss* is referred to as "transverse *cooling*". Correspondingly, a flux reduction means a *gain* in transverse momentum, which is thus called "transverse *heating*" [3].

In the very beginning after discovering cooling and heating it was clear that channeling theory must be extended, because all processes included so far were unable to reproduce this effect, as was shown by computer simulations [7]. Since energy loss can at best lead to a very small amount of cooling, but principally never to heating, another mechanism had to be found, and the idea came up that it may be charge exchange which could possibly lead to a violation of the rule of reversibility. This was strongly supported by first experiments with fully stripped ions, which still suffer a considerable energy loss, but where flux redistributions totally vanished. The problem in establishing this idea was the fact that there are basically no theories available for charge exchange of swift heavy ions around the maximum of the electronic stopping power, which is on the other side exactly the region where cooling and heating appears. Thus, the very first model must be considered as being rather qualitative in character with a few quite simple estimates. But these estimates were in accordance with the experiments present at that time. However, the following much more systematic study, as presented in this work, revealed a highly complex behavior in respect to cooling and heating. Such a result warns for any too simple explanations. Nevertheless, the merit of the first model was to give an insight into the possibility of charge exchange as a source for violating the rule of reversibility. Its basic assumption is a difference in the impact parameter dependence of electron capture and loss. It is well known that ions traversing matter reach an equilibrium charge state, around which the momentary charge state fluctuates due to electron capture and loss [8]. It was shown that if the mean capture radius is smaller than the mean loss radius, a net irreversible loss of transverse momentum follows, hence transverse cooling, while the reversed condition would lead to transverse heating [3]. Thus, for the first time, a possible theoretical understanding of heating was given. However, in face of the body of experimental data gathered in the meanwhile, a much more complex behavior was seen which prevents any explanation in such simple terms. Due to the lack of available theories, an own theoretical approach was undertaken in form of intensive computer simulations based upon the so-called "Classical Trajectory Monte-Carlo" (CTMC) procedure [9]. In the beginning of CTMC only one active atomic electron was taken into account, but the so-called "n-body CTMC" (nCTMC) considers all n electrons of the target atom [10]. All CTMC and nCTMC simulations are restricted to single ion-atom collisions, like in dilute gases, while channeling certainly requires to simulate the collisions of an ion with several atoms meeting the condition within dense solids. The specially developed "nN-CTMC" method, as done in this work, is an essential extension of the nCTMC method, whereby nN-CTMC calculates the simultaneous interaction of the ion with N atoms each carrying n electrons. As it is discussed in detail, nN-CTMC is not just a "multiplication" from nCTMC with "N=1" to nN-CTMC with $N \gg 1$, but requires to incorporate new concepts in order to adequately account for multiple charge exchange in solids. With these own simulations it was possible to not only reproduce

clear signatures of cooling and heating on one side, and measured shifts in charge state distributions of channeled vs. non-channeled ions on the other side, but also to reduce the underlying mechanism to the complex impact parameter and velocity dependent probabilities for charge exchange.
This work consists thus of two main parts: one experimental part, showing a large variety of different dependencies of cooling and heating, and one theoretical part, describing the own development of newly classical simulations in order to find an explanation for cooling and heating.

Chapter 2

Transverse Cooling and Heating

2.1 Channeling and Blocking

The effect of channeling is ultimately linked to the occurrence of correlated small-angle scattering of an ion traveling along a crystal direction [11]. If the angle of its motion relative to crystal strings or planes is smaller than a certain critical angle, then the ion experiences a guidance along these directions within the collective potential of the crystal atoms, thus, it is said to be "channeled". Fig. 2.1 shows the basic scheme of channeling together with relevant quantities. Channeling motion is possible by the suppression of large-angle scattering, because the distance of closest approach r_{min} in channeling is greater than the impact parameter required for large-angle Rutherford scattering. Hence, channeling is best characterized by the confinement to a certain impact parameter region preventing scattering to angles above the critical angle for channeling. As a consequence, yields are strongly reduced for all reactions which require small impact parameters, such as inner shell excitation or nuclear reactions, to

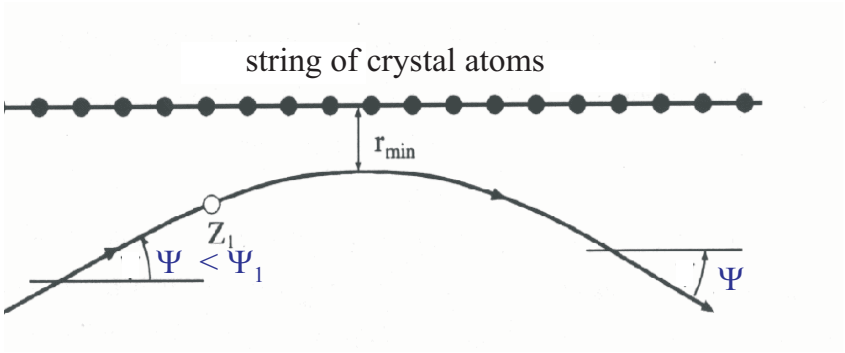

Figure 2.1: Basic scheme of channeling. Ions with an incident angle $\psi < \psi_1$ are guided along the string of crystal atoms by correlated small-angle scattering and are confined to impact parameters larger than r_{min}. Note that the scaling is unrealistic, because the ion passes several hundreds of crystal atoms during such a half-oscillation.

name a few.
The critical angle was derived by J. Lindhard, so-to-speak the "father" of channeling. He argued that an ion is channeled as long as a continuum description of the ion-crystal potential $U(r)$ is valid. This continuum potential is a collective potential averaged over all single ion-atom potentials $V(R)$, whereby R is the distance between the ion and a crystal atom at position z along the string direction, thus

$$U(r) \;=\; \frac{1}{d}\int_{-\infty}^{+\infty} V(\sqrt{b^2+z^2})dz, \tag{2.1}$$

with b being the distance from the ion to the string and d being the interatomic distance between the crystal atoms along one string. This continuum picture becomes invalid, when the ion gets so close to a single crystal atom that it suffers a large-angle scattering. From estimates comparing the product of the interaction time during the passage of one crystal atom and the ion's velocity on one side with the interatomic distance of the crystal atoms along a lattice string on the other side, the following critical "Lindhard" angle ψ_1 for *axial* channeling was derived:

$$\psi_1 \;=\; \sqrt{\frac{2\ Z_1\ Z_2\ e^2}{4\pi\epsilon_0\ E\ d}}, \tag{2.2}$$

where Z_1 and Z_2 are the nuclear charges of the ion and crystal atoms, respectively, and E the ion's energy.
In correspondence, the critical angle ψ_2 for *planar* channeling reads

$$\psi_2 \;=\; \sqrt{\frac{2\pi Z_1\ Z_2\ e^2\ a\ N_{at}\ d_p}{4\pi\epsilon_0\ E}}, \tag{2.3}$$

with N_{at} being the atomic density, d_p the interplanar distance, and a the Thomas-Fermi screening length defined by

$$a \;=\; 0.8853\ a_0\ (Z_1^{2/3} \;+\; Z_2^{2/3})^{-1/2}, \tag{2.4}$$

where a_0 is the Bohr radius. From the comparison of Eqn. (2.3) with Eqn. (2.2) follows that within the experiments performed in this work the axial critical angle is larger than the planar critical angle by a factor of about three.
For the axial critical angle there exists a correction due to thermal vibration of the crystal atoms, and finally one gets

$$\psi_c(\rho) \;=\; \frac{\psi_1}{\sqrt{2}}\cdot\left(ln\ \left[\frac{C^2a^2}{\rho^2}\right]\right)^{1/2}, \tag{2.5}$$

where $\rho = \sqrt{2}u_1$, with u_1 being the mean thermal vibration amplitude in the Debye approximation, which is about 0.08 Å in case of Si, while the distance of closest approach $r_{min} \approx a$ and therefore $r_{min} \approx 0.1$ Å (for convenience, lengths directly related to channeling dimensions are given in the unit of 1 Å= 0.1 nm). In this work the

critical angles are just used for orientations in graphs of angular flux distributions, and are thus not compared with measurements. In case of heavy ions deviations from the simple formulas can be expected due to screening by projectile electrons. Furthermore, in many cooling and heating experiments the thermal correction does not change the value according to Eqn. (2.2) very much, thus this equation is used throughout this work.
The validity of the continuum potential allows to decouple the forward motion from the transverse motion in respect to crystal directions. The transverse energy $E_\perp$ is then the sum of the kinetic energy that corresponds to the transverse momentum, and the potential energy $U(r)$, thus in total

$$E_\perp \;=\; E\psi^2 \;+\; U(r). \tag{2.6}$$

Note that for the experiments presented here the transverse energy is about 5 orders of magnitude smaller than the forward kinetic energy E, with ψ being in the order of a few tenth degrees. This decoupling especially means the conservation of the transverse energy, assuming that while this continuum picture is valid the ion's energy loss affects the forward kinetic energy only.

The blocking effect is just the complementary behavior to channeling, because here the ion starts from the position of a crystal atom or very nearby, for instance, as a recoil after a close encounter with a projectile. An ion in blocking cannot move along crystal directions, because the next few neighbors to its starting position scatter the ion away from the crystal direction, thus, this crystal direction is "forbidden", or blocked, respectively. This fact makes clear that channeling and blocking trajectories cannot be the same, because a channeling ion does not approach crystal atoms so close as where a blocking trajectory starts.
It is a bit surprising that detailed calculations of the blocking critical angles yield exactly the same result as the channeling critical angles [12]. On the other hand, Lindhard proved that channeling and blocking are related by the so-called "rule of reversibility", concluding that under idealized situations measurements of channeling and blocking with the same ions, crystals, and energies should give equal yields of detected particles. In this work, the rule of reversibility plays an essential role and is thus described in detail in section 2.2 below. The effect of blocking is just mentioned here in order to clearly point out that within the experimental conditions of cooling and heating experiments, which used an incident isotropic beam centered around an axial direction, the condition for channeling as well as for random motion is fulfilled, whereas blocking, for instance large-angle scattering on surface atoms, is negligible.

The motion of a channeled ion is not only governed by the collective potential $U(r)$, but also by scattering on the thermally vibrating crystal atoms. These scattering events can lead to an increase in transverse energy, and thus, finally to dechanneling if the transverse energy exceeds the critical transverse energy for channeling, which is $E\psi_1^2$ in axial case and $E\psi_2^2$ in case of planes. However, the same events of scattering are also experienced by non-channeled ions, which can, therefore, become channeled (rechanneling). In other words, de-channeling and re-channeling events lead to transitions

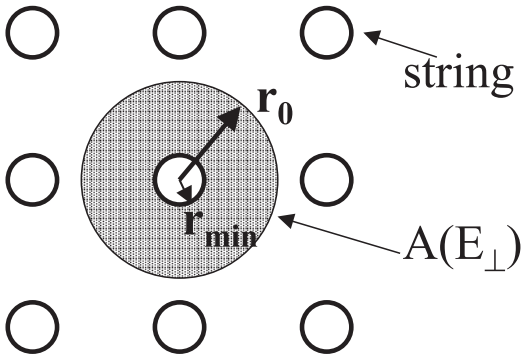

Figure 2.2: Accessible area $A(E_\perp)$ in the transverse plane along an axial channeling direction. The radius r_0 is the largest radius associated with each string, and r_{min} is the distance of closest approach to the string for an ion with transverse energy $E_\perp$.

from channeled to non-channeled ions and vice versa. The already mentioned rule of reversibility makes clear predictions about the probability for de- and rechanneling. As will be discussed below, it turns out that de- and rechanneling are equally probable, thus an initially isotropic beam should be conserved, in contrast to the appearance of cooling and heating. This *violation of reversibility* is the central theme of this work. Before turning to this rule and its violation by cooling and heating, further quantities relating to channeling are described. Since the value of the transverse energy must be non-negative, there is only a certain area $A(E_\perp)$ in the transverse plane which is accessible for a channeled ion, if at each position r of $A(E_\perp)$ the following condition is fulfilled:

$$E_\perp \geq U(r), \qquad \forall r \in A(E_\perp). \tag{2.7}$$

Lindhard has shown that in equilibrium all ions are equally distributed within their accessible areas, whereby such an equilibrium is reached after the ion passed about 1000 Å [1]. This means that the probability for finding an ion outside its accessible area is zero, whereas it is $1/A(E_\perp)$ for any point $\vec{r}$ within its accessible area. Fig. 2.2 shows the scheme of the transverse plane in axial channeling and relevant quantities. The size of the accessible area is

$$A(E_\perp) \;=\; \pi[r_0^2 \;-\; r_{min}^2(E_\perp)]; \quad \text{with } \pi r_0^2 \;=\; \frac{1}{N_{at}d}, \tag{2.8}$$

where r_0 is the maximal radius associated with each string, and $r_{min}(E_\perp)$ is the distance of closest approach to a string for an ion traveling with transverse energy $E_\perp$. Note that the distance of closest approach of all axial channeling trajectories would be $r_{min}(E_\perp = E\psi_1^2)$.

2.2 Rule of Reversibility

Since the so-called "Rule of Reversibility", or "Reversibility in Space", respectively, is the most central point in characterizing and discussing the effect of cooling and heating, its derivation according to Lindhard [13] is given in detail in this section.
Lindhard's aim was to arrive at a general framework for studying dynamical phenomena in statistical physics. In order for being quite general an abstract probability field $a(x,t)$ was introduced, whereby this field describes the statistical behavior of a system with x being the coordinate in a generalized space and t being the time. In context of channeling x will stand for the transverse energy. The state of the system is completely specified at a time t if $a(x,t)$ is given for all x.
Lindhard continues by introducing basic constraints from first-principles. The first one is that if $a(x,t)$ is given at a time t, then the state of the system is uniquely determined at any later time t'. The second constraint has to do with conservation of probability, that is, it is demanded that

$$\int \dot{a}(x,t)dx = 0, \tag{2.9}$$

with $\dot{a} = \frac{\partial}{\partial t}a(x,t)$. Further constraints are that $a(x,t)$ is real and non-negative due to its probability character, and that it describes a linear behavior. The latter point means that if $a_1(x,t)$ and $a_2(x,t)$ are solutions of the equation of motion, then also $\lambda_1 \cdot a_1(x,t) + \lambda_2 \cdot a_2(x,t)$, that is, superposition is imposed. The use of linearity was justified by the fact that in quite general cases of the dynamics of ensembles one is indeed concerned with linear equations of motion.
From the first constraint and superposition follows directly the equation of motion as used by Lindhard, concluding that if the field $a(x',t')$ is known at time t', then

$$a(x,t) = \int dx'\ T(x,t;x',t')\ a(x',t'), t > t', \tag{2.10}$$

where the quantity T is called the propagator, having the property of

$$T(x,t;x',t') = \delta(x-x'). \tag{2.11}$$

For later purposes it is more useful to treat the time derivative $\dot{a}(x,t)$ instead of $a(x,t)$, which receives a contribution from the point y through another function called $\Gamma(x,y,t)a(y,t)$. Therefore, one gets

$$\dot{a}(x,t) = \int dy\ \Gamma(x,y,t)a(y,t). \tag{2.12}$$

According to Eqn. (2.9) one must have

$$\int dx\Gamma(x,y,t) = 0, \qquad \text{for all y.} \tag{2.13}$$

Before reaching the fundamental equation for reversibility, the function $\Gamma(x,y,t)$ is re-written by introducing a function $G(x,y,t)$ with the property that

$$\Gamma(x,y,t) = G(x,y,t) - \delta(x-y) \int dx'G(x',x,t). \tag{2.14}$$

Following the constraints above about $a(x,t)$ being real and non-negative, it is found that the same must apply for $G(x,y,t)$. From this one gets the basic equation of motion which obeys all constraints,

$$\dot{a}(x,t) \;=\; \int dy\,[G(x,y,t)a(y,t) \;-\; G(y,x,t)a(x,t)]\,,\; G(x,y,t) \geq 0, \tag{2.15}$$

which is further reduced if only *time-independent* systems are treated, thus the final equation reads

$$\dot{a}(x,t) \;=\; \int dy\,[G(x,y)a(y,t) \;-\; G(y,x)a(x,t)]\,, \quad G(x,y) \geq 0. \tag{2.16}$$

In context of channeling, G is the differential scattering function and x is the transverse energy. Next step is to look at *equilibrium* distributions $a^0(x)$, defined by $\dot{a}^0(x) = 0$. According to Eqn. (2.16) such an equilibrium is reached by the following symmetry of the differential scattering function

$$G(x,y)\; a^0(y) \;=\; G(y,x)a^0(x). \tag{2.17}$$

The last step in deriving the rule of reversibility is to give a prove for the proposed symmetry (2.17) within the context of channeling. This is possible by the fact that at a fixed point $\vec{r}$ in transverse plane the scattering probability $p_{\vec{r}}(\vec{p}_{\perp,2};\vec{p}_{\perp,1})$ of an ion moving with transverse momentum $\vec{p}_{\perp,1}$ to another transverse momentum $\vec{p}_{\perp,2}$ is symmetrical [14], that is,

$$p_{\vec{r}}(\vec{p}_{\perp,1};\vec{p}_{\perp,2}) \;=\; p_{\vec{r}}(\vec{p}_{\perp,2};\vec{p}_{\perp,1}). \tag{2.18}$$

The transformation from transverse momentum to transverse energy is easily possible, because the corresponding volume elements in transverse momentum space and transverse kinetic energy space are proportional, $\pi d(p_\perp^2) \propto d\; E_{\perp,kin}$, and the potential energy is not changed by scattering, thus one gets

$$p_{\vec{r}}(E_{\perp,1};E_{\perp,2}) \;=\; p_{\vec{r}}(E_{\perp,2};E_{\perp,1}). \tag{2.19}$$

The transverse energies $E_\perp$ must exceed the transverse potential $U(r)$, so that the kinetic energies are non-negative before as well as after scattering. Therefore, the integration for averaging over the positions $\vec{r}$ must be performed within the accessible areas $A(E_\perp)$ in transverse plane corresponding to the transverse energies $E_\perp$. Finally one obtains

$$p(E_{\perp,1};E_{\perp,2}) \cdot A(E_{\perp,2}) \;=\; p(E_{\perp,2};E_{\perp,1}) \cdot A(E_{\perp,1}). \tag{2.20}$$

This equation is called "reversibility in space", that is, in phase space of the transverse energy, and satisfies the symmetry in Eqn. (2.17). It also qualifies as a "detailed balance", because its symmetry applies to *any* two transverse energies $E_{\perp,1}$ and $E_{\perp,2}$. Thus, the "rule of reversibility" implies that the probability for scattering of an ion moving with transverse energy $E_{\perp,1}$ to another transverse energy $E_{\perp,2}$ is the same as for the reversed transition, but with a correction for the change in the accessible areas

in the transverse plane. It must be pointed out here that the "reversibility in space" must not be confused with the well-known *Bewegungsumkehr* in elastic scattering, which is the time reversibility of the corresponding equations of motion. The main difference between *Bewegungsumkehr* and "reversibility in space" is that the latter may be derived without reference to time reversibility of *individual* trajectories, that is, only the reversibility of a whole *ensemble* is meant. In channeling, time reversibility of individual trajectories is not fulfilled due to the presence of statistical fluctuations caused by scattering on target electrons. But this scattering is certainly included in the derivation of the "reversibility in space" by Eqn. (2.18). Thus, time reversibility of individual trajectories can only be applied to elastic scattering on the thermally displaced atomic nuclei. However, for well channeled ions this nuclear scattering is strongly suppressed due to the confinement to larger impact parameters, while electron scattering is always present.
In order to derive transition rates from transition probabilities, one must keep in mind that in case of non-channeled ions the accessible area in transverse space is not infinite, but πr_0^2. Furthermore, for an isotropic beam the number of ions within the accessible areas is proportional to the areas, that is, $N(E_\perp) \propto A(E_\perp)$. Thus, according to Eqn. (2.20) for an isotropic flux, which populates all transverse energies according to their accessible areas, the transition rates from channeled to non-channeled motion and vice versa are equal. Therefore, an initially isotropic flux is expected to be conserved, thus not showing any flux redistributions.

2.3 Cooling and Heating

The first hint for the occurrence of flux redistributions was found by S. Karamian [6]. He studied the flux distribution in a blocking geometry. Since this type of scattering is certainly a large-angle scattering, a blocking image is to be expected. However, by varying the entrance energy of Ar projectiles, and thus the depth inside a Si crystal in which these projectiles are scattered due to the energy dependence of Rutherford scattering, he found that ions emerging from a larger depth did not show a blocking, but a channeling distribution. This type of experiment did not provide a one-to-one relation between exit energy and the starting point inside the crystal because of the difference in the energy loss of channeled vs. non-channeled ions. In the experimental section a more definite scattering geometry, which was used throughout this work, is described. This geometry allows to produce a quasi-isotropic flux around an axial direction of aligned crystals [15]. Since each ion that enters the crystal is also detected, no selection effects related to different energy losses distort the exit angular distribution. Typical results with the advanced scattering geometry are shown in Fig. 2.3. One can clearly see a significant redistribution of the flux along crystal directions. As the initial flux distribution is isotropic, a flux enhancement means that some more ions leave the crystal along lattice directions than entered there in the beginning. Therefore, these ions must have lost a considerable amount of their transverse momentum relative to these marked directions. Thus, a flux enhancement (loss of transverse momentum)

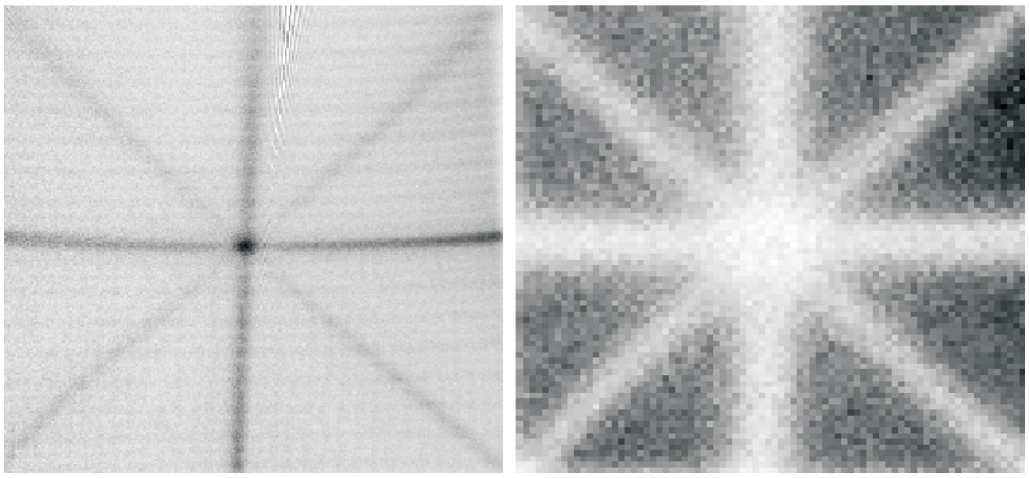

Figure 2.3: Strongest examples of flux redistributions: (left) flux enhancement up to a factor of 4 along crystallographic directions, cooling, of 187 MeV Ni ions after transmission of a 13.6 μm thin Si(001) crystal; (right) flux reduction by a factor of 5, heating, of 92 MeV Au ions in a 2.9μm thin Si(001) crystal.

was called "transverse cooling", and with the same logics a flux reduction (gain of transverse momentum) was called "transverse heating". Throughout this paper the adjective "transverse" is dropped, because there is no misunderstanding possible, as all channeling effects refer to the *transverse* component of motion.

Since according to the rule of reversibility one does not expect any angular flux redistributions, the occurrence of cooling or heating is clearly a violation of this rule. However, one must keep in mind that this rule was derived under the assumption of *time-independent* situations, thus certainly neglecting energy loss, which would indeed violate the symmetry in Eqn. (2.18). But, as will be shown by experimental results, there are conditions under which cooling and heating disappear, thus satisfying the rule of reversibility, despite presence of energy loss. Furthermore, one can estimate upper limits of the degree of flux redistributions due to energy loss alone. This is shown in the theoretical section, where it turns out that this kind of violation is just "weak" as compared to experimentally found redistribution strengths. Therefore, another mechanism over and above energy loss effects must be found. In the next chapter the systematic experimental study is presented, yielding a quite complex behavior of cooling and heating. Theoretical approaches towards an understanding of this effect are then discussed in the theory chapter.

Chapter 3

Experimental

The most important condition of any experiment for studying changes in flux distributions of ions after transmission through crystals is to avoid any selection effect. If only a part of the initial ion flux is detected, then it is impossible to infer from that to a change in the *total* flux, as it is always possible that the undetected part may just compensate any measured flux changing. In order to have a direct comparison of the channeled with the non-channeled flux it is reasonable to generate an *isotropic* flux around a crystal direction which extends significantly above the corresponding critical angle. This is the reason for using an isotropic flux in contrast to well collimated beams as they are typically used in channeling measurements. The use of such typical beam geometries may explain why the effect of cooling and heating was not discovered earlier, taking into account that channeling is known for over 40 years.
This chapter is divided into two parts, whereby the first treats the experiments directly related to cooling and heating, and the second part describes measurements of charge state distributions performed within the energy regimes of cooling and heating, thus giving insights into the mechanisms of charge exchange, which is possibly responsible for cooling and heating, as discussed in detail in chapter 4 about the undertaken theoretical approaches.

3.1 Transverse Cooling and Heating

3.1.1 Setup

The scheme of the scattering geometry is displayed in Fig. 3.1. The focused ion beam from the Munich 15 MV Tandem accelerator is scattered on $150 - 200\ \mu g/cm^2$ thin W- or Os foil in order to produce a quasi-isotropic flux incident on the crystals. The entrance ion energy into the crystals is adjusted by inserting Al degraders in front of the crystals. The scattering angle θ was usually as small as 12.5°, which causes due to the scattering geometry the danger of beam damage of the crystals by the unscattered beam. In order to avoid that an aperture was put in between the Al degrader and the crystal. The distance from the scattering foil to the crystal was 22 mm. All

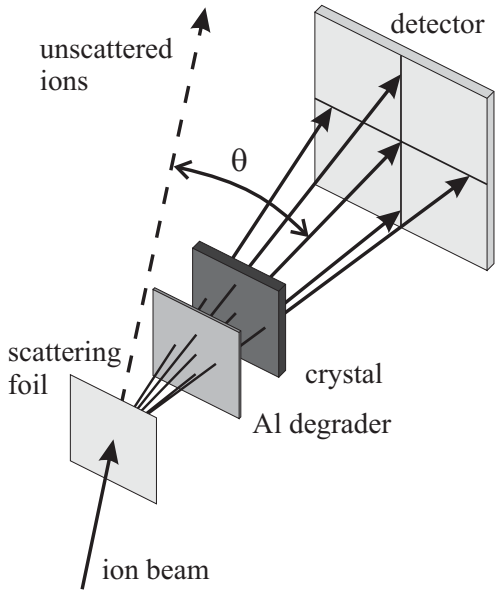

Figure 3.1: Basic scattering geometry. The ion beam from the Tandem accelerator is scattered on very thin scattering foils into a quasi-isotropic ion flux entering the crystals. The ion energy is adjusted by inserting degrader foils. The ion flux after transmission is detected by position sensitive detectors.

three components, scattering foil, Al degrader, and crystal, were mounted on a 5-axes positioning system (goniometer) in a high-vacuum chamber. The Si(001) crystals were produced at the Forschungszentrum Rossendorf by electrochemical etching with an ion-implanted etch stop [16], while the Ni(001) and Pt(001) crystals were produced by molecular beam epitaxy at the University of Aarhus, Denmark.
The choice of the scattering angle $\theta = 12.5^0$ has the advantage that the Rutherford scattering cross section is very high at low scattering angles, and thus a large number of ions could be detected in a relatively short time. In order to get final angular distributions with satisfying statistics about 4 million ions have to be measured, which takes about one hour. On the other side, such a small scattering angle bears a large variation in the angle dependence of the Rutherford cross section within the detected solid angle by a factor of three. Therefore, in order to imitate a purely isotropic ion flux, the detected flux must be corrected in such a way as if the initial beam were perfectly isotropic. In the following the applied detectors and the corresponding data acquisitions as well as the Rutherford correction and further data processing are described in detail.

3.1.1.1 Detectors

Most experiments, except the ones with protons and lead ions, were performed with an already existing setup at the Tandem lab, which is supplied with a position sensitive

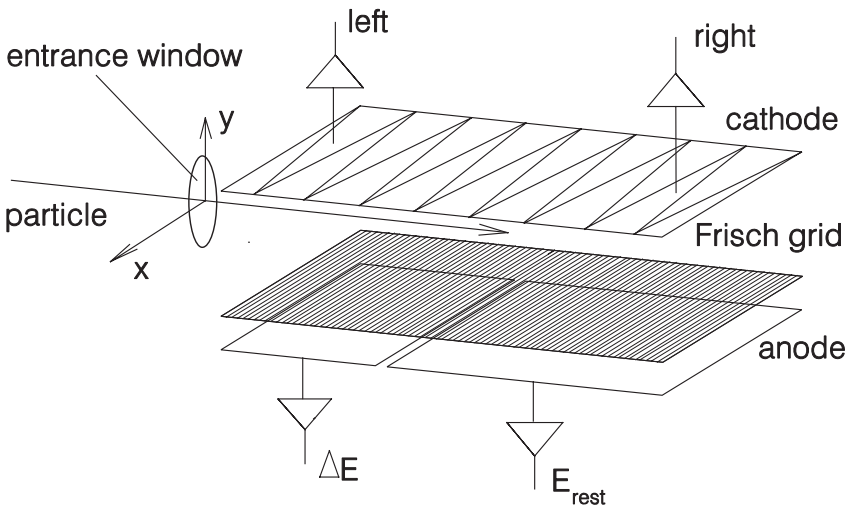

Figure 3.2: Principle scheme of the ionization chamber. Ionized electrons are detected at the anode, which is screened from the gas volume by the Frisch grid. Image charges induced in the Backgammon-structured cathode allow to determine the x-position of the ion trajectory in the chamber. The y-position is yielded by the ratio of the total cathode signal, $left + right$, and the total deposited energy, which is the sum of the two separate anode parts $\Delta E + E_{rest}$.

ionization chamber. In cases of exit energies below the threshold of the chamber nuclear track detectors (CR39) have been used.
Within the gas volume of the ionization chamber there is isobutene gas with a purity of 99.999 % and a pressure of about 20–70 mbar. Since the scattering chamber is under high-vacuum of a pressure of about 10^{-7} mbar, there must be an entrance window separating these two different pressure areas, but still allowing for transmission of the ions. This window consists thus of a 0.5 μm thin polypropylene foil which is mechanically stabilized by a supporting grid with 0.1 mm thin wires and a mesh size of 1 mm.
Fig. 3.2 shows the principal structure of the ionization chamber that was used in the experiments. If an energetic ions enters the gas volume of such a chamber, it ionizes the target gas, and these ionization electrons are drawn to the anode. In order to make the anode signal independent from the positions of the ionization events and from the charge of the ionized gas atoms, a so-called Frisch Grid is inserted for screening the anode. The ionized gas atoms move towards the cathode within the applied electrical field. The anode is divided into two decoupled parts, whereby the first gives the so-called $\Delta E-$signal, while the longer part yields the $E_{rest}-$signal. The chamber was operated in the ionization mode, that is, the number of produced charge carriers is directly proportional to the deposited energy in the gas volume. Thus, if the

ion is stopped within the gas volume above the total anode, the deposited energy is proportional to the sum of both anode signals. In order to make the chamber position sensitive two further signals are needed. The so-called R-signal (right) and L-signal (left) come from the "Backgammon structure" of the cathode. The ions generate an image charge in the cathode, and its contribution to the R- and L-signal depends on the x-coordinate: the more to the left the ion enters the chamber, the stronger the L-signal. Thus, the x-coordinate can be gained by

$$x = \frac{R-L}{R+L}. \tag{3.1}$$

In order to calculate the y-coordinate it must be taken into account that the produced image charge on the cathode (R+L) is directly proportional to the ion energy $E = \Delta E + E_{rest}$ and indirectly proportional to the distance from the ion to the cathode. From this follows if y is taken as the inverse of the ion–cathode distance,

$$y = \frac{R+L}{E} \tag{3.2}$$

Each detected ion produces the four signals R, L, ΔE, and E_{rest}, from which it is possible to infer the ion flux distribution behind the crystals according to the two equations above. These signals are processed by a chain of electronic devices, such as pre-amplifiers, amplifiers, Linear Gate Stretchers, digitalized by a ADC (analog–digital–converter) and stored on a computer disc [15].
Any ionization chamber has a certain energy threshold arising from the condition that the signal-to-noise ratio must be sufficiently large. It was found in earlier measurements [17] that the minimum energy deposition must be above 10 MeV. There are basically two reasons why ions may deposit less than this energy: either they enter the entrance window with such a low energy that after transmission of the window their rest energy is too little in order to reach the $E_{rest}-$part of the anode, or their total energy is so high that they cross the active gas volume and deposit less than 10 MeV therein. For such cases the chamber cannot be used and nuclear track detectors are applied instead. A nuclear track detector consists of a material in which energetic ions can create structural defects by breaking the bonds between the target atoms so that stable "nuclear tracks" are formed [18]. Such primarily generated defects can be made visible by etching these ion tracks up to a size of a few microns. We have used two materials, CR39, and quartz glass. The advantage of glass is a very fast etching procedure that shows the ion flux distribution within a few minutes. However, special care has to be taken due to the use of 4% HF acid. The disadvantage of glass is its relatively high energy threshold for light ions (the creation of tracks depends very much on the deposited *local* energy *density*, which is smaller for lighter ions). The threshold of CR39 is very low, around 1 MeV [19], but CR39 requires a long etching procedure of up to 5 hours within a 70° warm bath of 1 liter of water, 200 g NaOH and 20 g $NaHCO_3$.

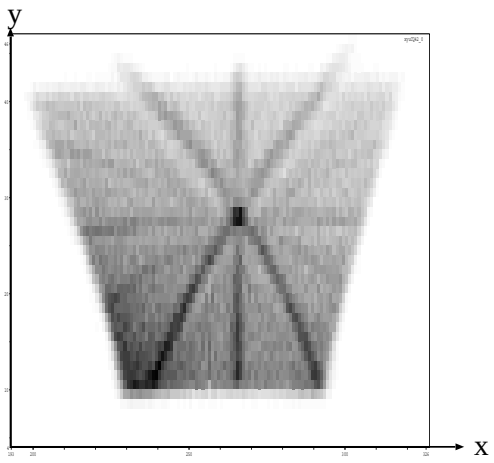

Figure 3.3: Distorted, yet uncorrected, position spectrum as seen by the ionization chamber. A larger fluence is indicated by a darker color. The distortions affect both the x- and y-direction. The flux distributions of channeled ions, that is, the enhanced flux in this spectrum, is shifted upwards as compared to the random flux.

3.1.1.2 Data Acquisition and Processing

In order to generate the ion flux distribution after transmission of the crystals the raw data of the used detectors must be transformed into two-dimensional position spectra in which each position is associated with a certain solid angle and containing the measured fluence.
In case of the ionization chamber the raw data consist of the four signals as described above. Fig. 3.3 shows a position spectra calculated from the raw data according to Eqn. (3.1) and (3.2). The clearly visible distortions have their origin in the fact that the electric flux lines do not end on the cathode in the region close to the entrance window, which is grounded. Therefore, the produced ionization electrons in this region do not contribute to the cathode signal, but still to the anode signal. Thus, for compensation a certain energy offset E_{off} must be subtracted from the anode signal E. Hence, Eqn. (3.2) reads now

$$y = \frac{R+L}{E-E_{off}}. \tag{3.3}$$

The amount of undetected charges on the cathode depends on the ion energy, which in turn depends on the scattering angle, and thus on the x-coordinate. As a result the energy offset correction must be a function of x, and in first approximation a linear dependence appeared suitable [17], so finally one gets

$$y = \frac{R+L}{E-E_{off}(\alpha\ x+\beta)}. \tag{3.4}$$

Both parameters α and β must be determined for each single position spectra. The effect of α is to make the position spectra leveled out. One gets the parameter β by

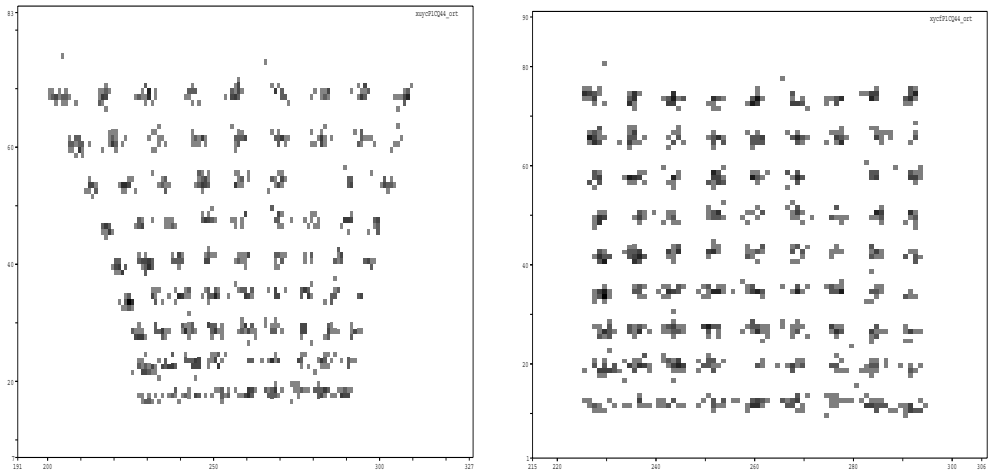

Figure 3.4: Result of the correction of the mask position spectrum : (left) uncorrected (as in Fig. 3.3), (right) corrected mask spectrum.

a comparison of the energy selected position spectra of the channeled ions with the position spectra of the non-channeled ions, whereby both groups of ions can easily be discriminated by their different energy loss with the help of the measured energy spectra. The latter spectra are shifted against the first due to the lower exit energies E of non-channeled ions which causes different y-values according to Eqn. (3.2).
The offset correction has only an effect on the y-coordinate, but Fig. 3.3 also shows distortions in the x-direction. This is taken care of by a two-dimensional transformation of the measured position spectrum of a mask consisting of equidistant holes onto a quadratic matrix, as shown in Fig. 3.4. The parameters for that mask transformation are then used to also transform the actual position spectrum.
Since in all measurements the ions to be measured were the projectiles from the Tandem accelerator, the position spectra contain only a very small amount of other elements, namely recoils from the scatter foil, Al degrader or from surface contaminations of these components. These ions can be easily excluded from the data analysis, because ions detected by the ionization chamber are separable by their nuclear charge, if the two energy signals ΔE and E_{rest} of each ion are plotted in a two-dimensional scatter plot.

In case of nuclear track detectors the raw data consist of a list of objects that an automatic scanning microscope has found via a computerized image recognition system [20]. If the data of these objects, such as central brightness or diameter of the tracks, are plotted in suitable scatter plots, real ion tracks can be distinguished from artifacts, for instance, surface defects or inhomogeneities within the etching procedure [17]. The corresponding position spectra are not distorted as in case of the ionization chamber. The total fluence upon track detectors is very much limited as compared to the ionization chamber, because after etching the tracks may overlap if their density is too high. Such overlaps prevent from counting single tracks and thus one cannot infer

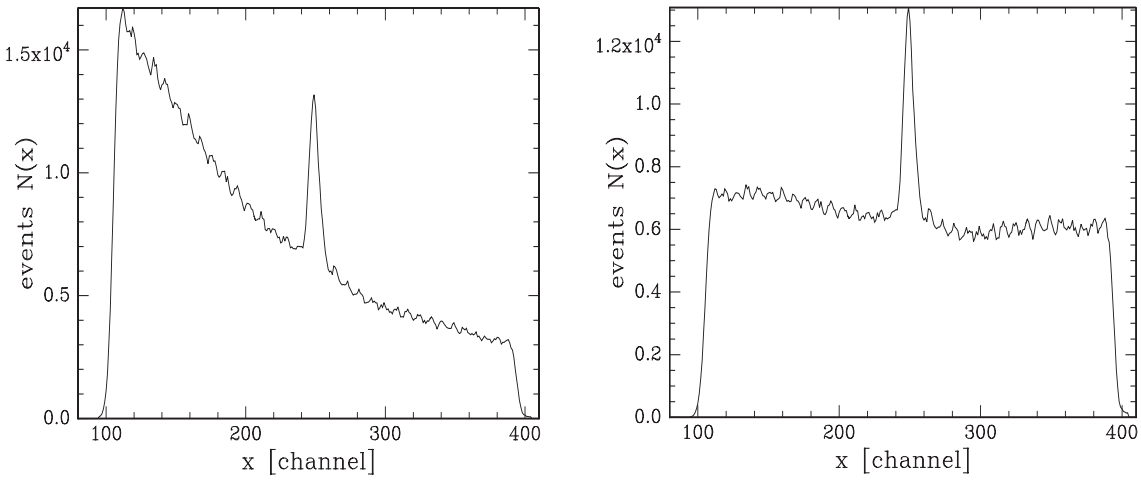

Figure 3.5: Projections of position spectrum onto the x-axis, which corresponds to the scattering angle: (left) the angular dependence of the Rutherford scattering cross section is clearly visible, which can be corrected by an angle dependent factor, Eqn. (3.5), (right). The small wiggles in the projections come from small oscillations in the position spectrum by artifacts generated in the ionization chamber in case of high energy ions where the signal-to-noise ratio allows to resolve such structures.

the original ion fluence. While in case of the ionization chamber the fluence is just restricted by the measurement time, track detectors can practically only contain about 10^5 tracks/cm^2. As a consequence, the statistical errors are much larger than in case of the ionization chamber. Thus, track detectors have only been used if the ion energy was below the threshold of the ionization chamber, like for proton and He ions, or in the case of 1 GeV lead ions which were measured at the GANIL accelerator in Caen (France).

3.1.1.3 Angular Distributions

After the basic procedures yielding the two-dimensional position spectra a correction for the angular variation of the Rutherford scattering cross section must be applied. This correction is not a deconvolution, but just a simple angle dependent factor according to the scattering cross section. If $N(x, y)$ is the fluence in the position spectrum at position (x, y), then the angular corrected value $N'(x, y)$ reads

$$N'(x,y) \;=\; N(x,y) \cdot \frac{sin^4[\Theta(x,y)/2]}{sin^4[\theta/2]}, \tag{3.5}$$

whereby $\Theta(x, y)$ is the scattering angle associated with the $(x, y)-$coordinates and $\theta = 12.5°$. Fig. 3.5 shows the effect of this correction with the projections of the uncorrected and corrected position spectrum onto the x-direction. It was expected that the initial Rutherford-distorted flux may become smeared out due to multiple scattering on target nuclei and electrons within the crystals. However, it was found that in

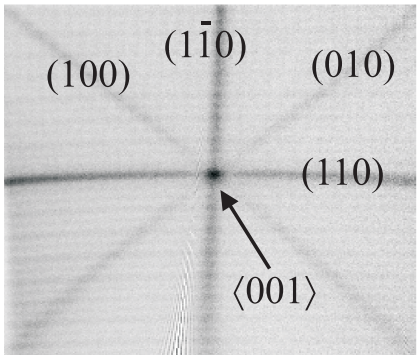

Figure 3.6: Rutherford corrected position spectrum with all relevant axial and planar crystallographic directions indicated.

case of Si and Ni crystals this influence was negligible, but for Pt crystals an effective scattering angle $\theta_{eff} < \theta$ had to be applied in order to account for the smearing out by multiple scattering [17].
Fig. 3.6 shows a position spectrum after all corrections, also indicating major crystal axial and planar directions. The final step in the analysis procedure is to produce the corresponding axial and planar angular distributions of each two-dimensional position spectrum. For the axial case a circular averaging about rings centered at the axis is performed. Each such ring corresponds to a polar angle ψ in respect to the axial direction, with $\psi = 0$ pointing exactly along the crystal axis. For planes the averaging is done along "stripes" parallel to the plane in question, whereby other planes were excluded from being counted by a cut. The contributions of the planes to the axis are negligible, as they cancel out by the circular averaging, taking into account the conservation of particles. The counts $\chi(\psi)$ are then normalized to the largest measured angle $\psi_{max} \gg \psi_1$, which refers to random directions. Therefore, $\chi = 1$ stands for the normalized random flux, and $\chi(0) \equiv \chi(\psi = 0)$ is a possible measure of any angular flux redistributions, as it gives the ratio of the fluence of ions exiting along a crystal direction and the initial flux along this direction.
The experimental errors in the angular flux distributions are determined by the statistical errors alone. It was found that systematic errors, such as ill-placed axial centers for the circular averaging in the position spectra, can be reduced to be smaller than the statistical errors. Comparisons of angular flux distributions from measurements of one and the same case with both the ionization chamber and nuclear track detector yielded an agreement within the statistical errors [17].

The validity of the Rutherford correction was verified by two independent means. The angular variation of the Rutherford cross section only affects the x-direction, but not the y-direction. Therefore, a simple check is to compare planar angular distributions that are derived from the same plane, say once the vertical (1$\bar{1}$0) and another time from the horizontal (110) plane, according to Fig. 3.6. After Rutherford correction both planar distributions were found to be equal. An experimental check for the validity of

the correction in case of an axis was the comparison of angular distributions that were gained by two different scattering angles, once with $\theta = 12.5°$ and another time with $\theta = 50.0°$, where the angular variation of the Rutherford scattering cross section is negligible. The Al degraders were chosen in such a manner that both experiments led to the same exit energy. It was found that the Rutherford corrected result was, within the experimental errors, the same as the uncorrected result under the larger scattering angle.

The angular resolution of the detectors is determined by their position resolution, their distance to the scattering foil and the beam spot size, which was typically 1 mm^2. The position resolution inside the ionization chamber was found to be about 0.6 mm, the distance from its entrance window to the scattering foil was 614 mm. In case of the nuclear track detector the position resolution is in the order of a few micrometer, and its distance to the scattering foil was 535 mm. From these numbers follows that the main influence on the angular resolution in case of the nuclear track detector is the beam spot size, while in case of the ionization chamber the beam spot size matters about as much as the position resolution, whereby in total the final angular resolutions of both detectors are estimated to be about the same [17]. This was confirmed by experiments, where no significant differences between the two detectors were found, and their resolution of about 0.05° is good enough in order to resolve typical critical angles in the range of a few tenth degrees. Since the ionization chamber is fixed it was only possible to enlarge the detector distance by a factor of two with the track detector. This experiment yielded the same width in the angular flux distribution, thus indicating that these widths are mostly determined by the effect of cooling and heating itself, and not dominantly by the detector resolutions.

3.1.2 Results

In contrast to the earliest experimental findings, the systematic study of the effect which is presented in the following, shows a large variety of different dependencies [21, 22].
First of all, an important result is described in respect to the energy region in which the effect can appear. Then the large body of data corresponding to the transition from cooling to heating is discussed, as well as detailed presentations of the dependence on ion energy, crystal thickness and orientation. All data refer to Si crystals, except the data for Ni and Pt crystals reported in section 3.1.2.7.

3.1.2.1 Fully Stripped Ions

In the very beginning it became clear that the effect disappears in case of fully stripped ions, as shown in Tab. 3.1 by the $\chi(0)$ measure of the cooling strength [3, 17].
It is obvious that the angular redistributions fade out if the mean charge state of the ions comes closer and closer to the nuclear charge state. Due to the available energies

Ion	E_{in} [MeV]	E_{out} [MeV]	$\overline{Q}$	$\chi(0)$
O	96	90	7.9	$< 1.04 \pm 0.02$
O	70	63	7.7	1.28 ± 0.05
O	55	46	7.4	1.33 ± 0.05
O	37	25	7.0	1.45 ± 0.05
C	41	36	5.8	1.12 ± 0.05
C	26	19	5.4	1.48 ± 0.12
He	4.5	3.1	1.97	1.18 ± 0.05
He	3.5	1.7	1.88	1.32 ± 0.05
p	1.0	0.58	1.0	< 1.05
p	0.72	0.12	0.9	1.22 ± 0.05

Table 3.1: Cooling strengths $\chi(0)$ in dependence of the ion entrance energy E_{in} and the corresponding exit energy E_{out}, as well as the mean charge states $\overline{Q}$ from tabulated values [23] corresponding to the mean value of entrance and exit energy. The closer the charge state approaches the value of the nuclear charge, the weaker appears the cooling effect.

at the Tandem accelerator experiments with fully stripped ions are restricted to light ions. These results are very important as they point to the apparent condition that ions must not be fully ionized in order to show the cooling effect. Furthermore, as becomes clearer in the sections further below, at the high energy end of the redistribution effect, the ions always show cooling, that is, during decreasing their energies down to values at which they start being dressed with one or more electrons, they always start showing cooling patterns, but never heating patterns. In case of such high energies where the ions are fully stripped, the cooling effect disappears and the rule of reversibility is strictly fulfilled - despite the still present energy loss. This finding is another strong evidence that cooling does not appear due to energy loss, but must require another irreversible mechanism. The degree of the possible violation of reversibility because of energy loss is discussed in more details in section 4.1.

3.1.2.2 Dressed Ions: Transition from Cooling to Heating

Probably the most puzzling and surprising feature of the effect of cooling and heating is the appearance of transitions from one "phase" to the other. It was found that when the ion energy is decreased, the cooling patterns turn steadily into heating patterns. This result was surprising in the sense that the earlier measurements only showed *either* cooling *or* heating, with Cu ions as an exception, because they showed simultaneously both features [3]. It was back then argued that cooling and heating is just a matter of

the ion nuclear charge, and this trend could be predicted by estimates of the very first qualitative charge exchange model as discussed in the theoretical part below, section 4.2. However, within this work it became clear that cooling and heating is in fact a matter of the ion *energy*, not its nuclear charge. The reason why this was not found earlier lies in the fact that in the first experiments all tested ions were each studied at basically only one certain energy, and within the probed energy regions the light ions do indeed only show cooling, while the heavy ions only show heating. Fig. 3.7 shows the case of Y ions transmitted through a 3.4 μm thin Si(001) crystal in three different energy regions. The cooling flux distribution turns into a heating distribution as the ion energy is decreased, running through an intermediate stage. The figure also displays the corresponding angular flux distributions for the $\langle 100 \rangle$ direction, where the cooling case is well presented by a clear flux enhancement along crystal directions, even extending far beyond the critical angle according to Eqn. (2.2). The same kind of extension behavior is seen in the heating case. Only the intermediate stage shows a flux enhancement restricted to channeled ions, which does, however, not mean that the redistribution affects only channeled, but not non-channeled ions, because else the flux of channeled ions could not be enhanced only, but would need a compensation by a corresponding flux reduction. Therefore, at any stage the mechanism for cooling and heating does not only work for channeled, but also for non-channeled ions.
In general, cooling cases are further characterized by a half angle (HWHM) that is smaller than the critical angle, whereby the ratio is typically between 1/2 and 1/3. In some, but not all, heating cases the angular flux shows a local minimum, so that the $\chi(\psi = 0)$ value is significantly larger than the χ value at somewhat greater angles ψ, as visible in the bottom part of the figure above. It seems that in these cases the heating process is less effective at very small angles ψ, which corresponds to very large impact parameters, that is, the best channeled ions. Such a minimum was not observed for Au ions, and this may very well be due to their much stronger multiple scattering on target electrons which can smear out such weak local minima.
The systematic study of the transition behavior requires a well-defined criterion for determining the "transition energy", that is, the ion energy at which the cooling condition turns into the heating condition. For this reason the following volume measure V is introduced for axial angular distributions:

$$V \;=\; 2\pi \int_0^{\psi_{max}} [\chi(\psi) \;-\; 1]\; \psi d\psi; \qquad \text{with } \psi_{max} \gg \psi_1. \tag{3.6}$$

This measure allows to distinguish between a cooling and a heating case, because for cooling $V > 0$, while for heating $V < 0$, due to the fact that V reflects the total angular flux redistribution. Despite the conservation of particles in the experiment, volume measures V different from zero are possible, because V refers only up to a certain maximum observation angle ψ_{max}, and one has to take into account here that the normalization procedure is also restricted to the observable region up to ψ_{max}, which should be considerably larger than the critical angle ψ_1. Thus, it is reasonable to associate the case with $V = 0$ to the transition from cooling to heating. However, it is, at first sight, not quite clear of how to deduce the transition energy from measured

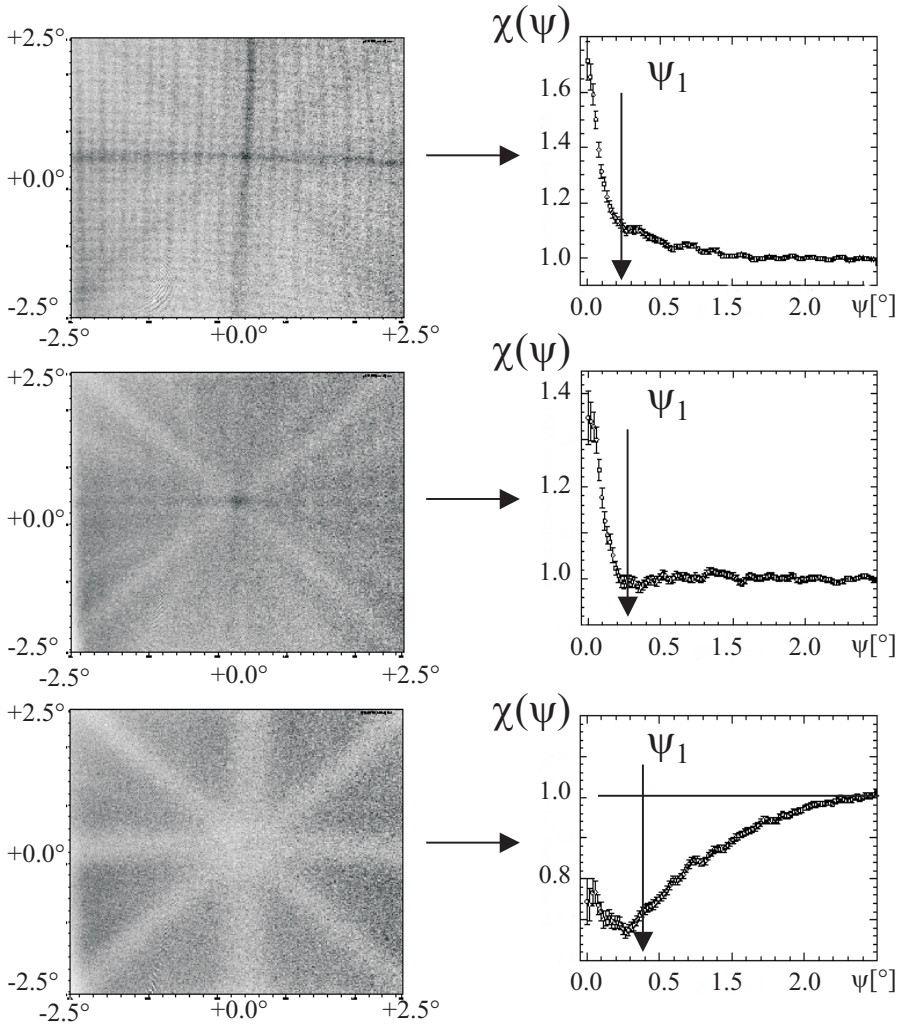

Figure 3.7: Flux and axial angular distributions of Y ions transmitted through a 3.4 μm thin Si crystal at three different exit energies: 177 (top), 117 (middle), and 63 MeV (bottom). The top case shows pure cooling, and the bottom case pure heating, while the middle case is an intermediate stage. The HWHM of the first two angular distributions are $(0.09 \pm 0.01)^\circ$ and $(0.10 \pm 0.01)^\circ$, while the corresponding critical angles are 0.23° and 0.28°.

angular distributions, which clearly depend on the exit energy as seen above. The reason for that is the fact that all measurements are performed with crystals of finite thickness with a considerable amount of energy loss. The "true" transition energy must therefore be in between the entrance and the exit energy of all such cases that lead to angular distributions with $V = 0$. Usually the difference between entrance and exit energy, that is, the energy loss, is about 20-30 MeV. Furthermore, it is possible that even if the *exit* angular distributions have a volume measure $V = 0$, the conditions in

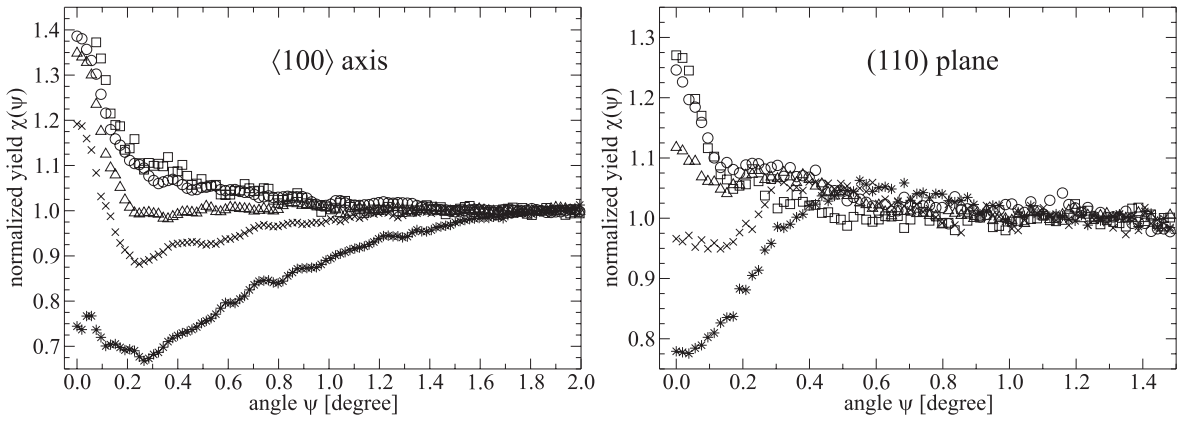

Figure 3.8: Axial and planar angular distributions of Y ions after transmission of a 3.4 μm thin Si(001) crystal. The exit energies are 177 (squares), 141 (circles), 117 (triangles), 92 (crosses), and 63 MeV (stars). Within this energy range a transition from pure cooling to pure heating patterns is seen.

a large part of the trajectories through the crystals may very well be in the cooling regime, such that in the beginning there is a building up of a cooling pattern, while towards the end of the crystal there is the transformation to the observed exit result of $V = 0$. Therefore, the crystal thickness can possibly distort the measurement of the transition energies.

Fig. 3.8 shows axial as well as planar angular distributions of the case with Y ions transmitted through Si(001) at five different exit energies in steps of about 30 MeV. While the first two high energy cases yield the same distributions, a rather fast change is seen down to the lowest energy. The exit energy that fulfils the $V = 0$-criterion would be a bit lower than the 117 MeV case. The figure clearly shows that in the axial case the $\chi(\psi \approx \psi_1)$ values are equidistant for the 141 MeV and 92 MeV case when compared to the 117 MeV case. The same finding was also seen in all other transition measurements. This points to a decreasing of the $\chi(\psi \approx \psi_1)$ values that is about linear and surprisingly rapid: the relative change in the corresponding ion velocities is, in general, of the order of only 15 %. This observed rapidness is surprising, if one takes into account that the width of the ion exit energy distributions are in the order of about 10-15 % due to energy straggling in the Al degrader and within the crystal. The linear decrease of the $\chi(\psi \approx \psi_1)$ values is thus observable within exit energy changes that are significantly smaller than the typical energy loss and energy distribution widths in the thinnest used crystals. This finally means that one must assume a very sharp distinction between cooling and heating condition. However, according to Fig. 3.8 the change from cooling to heating first starts around the critical angle, while best channeled ions are still enhanced, that is, for these ions there is still some cooling active. This finding is best seen by the 92 MeV case in the figure above. A change at larger angles ψ affects the volume measure V much more than changes at small angles due to the factor ψ in the integrand.

Taking all the facts above into account, then it seems that for defining the transition energy E_t it is a reasonable choice to take the exit energy which leads to an angular distribution with $V = 0$. Of course, this choice is arbitrary in the sense that one could have equally well chosen the mean energy between entrance and exit energy, or the entrance energy. The point hereby is not so much a unique *absolute* transition energy, but rather its systematic dependence in respect to the nuclear charge of the ion, as well as to the crystal atoms' nuclear charge and the crystal orientation. The discussion above also shows that the accuracy of the so-defined transition energy can be as good as $\pm\ 5MeV$.
There remains the question of how much the transition energy is influenced by the thickness of the used crystals. Crystals considerably thinner than the used ones, but not available for our group, may probe the ion energy dependence of cooling and heating conditions much more accurately, and thus may yield transition energies different from the ones given here. On the other hand, as stated above, it is not so much the absolute value of a transition energy, but rather "relative" transition energies that are equally defined for all ion and crystal combinations.

Fig. 3.8 also shows that the transition behavior of the (110) planes is strongly distorted by the appearance of a shoulder, which is most likely a "pile-up" of heated ions, that is, of ions that are transferred from channeled to non-channeled motion, but not quickly enough transferred further to even larger angles ψ. This behavior makes it difficult to introduce a criterion for the transition energy in correspondence to the volume measure in the axial case. The pile-ups would pretend falsely a flux enhancement in the sense of "cooling", but in fact they are just a consequence of heating. It is noted here that the appearance of a local minimum in the (110) angular distributions, as seen for the 117 MeV case in Fig. 3.8, coincides for all measured cases with the transition in the axial case.

The simplest transition behavior was found for the (100) planes: their cooling flux enhancements turn into heating flux reductions through their complete disappearance within the total flux distribution. Thus, the (100) transition energies are taken as the exit energies of flux distributions in which there are no flux redistributions along the (100) directions.

The compilation of all $\langle 100 \rangle$ and (100) transition velocities v_t, corresponding to the transition energies deduced from the measurements as described above, is shown in Fig. 3.9. Despite the somewhat arbitrary definition of the transverse energies and experimental restrictions, such as the limited number of trials for finding the exit energy that leads to a $V = 0$ axial angular flux distribution, or the disappearance of the (100) planes, respectively, a remarkably general trend is clearly seen: both curves can be fitted according to the function $v_t = \alpha \cdot Z_1^{1/2}$, with $\alpha_{axis} = 1.13 \pm 0.01$, $\alpha_{plane} = 1.36 \pm 0.02$, and the use of atomic units ($[v] = v_0$, with $v_0 \approx 2.19 \cdot 10^6 m/s$ being the Bohr velocity). Therefore, the corresponding transition energies E_t scale with Z_1^2 ($E_t = \frac{1}{2} m v_t^2 \sim Z_1 \cdot v_t^2 \sim Z_1^2$). Furthermore, the choice of the transition energy as the *exit* energy, as described above, leads to the nice side effect that in this case a fit to the measured transition energies is of the type $E_t = \beta \cdot Z_1^2$ without any offset at

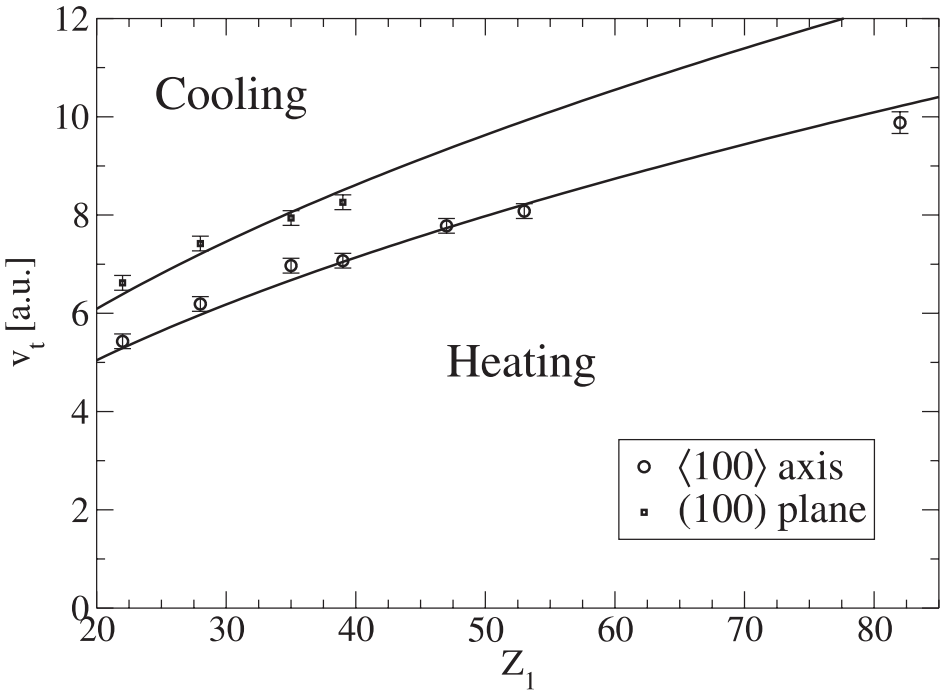

Figure 3.9: Transition velocities of all measured ions along the Si ⟨100⟩ axial and (100) planar directions. In atomic units, the scaling of the velocities is $v_t = \alpha \cdot Z_1^{1/2}$, with $\alpha_{axis} = 1.13 \pm 0.01$, $\alpha_{plane} = 1.36 \pm 0.02$. Ions with faster velocities are cooled, whereas they are heated at lower velocities than the corresponding transition velocities.

"$Z_1 = 0$", with $\beta_{axis} = (0.074 \pm 0.001)$ MeV and $\beta_{plane} = (0.10 \pm 0.01)$ MeV.
It must be noted here that the fit according to $Z_1^{1/2}$ is better by one order of magnitude in the χ^2-deviation from the data than a $Z_1^{2/3}$ scaling.
It is commonly assumed [24] and confirmed by the simulations of this work that the mean ion charge state *inside* (amorphous) solids is the same as the measured charge state behind the solids. Therefore, it is possible to associate mean ion (random) charge states to all measured transition energies with the help of tabulated values. The used table [23] entails data for C foils only, but it has been shown that they do not differ by more than one elementary charge from the case of Si [25]. If thus determining the mean ionization degree, one finds that the transition from cooling to heating occurs if the ions have lost $(60 \pm 3)\%$ of their electrons compared to their neutral charge state. Therefore, it can be concluded that the transitions have nothing to do with the closing of shells in the ion ground state, contrary to estimates from the first experimental case of such a transition, namely with Ni ions, where the "transition charge state" occurs at the closure of the L-shell, if the ion would be in ground state [17].

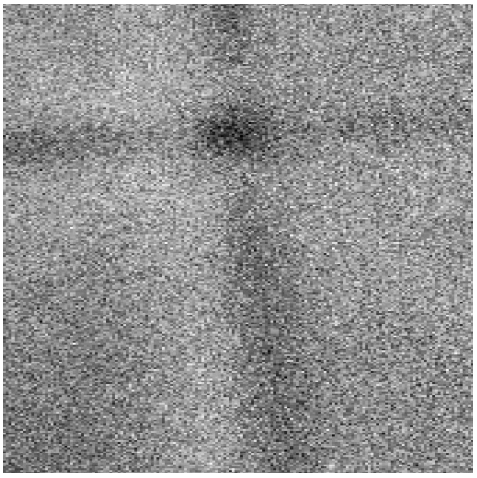

Figure 3.10: Flux distribution of S ions with an exit energy of 7 MeV. Both the ⟨100⟩ axial and (110) planar directions show strong flux enhancements, which are embedded in regions with flux reduction. Still the axial volume measure is positive, thus indicating an overall cooling effect. There is no flux redistribution along the (100) planes.

3.1.2.3 Disappearance of Transition

A very puzzling result is the disappearance of the transition behavior for ions lighter than Ti. It was found that He, C, O, F, S, and Ca ions show only cooling patterns at the lowest observed exit energies. For S and Ca ions their lowest exit energies have been significantly below the extrapolated transition energies E_{extra}:
7 MeV S (E_{extra} = 19 MeV) and 22 MeV Ca ions (E_{extra} = 30 MeV). In both cases strong cooling patterns with no signs of flux reduction were found. It is remarkable that Ca ions (Z_1 = 20) are not heated, while Ti ions (Z_1 = 22) are, while they are almost direct neighbors in the Periodic Table. He ions with 0.5 MeV (E_{extra} = 0.3 MeV) and 7 MeV F ions (E_{extra} = 6 MeV) showed also strong cooling patterns that were clearly distinct from possibly intermediate transition patterns. One must keep in mind that, despite the fact that their mean exit energies were still above the extrapolated transition energies, the widths of the corresponding exit energy distributions were presumably rather large due to straggling in the relatively thick Al degraders and could thus entail considerable fractions of ions with exit energies below the extrapolated energies, especially in case of F ions. Furthermore, if their cooling strengths were about to start being decreased towards possible heating, the observed flux redistributions would have been expected to be much weaker, if one also takes into account the counteracting multiple scattering of the ions on target electrons, which is very strong at such low ion energies. It is thus concluded that even the lightest ions do not show a transition to heating. Fig. 3.10 shows the case of 7 MeV S ions, measured with a nuclear track detector. A strong axial flux enhancement is seen embedded in a region with flux reduction, but with a still positive volume measure. The same qualitative behavior is observed for the strong (110) planes, but the (100) directions are not seen.

This, however, does not necessarily mean that the (100) planes undergo their transition just at this energy. Their disappearance at such low energies was also observed for the other measurements, and this result is interpreted as the disappearance of cooling due to the much stronger multiple scattering on target electrons which always works against any form of flux redistribution and whose strength increases at decreasing energy. Thus, the cooling strength along the axis and the (110) planes is still stronger than the multiple scattering along these directions.
Another form of absent transition behavior was found for all ions at all energies along the $\langle 110 \rangle$ axis, which is reported within the orientation dependence section 3.1.2.6 below.

3.1.2.4 Energy Dependence

It was already discussed in section 3.1.2.1 above that fully stripped ions do not show any redistribution effect. The ion energies available at the Tandem accelerator are not high enough in order to produce fully stripped ions heavier than S. Besides the effect observed for naked ions, it is also interesting to look at the cooling strength in dependence of the ion energy below the threshold of fully stripped ions. Fig. 3.11 shows the cooling strength according to the $\chi(0)$ measure plotted against the mean ion energy for S, Ti, Cr, Ni and Br ions. The case of S ions is the only case where the entire energy region can be probed, from lowest values up to the stage of being fully stripped at around 200 MeV [23]. It is seen that while decreasing the energy from the high energy end the cooling strength increases until it reaches a maximum. Also Ti and Cr ions show a maximum, while the even heavier Ni and Br ions only show an increase in cooling strength with increasing energy. This behavior may be understood by the decrease of the strength of multiple scattering on target electrons working against cooling. In case of Ti and Cr ions multiple scattering also decreases with increasing energy, but it looks like that also the cooling mechanism becomes weaker, although both ions are still far away from being fully stripped; for instance, the energy for making Ti ions fully stripped is far above 300 MeV [23]. It is clear that the cooling strength fulfils two boundary conditions, namely vanishing at high energies, where the ions are fully stripped, and at low energies, either because the ions undergo a transition to heating or because cooling disappears towards zero ion energy. Thus, it is also expected that Ni and Br ions show a maximum. After all, such a maximum indicates the optimal energy in respect to strongest possible cooling compared with the counteracting multiple scattering. It is clear that the optimum depends mostly on the ion, but not so much on the target, say for instance a certain orbital velocity of a target electron shell, because in such a case the maximum would be at a certain, fixed ion velocity. Furthermore, the maximal cooling strength possible for a certain ion seems to be a non-monotonic function of the nuclear charge, because the light S ions and the heavier Ni and Br ions can be cooled more strongly than the "intermediate" Ti and Cr ions. This may also reflect the interplay between cooling and multiple scattering, the latter monotonically increasing with increasing nuclear charge and decreasing ion energy.

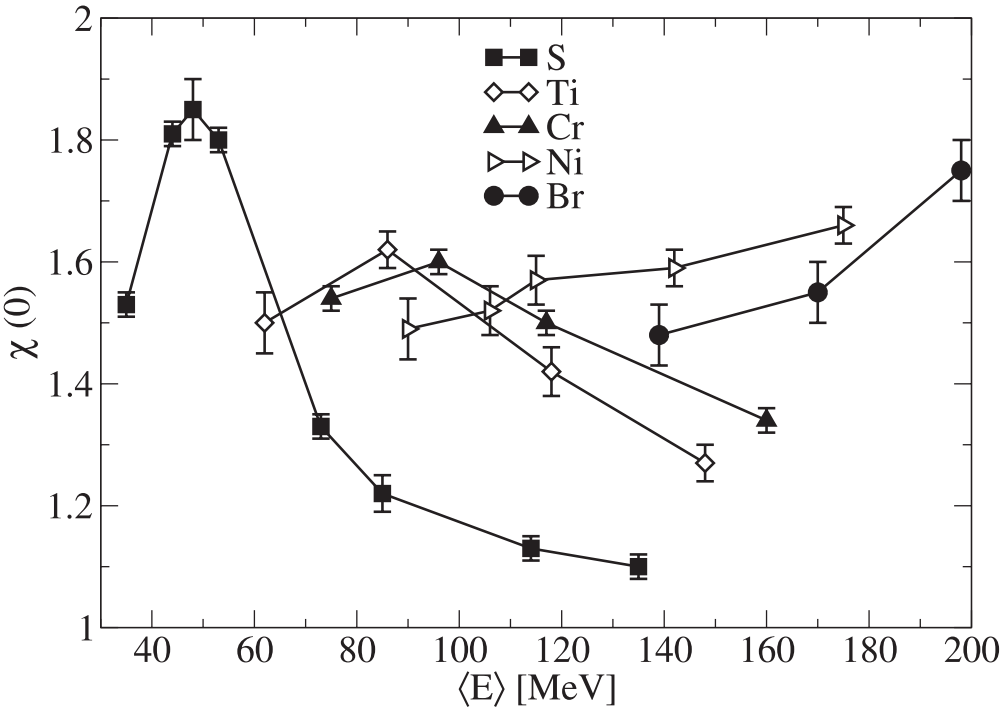

Figure 3.11: Cooling strengths, measured by terms of $\chi(0)$, plotted vs. mean ion energy $\langle E \rangle = 0.5 \cdot (E_{in} + E_{out})$. For better clarity only those data are included that refer to pure cooling cases, that is, transition and heating cases are excluded (note that S ions never show heating). S, Ti, and Cr ions show a clear maximum, indicating an optimal energy for strongest cooling, whereas Ni and Br ions do not show such a maximum within the tested energy range. Also clearly visible is that the "intermediate" Ti and Cr ions cannot be as strongly cooled as the lighter S ions and the heavier Ni and Br ions.

3.1.2.5 Thickness Dependence

When studying the cooling strength, measured as $\chi(0)$, with crystals of different thickness, one must keep in mind that this thickness dependence is linked with the energy dependence reported above. The reason for this is that in the tested energy range the ion energy decreases about linearly with increasing depth inside the crystal. Two requirements must be fulfilled for testing the thickness dependence of the cooling strength. First, the exit energies must be significantly above possible transition energies, and, secondly, the entrance energies must be below the regime of fully stripped ions. Otherwise the cooling effect would disappear in the first part of the crystals, and thus distort the thickness dependence to be measured. Fig. 3.12 shows the result of the cooling strength plotted against the thickness of different Si(001) crystals. In case of Ni ions a linear increase with thickness was found. It must be noted here that the energy dependence in the range of energies used for the Ni thickness dependence was almost constant. Therefore, if the counteracting strength of multiple scattering on

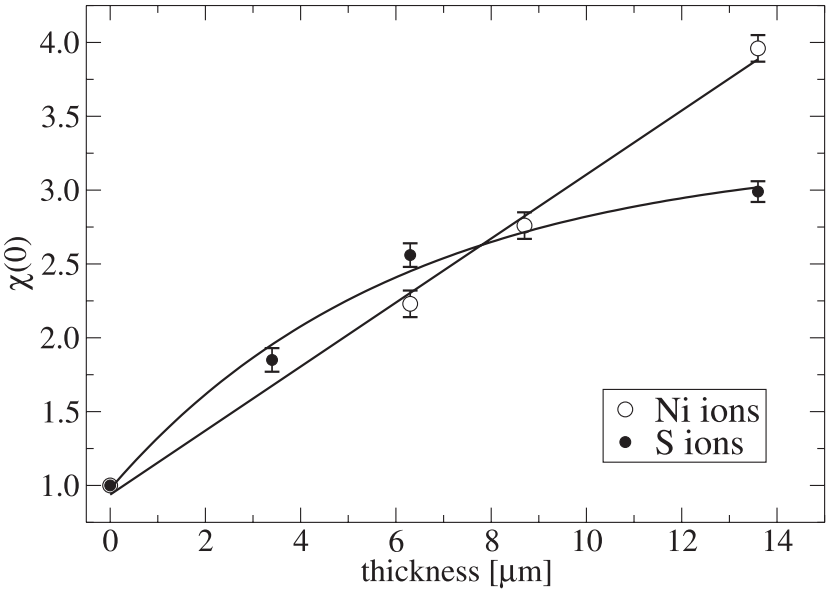

Figure 3.12: Cooling strength, measured by $\chi(0)$, plotted against crystal thickness. While Ni ions, with constant entrance energy of 187 MeV, show a linear increase, S ions, with constant exit energy of 57 MeV, show a saturation behavior.

target electrons is negligible, a linear increase of the cooling strength is to be expected as observed for Ni ions, and also for Ti ions (not shown). In contrast, S ions and O ions (not shown) exhibit a saturation behavior, when the exit energies are kept constant. This is also explained in accordance to the energy dependence. For very thick crystals the entrance ion energy must be large enough in order for the exit energy to reach the same value for every thickness. But at very high energy the energy dependence in Fig. 3.11 shows a strong decrease of cooling, only towards lower energies an increase. Therefore, in thick crystals only the last part in which the ion energy decreases sufficiently to small, but effective cooling energies, contributes to a considerable cooling strength.

3.1.2.6 Orientation Dependence

A distinct dependence on the crystal directions was already discussed in terms of different transition behavior, see section 3.1.2.2. For instance, the transitional angular distributions of (110) planes show shoulders, or pile-ups, which do not appear in the $\langle 100 \rangle$ axial case, and the (100) planes undergo their transition from cooling to heating through a stage of complete disappearance of any flux redistributions. Furthermore, as shown in Fig. 3.9, the transition velocities are significantly different along the $\langle 100 \rangle$ and (100) directions.
Another type of orientation dependence was found in respect to different cooling strengths along the $\langle 110 \rangle$ and $\langle 100 \rangle$ axis with the same crystal thickness (thus avoiding

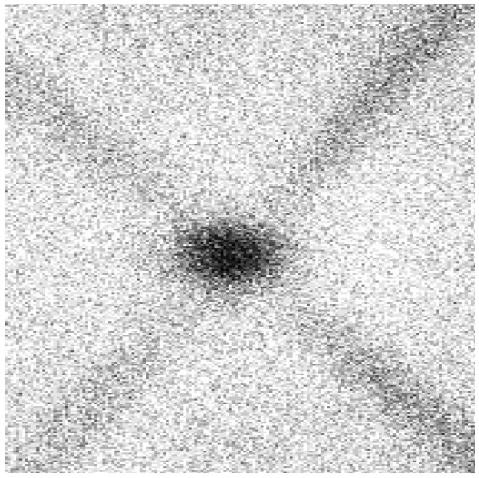

Figure 3.13: Flux distribution of lowest measured exit energy for Ni ions along the $\langle 110 \rangle$ Si axis at 5 MeV. Despite such a low energy there is no heating seen as compared to the $\langle 100 \rangle$ Si axis. Also seen are the (111) planes, which show no heating either.

a possible distortion due to thickness dependence). The cooling strength of the first axis is larger than that of the latter by about 30 % [17]. Furthermore, a much more puzzling result was the complete disappearance of any transition behavior along the $\langle 110 \rangle$ axis. A possible transition was looked for with Ni, Br, Y, and Ag ions at various energies far below the transition energies in case of the $\langle 100 \rangle$ axis, but only a cooling pattern was observed with no transition to heating. Fig. 3.13 shows the flux distribution of 5 MeV Ni ions transmitted along the $\langle 110 \rangle$ axis. A strong cooling pattern is seen both for this axis and the (111) planes, which do not show any transition behavior either. This finding was found to be the same for all tested ions.
There are two relevant differences between the $\langle 110 \rangle$ and $\langle 100 \rangle$ axes. One is that the interatomic distance along the $\langle 110 \rangle$ axis is reduced by the factor $1/\sqrt{2}$ as compared to the $\langle 100 \rangle$ channel. Secondly, the $\langle 110 \rangle$ strings are arranged in close-lying pairs which in effect enlarges the transverse area. Therefore, ions channeling along the $\langle 110 \rangle$ axis probe a larger impact parameter region, because the channel width is larger by the factor $\sqrt{2}$ as compared to the $\langle 100 \rangle$ axis.

3.1.2.7 Ni and Pt Crystals

All results so far referred to the case of Si crystals only. In order to study the dependence of cooling and heating on the target crystal, 1.0 μm thin Ni(001) and Pt(001) crystals were used. The latter have a face-centered cubic structure, while Si crystals are diamond-like. Besides different interatomic distances and different channel widths, the main difference to the Si crystals lays in the much larger nuclear charges corresponding to a much larger electron density in close ion-atom collisions in case of the heavier crystals.

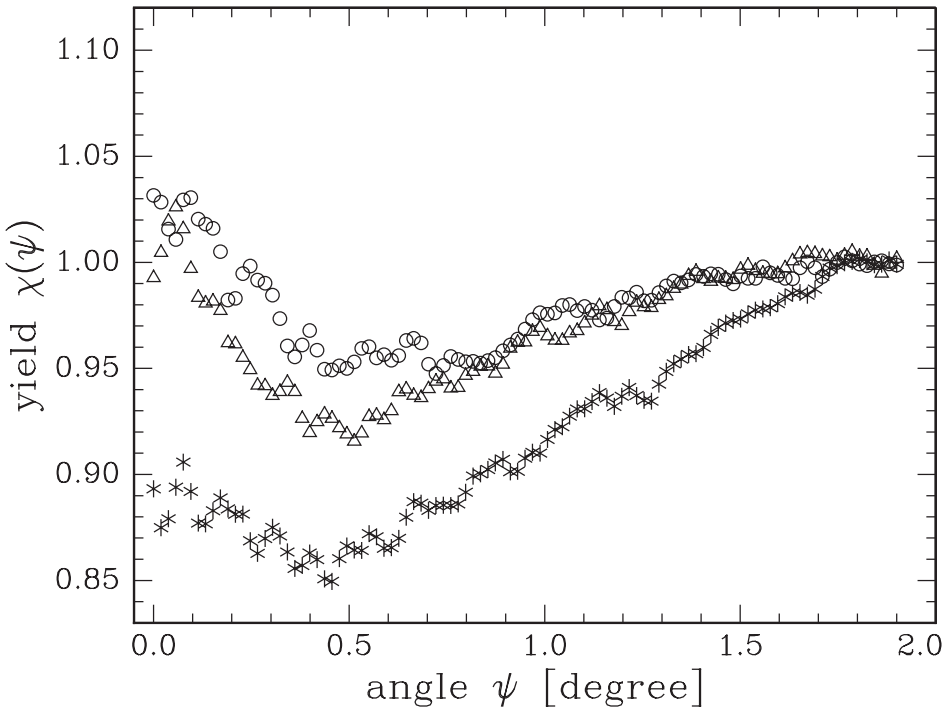

Figure 3.14: Axial angular distribution of Ni (circle), Cu (triangles), and Zn (stars) ions after transmission of a 1.0 μm thin Ni(001) crystal at the same exit energy around 40 MeV. Whereas the flux of best channeled Zn ions with low exit angles is clearly reduced, best channeled Ni and Cu ions are enhanced.

Ni crystals also show a transition behavior from cooling to heating, when the ion energies are decreased. The transition velocities (in atomic units) read for the $\langle 100 \rangle$ axis as follows: 7.50 ± 0.15 for Br, 7.98 ± 0.14 for Y, and 8.65 ± 0.18 for I ions, thus being significantly larger than the corresponding values in case of the Si-$\langle 100 \rangle$ axis.
Due to the puzzling finding of the disappearance of a transition behavior in case of Si crystals, the Ni crystals were also studied in order to find the nuclear charge below which there may be no heating any more. Fig. 3.14 shows $\langle 100 \rangle$-axial angular distributions of Ni, Cu, and Zn ions with the same exit energy of about 40 MeV. At first sight one may think that all such ions show a transition behavior, whereby Ni and Cu ions seem to just undergo the transition, while Zn ions already show a clear heating case. It is obvious that in all three cases the corresponding volume measures V, Eqn. (3.6), are negative, indicating heating. However, while indeed Zn ions show a clear heating case, and thus a transition behavior like in the case of the Si-$\langle 100 \rangle$ axis, the axial angular distributions of the Ni and Cu ions remain qualitatively the same as shown in the above figure. This means, that at even lower energies they show a small flux enhancement at small angles, but a large "depletion zone" at intermediate angles, extending beyond the critical angle and causing a negative volume measure. In other words, ions lighter than Zn ions, that is, ions with $Z_1 < 29$, seem to get "stuck" in an intermediate stage

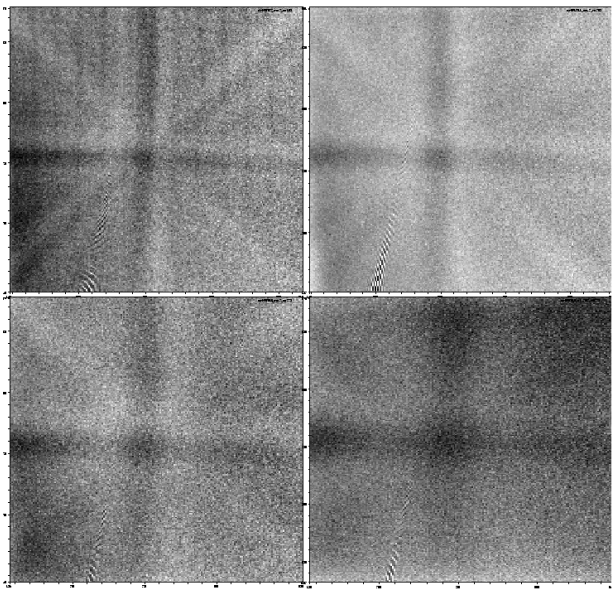

Figure 3.15: Flux distributions of Br ions after transmission of a 1.0 μm thin Pt(001) crystal at four different exit energies: 96 MeV (top left), 58 MeV (top right), 42 MeV (bottom left), and 27 MeV (bottom right). For all energies there is a qualitatively unchanged pattern of strong flux enhancement embedded in a depletion zone. The widths of the flux enhanced regions scale with the critical angles, which are 0.83°, 1.06°, 1.25°, and 1.56°, respectively. The shown angular windows are about 4° in both direction.

of a transition from a pure cooling pattern towards a pure heating pattern which they do not really reach. In this sense there is a difference in the transition behavior found with Ni crystals as compared to Si crystals. Here the "disappearance" of the transition is rather a disappearance of pure heating patterns, whereby a pure heating angular distribution is defined by a flux reduction at any channeling exit angle. While best channeled Zn ions with very small exit angles can show a strong flux reduction, the corresponding best channeled Ni or Cu ions show a flux enhancement only. It is again remarkable that neighbors in the Periodic Table can exhibit such a different behavior.

A further type of "transition" behavior was found with Pt crystals as compared to the Ni and Si cases. Fig. 3.15 shows the flux distribution of Br ions at four different energies after transmission along the Pt-$\langle 100 \rangle$ axis. There is no qualitative change any more in the flux distributions, no matter at which energy there were measured. Strong flux enhancements are always embedded in "depletion zones", whereby the corresponding volume measures as defined in Eqn. (3.6) are all close to zero, if ψ_{max} is set to the critical angle ψ_1. This means that there is a flux redistribution for channeled ions only, with the depletion zone just compensating the enhancement of best channeled ions and leaking out beyond the critical angle due to diffusion. This was confirmed by the finding that the widths of the enhancement regions scale with the critical angles.

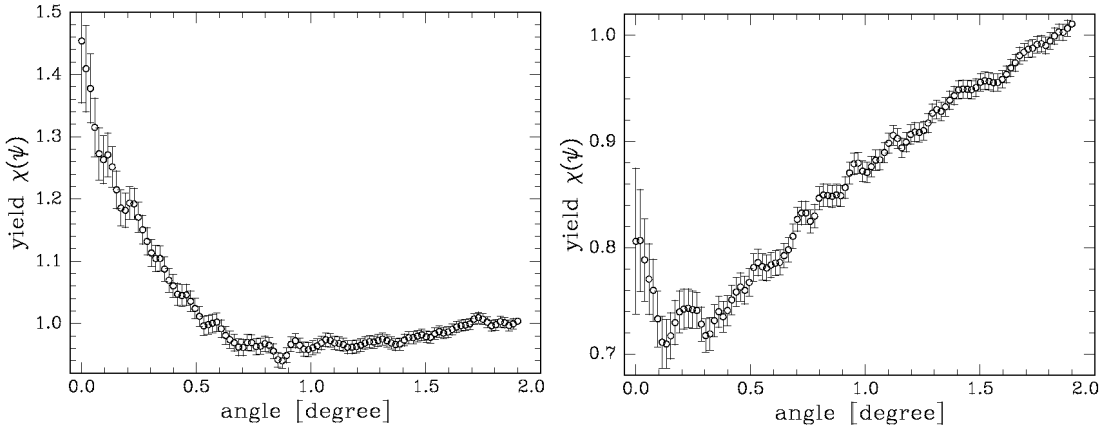

Figure 3.16: Axial angular distributions of 100 MeV Ag ions with the same exit energy around 68 MeV after transmission of 1.0 μm thin Ni(001) crystal (left) and Pt(001) crystal (right). Despite the same energy the two cases are clearly distinguished by strong flux enhancement of channeled ions with a depletion zone in case of Pt and a pure heating pattern for the Ni case. The critical angles are 1.18° and 0.71°, respectively.

In order to point out the qualitative difference between pure heating in Ni crystals and the unchanging Pt patterns, Fig. 3.16 shows $\langle 100 \rangle$ axial angular distributions of Ag ions transmitted once through a Ni crystal and the other time through a Pt crystal at the same low "heating-velocity". It is concluded that the behavior of cooling and heating depends not only on the state of the ion itself, such as energy or charge state (which is about equal at the same ion energy [25]), but also strongly on the ion-crystal combination.

The same result of qualitatively unchanging flux distributions with strong flux enhancements embedded in depletion zones were also observed with Ni, Br, Y, Ag, I, Au, Pb, and even Th ions. Even for the two heaviest ions, Pb and Th, no pure heating patterns were observed, whereby the lowest ion energy was 320 MeV for Pb ions (measured at GANIL accelerator), while their Si-$\langle 100 \rangle$ transition energy is 500 MeV, and 122 MeV for Th recoils (for that case Au ions produced recoils from a thin Th scattering foil).

Summing up, the behavior in respect to transitions from cooling to heating are quite different in Si, Ni, and Pt crystals. While there are clear transitions from pure cooling to pure heating patterns in case of the Si crystals, as long as $Z_1 \geq 22$, and only cooling patterns with $V > 0$ for lighter ions, clear transitions were observed in Ni crystals for all ions with $Z_1 \geq 30$, but intermediate patterns with $V < 0$ for all lighter ions, whereas in case of Pt crystals there are energy invariant qualitatively unchanging patterns of strong flux enhancements embedded in depletion zones restricted to channeled ions only.

3.2 Charge State Measurements

Since the transition from cooling to heating was only observed for dressed ions and since cooling disappears for fully stripped ions, it seemed very important to study the charge states of channeled vs. non-channeled ions, both for cooling and heating ion energies. Furthermore, the first model for describing the effect of cooling and heating was a charge exchange model based upon different impact parameter dependencies for electron capture and loss. This will be described in more details in section 4.2 below. According to this model, for cooling the mean channeling charge states should be higher than along random directions, implying that electron capture happens mostly when the ion is close to the strings. Thus the ion approaches strings with a higher charge state, but leaves them after electron capture with a lower charge state. Since the potential part of the transverse energy depends on the ion charge state, such a cycle of electron capture and loss means an irreversible change of transverse energy, thus cooling [3]. In case of heating, the situation of channeling vs. random charge states was supposedly reversed.
Differences between channeling and random charge states have indeed been found by other groups, but the aim here was to study these differences in dependence on different ion energies corresponding to cooling and heating regimes for one and the same ion species. These earlier measurements found out that the channeling charge states of 40 MeV I ions along the Au-$\langle 100 \rangle$ channel was lower by 2.5e than along random direction [27], while in case of O ions also channeled along Au-$\langle 100 \rangle$ direction their charge state was higher by 0.5e than in random direction [26]. A negative shift to lower channeling charge states was interpreted in such a way that the impact parameter dependence for electron capture is concluded to be less steep than for electron loss, thus at large impact parameters electrons are rather captured than lost and a lower charge state appears [27]. In case of a positive shift to higher channeling charge states the conditions are supposedly reversed. These conclusions are in accordance to the first charge exchange model as mentioned above. In the beginning of cooling and heating experiments the experimental picture was quite simple, where light ions were only cooled and heavy ions only heated. This first finding was in correspondence with the experiments about the shifts in the charge states of channeled vs. non-channeled ions, as light ions show a positive shift, while heavy ions show a negative shift. However, in the meanwhile the transition from cooling to heating was discovered, and this raised the question about whether or not the shifts in the charge states would be generally linked to the appearance of cooling or heating, that is, whether or not the shifts are reversed when cooling turns into heating.

3.2.1 Setup and Data Acquisition

For all measurements related to the charge state distributions we used the Q3D magnet spectrograph of the Munich Tandem accelerator lab [28]. Since the appearance of cooling and heating has already been determined by the experiments presented in the sections above, the aim of the measurements at the Q3D setup was solely to study the

impact parameter dependence of the ion charge states, at least the difference between channeling and random mean charge states. Therefore, not the isotropic ion flux was to be used as in the flux distribution measurements above, but a well collimated beam as typically done in all other channeling experiments. The area of the outermost ring in the accessible transverse planes of channeling directions (see section 2.1) are small enough when compared to the total accessible area, therefore in case of such collimated beams the majority of ions is well channeled with low transverse energy, and thus the mean charge states averaged over all measured ions correspond well enough to the charge states of well channeled ions. For comparison, the mean *random* charge states can be measured by tilting the crystal away from major axial and planar directions.
The basic setup is shown in the top part of Fig. 3.17. We have prepared a well collimated beam in transmission geometry with a divergence of about 0.01°, a beam spot size of about $100\mu m \times 100\mu m$, and a beam intensity of only a few thousand particles per second in order to prevent beam damage of the crystals and pile-ups in the detector system. The acceptance angle of the Q3D magnet spectrograph was in all cases at least three times larger than the corresponding critical angles for channeling, thus avoiding any selection effect. It would have been certainly more helpful to correlate exit charge states with their exit angle, but with the available system it was not possible to resolve the exit angles. In fact, the Q3D (one quadrupole, three dipoles) was run in a mode where ions with different exit angles, but same charge state and momentum were focused on one point in the focal plane [29]. Each point of the focal plane refers to a certain ratio of ion momentum over charge state with a dispersion of $\delta x/(\delta p/p) = 20\ cm/\%$. The position of the ions in the focal plane were measured with a position sensitive ionization chamber [30], yielding basically two signals, allowing to create a scatter plot as shown in the bottom part of Fig. 3.17: total ion energy E and position x in focal plane, whereby $x \sim \sqrt{E}/q$ for an ion with charge state q. The measured charge states q were directly associated with the exit charge states right behind the crystals, because alterations of the exit charge states due to charge exchange in the rest gas of the Q3D can be neglected [28] as well as Auger decays whose contribution to charge exchange per ion is less than 1 % [31].
The length of the focal plane detector and the magnetic rigidity of the Q3D determines an energy acceptance window of about $\Delta E/E = 10$ %. But since the widths of the exit ion energy distributions are of the order of 10-20 %, only a part of the energy distribution per charge state could be detected by one fixed value of the magnetic field in the Q3D. Therefore, in order to measure the entire energy distributions of a charge state distribution, the magnetic field had to be tuned through different fixed values and all resulting measured parts had to be put together for the entire spectrum [28]. Fig. 3.18 shows the energy spectrum of axially channeled and random ions for two different energies, corresponding to cooling and heating regime. A clear shift to lower values of the energy loss of channeled ions as compared with random ions is visible, which is 4.3 % for high and 12.8 % for low energy. Channeled ions lose less energy because of their reduced interaction strength with the crystal due to their confinement to larger impact parameters [12]. By this knowledge it is possible to align the crystal with an axis pointing into the beam direction. This means that one has to search for

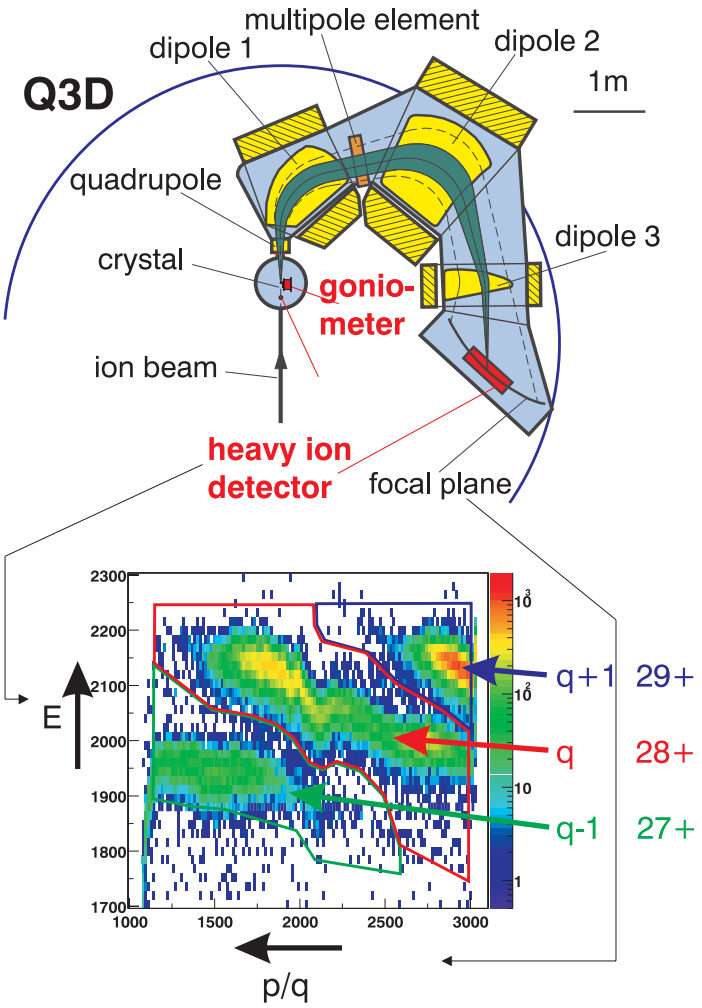

Figure 3.17: (Top): Basic scheme of the Q3D magnet spectrograph used for measuring charge state distributions of channeled vs. non-channeled ions. In order to normalize the distributions onto equal fluences, a PIN diode could be moved into the beam. The ions are deflected by the magnetic field of the detector due to their momentum p and charge state q, and are detected by a position sensitive ionization chamber, yielding two signals, as shown in the bottom part: ion energy E and position in focal plane, which scales with p/q. For each value of the magnetic field parts of three different charge states are visible, as indicated.

the alignment of the crystal by looking for the smallest energy loss, thus indicating best alignment along a channeling direction. The procedure of putting all measured parts into a whole, calibration measurements, and all further details about data processing can be found in reference [28].

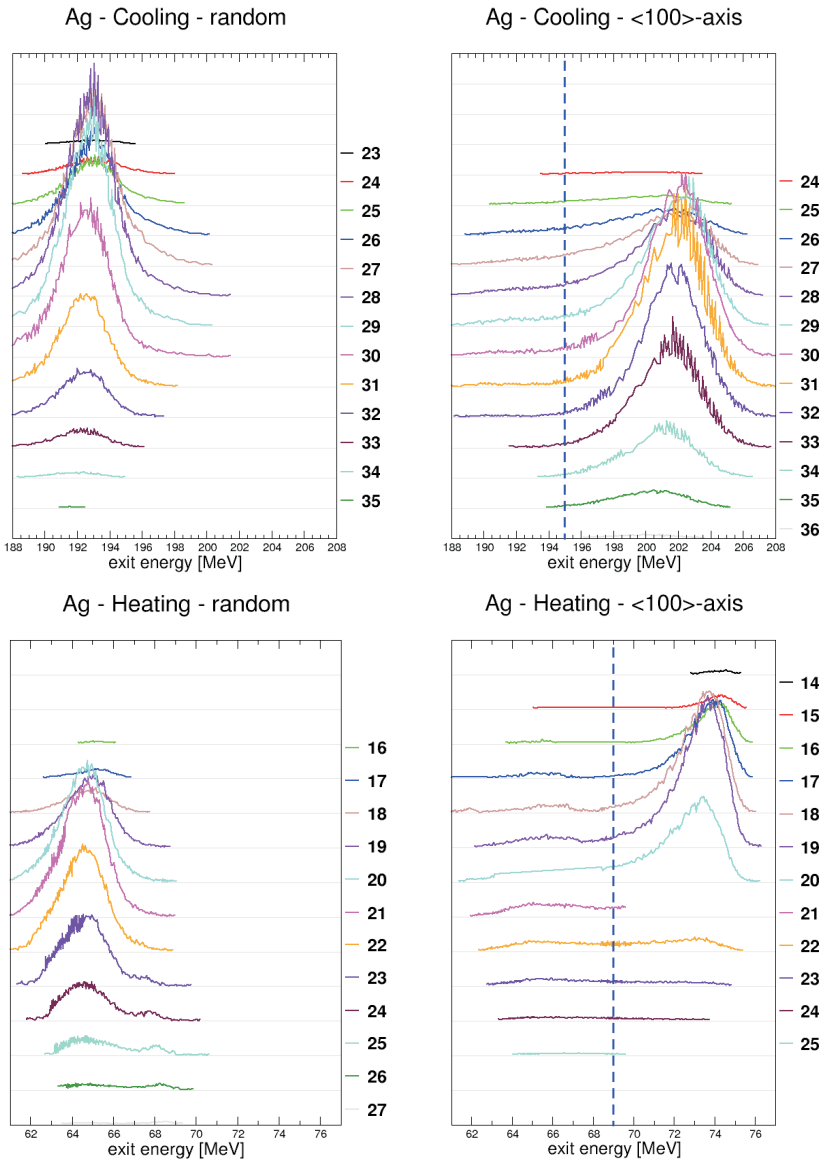

Figure 3.18: Exit energy distributions of 240 MeV Ag ions after transmission of a 3.0μm thin Si(001) crystal along $\langle 100 \rangle$ axial and random direction (top), and same distributions of 100 MeV Ag ions (below). A clear difference in axial energy loss as compared to the corresponding random energy loss is seen. The colors indicate different charge states, showing that at high (low) energy the mean channeling charge states are higher (lower) than in random direction. Detailed numbers are given in Tab. 3.2.

3.2.2 Results

First the results in respect to shifts in the charge state distributions are given for all three used crystals. The last section then deals with an experiment in which the Pt crystal was tilted steadily away from best alignment to random orientation in order

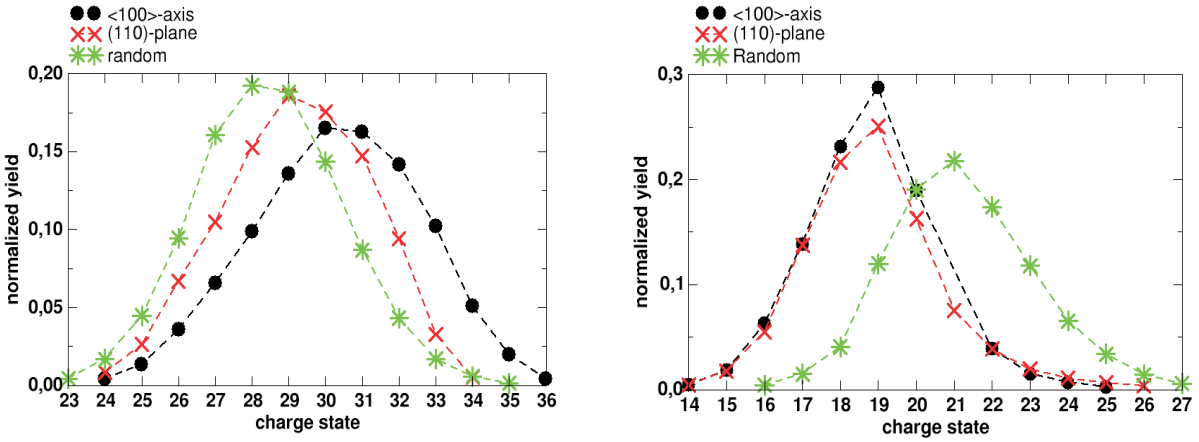

Figure 3.19: Axial and planar charge state distributions of 240 MeV Ag ions (left) and 100 MeV Ag ions (right) after transmission of a 3.0 μm thin Si(001) crystal. At high energy, channeling charge states are shifted towards higher values when compared with random charge states, but shifted to lower values at low energy.

to probe the accessible impact parameter regions. Two energy regimes according to cooling and heating were tested, namely the "low" energy case of 100 MeV Ag ions and the "high" energy cases with 240 MeV Ag ions, or 220 MeV Ag ions, respectively. In Si and Ni crystals 100 MeV Ag ions are heated, while Ag ions above 160 MeV are cooled, see sections 3.1.2.2 and 3.1.2.7. In contrast, 100 MeV Ag ions do not show heating in case of Pt crystals, but a strong flux enhancement of best channeled ions, see Fig. 3.16, which is also seen at high energies. Therefore, if there should be a general correlation between channeling charge state shifts and the appearance of flux enhancement/flux reduction, the charge state distributions should show different shifts in case of Si and Ni crystals, corresponding to the observation of energy dependent cooling or heating, but no change in the charge state distribution was expected in the Pt case [32].

3.2.2.1 Si, Ni, and Pt Crystals

The charge state distributions of 240 MeV and 100 MeV Ag ions transmitted through Si crystals are presented in Fig. 3.19.

At high energy, both the planar and axial channeling charge state distributions are shifted to higher values compared to the random case, while at low energy these shifts are reversed. This finding is in agreement with the prediction of the estimates of the first charge exchange model. However, Fig. 3.20 shows a clear discrepancy between expectation and experiment, because despite different behavior in respect to cooling/heating, the charge state distributions in case of Ni crystal (heating) and Pt crystal (cooling, at least strong flux enhancement of best channeled ions) are qualitatively the same as both show a negative shift of channeling charge states. Tab. 3.2

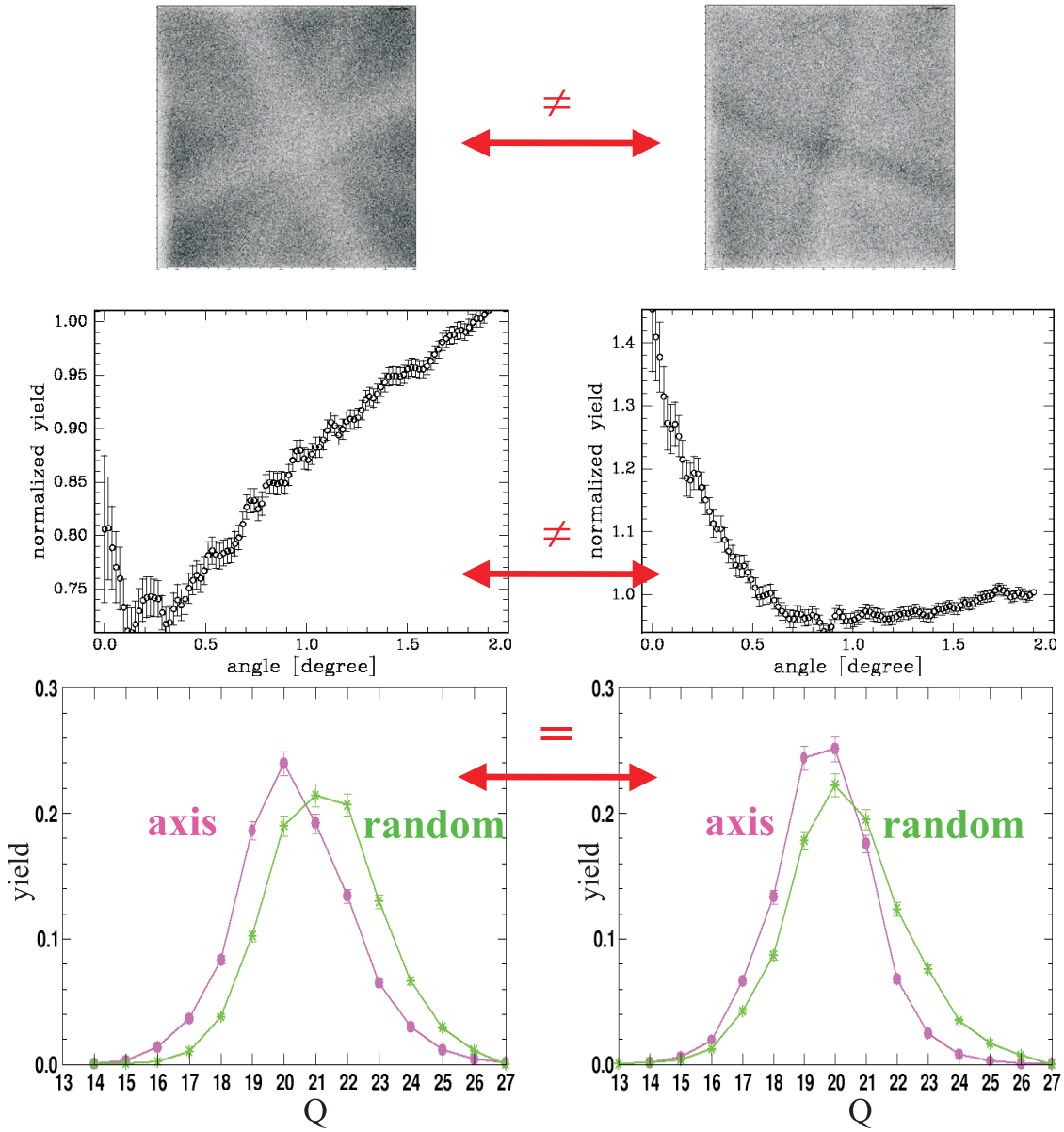

Figure 3.20: Flux, corresponding axial angular and charge state distributions for the case of 100 MeV Ag ions transmitted through 1.0 μm thin Ni(001) (left column) and equally thin Pt(001) crystal (right column). The Ni case is a pure heating case, while Pt shows a strong flux enhancement of ions with low exit angles. Despite clearly different cooling/heating behavior, the charge state distributions are qualitatively the same, that is, a shift of the axial channeling charge states to smaller values than for random direction.

summarizes all measurements and gives the observed shifts in mean channeling charge states as compared to the corresponding random values.

The result is a unique correlation between the sign of the channeling charge state

Ion	v [a.u.]	Crystal	Q_{random}	ΔQ_{axis}	ΔQ_{plane}	regime
100 MeV Ag	6.15	Si	21.04 ± 0.03	-2.25 ± 0.06	-2.35 ± 0.06	heating
240 MeV Ag	9.52	Si	24.09 ± 0.03	$+2.02 \pm 0.06$	$+0.90 \pm 0.06$	cooling
100 MeV Ag	6.15	Pt	20.40 ± 0.05	-0.79 ± 0.06	-0.34 ± 0.06	cooling
220 MeV Ag	9.12	Pt	25.98 ± 0.03	$+0.80 \pm 0.06$	$+0.26 \pm 0.06$	cooling
100 MeV Ag	6.15	Ni	21.20 ± 0.05	-0.73 ± 0.06	-0.45 ± 0.06	heating

Table 3.2: Shifts in mean channeling charge states, $\Delta Q_{channel} = Q_{channel} - Q_{random}$, as compared to corresponding random values for axial and planar directions. These shifts are positive (negative) at high (low) velocity.

shifts and the ion *velocity*, but not with the appearance of cooling and heating due to the Pt case at low velocity. Thus, in order to study this latter case in more details, a tilting experiment was performed, as described in the following.

3.2.2.2 Tilting of Pt crystal

The above findings in case of the Pt crystal raised the question of whether the conditions for cooling and heating may be different in different impact parameter regions. Ions exiting the crystal with relatively large exit angles will have probed also smaller impact parameters, while ions with very low exit angles were only confined to large impact parameters. But since exit angles were not resolvable with the available setup, an increase of the transverse energy, and thus an increase of the accessible impact parameter region, averaged over all channeled ions, could be reached by tilting the crystal from best to random alignment. Fig. 3.21 shows the result of mean axial channeling charge states plotted against the tilting angle, where all mean channeling charge states remain below the value of random ions. It is thus concluded that this result does not give evidence for different cooling/heating conditions in different impact parameter regions.

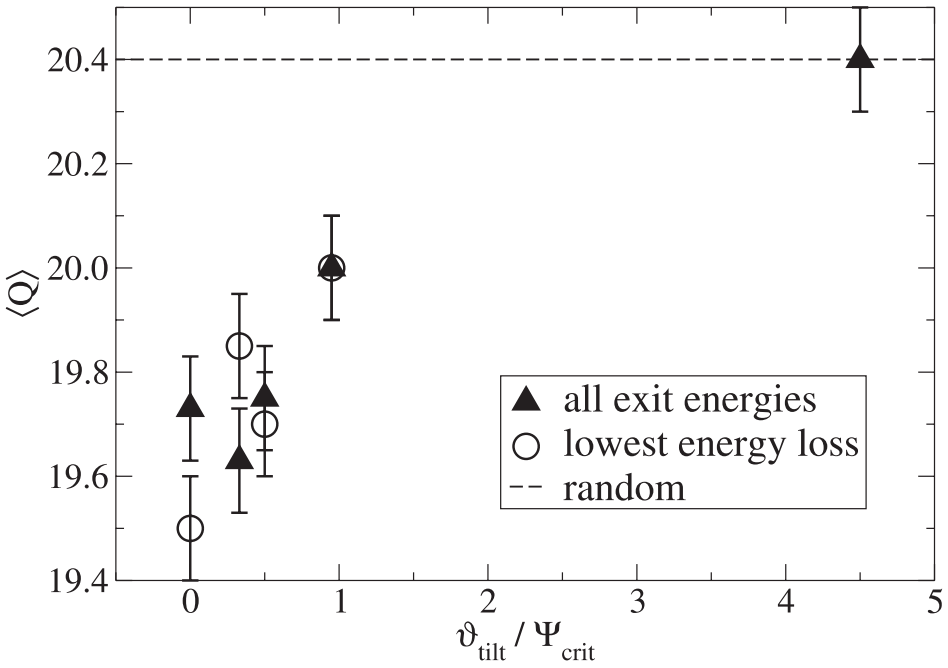

Figure 3.21: Tilting of Pt(001) crystal with 100 MeV Ag ions: mean axial channeling charge states plotted against the tilting angle in units of the critical angle, once averaged over all ions (all exit energies), and once only for channeled ions (lowest energy loss). The horizontal line refers to the random value. It is seen that independently from tilting all charge states stay below the random value.

Chapter 4

Theory

The experimental findings clearly point to a violation of the rule of reversibility. Thus, in order to find an explanation for this effect, an extension of the standard channeling theory is necessary. This means that some additional mechanism must be found which is responsible for the unpredicted phenomenon. Computer simulations, such as CRYSTAL-TRIM [7], that entail any process considered by the standard channeling theory, are not able to reproduce cooling or heating [15, 3]. It is thus concluded that the mechanism in question must be a process which is not included in these simulations. Up to now channeling is described by time-independent transverse potentials $U(r)$ (see section 2.1). It is clear that the rule of reversibility is violated by the presence of any time dependence. Therefore, one must find a mechanism which transforms $U(r)$ into a time-dependent form $U(r,t)$. Such a time dependence breaks the conservation of the transverse energy and can thus possibly lead to cooling or heating. In the next section it is shown that a violation of the rule of reversibility due to energy loss cannot be as strong as the observed redistributions. Furthermore, since experiments with fully stripped ions showed no flux redistributions despite significant energy loss, the rule of reversibility is fulfilled in this case. This has raised the idea that cooling/heating has something to do with charge exchange, which was not included in the early simulations. The transverse potential guiding the ion along channeling directions depends on the charge state of the ion. It is commonly known that the charge state of an ion traversing matter fluctuates around an equilibrium charge state due to electron capture and loss events. In contrast, if the equilibrium charge state of an ion is its nuclear charge, then this fully stripped ion does not experience any electron capture, or, at most only a negligible number of such events, respectively. If the charge state of the ion is not just a function of its impact parameter, but depending on time, then the transverse potential must have the form $U(r,t)$, expressing a time asymmetry. Since channeling is an oscillatory behavior, the term time asymmetry is meant here as an asymmetry between the ion's approaching a crystal string or plane and leaving it.
It is, therefore, conceivable that if an ion runs through an irreversible cycle of charge exchanges, this may finally lead to an irreversible change of its transverse energy, whose potential part strongly depends on the charge state. The first model that was devel-

oped utilizes different impact parameter dependencies for electron capture and loss [3]. This analytical model will be shortly discussed in a subsequent section, because it was the starting point of further theoretical approaches.
So far no working alternatives to charge exchange as the underlying mechanism of cooling and heating were found. Despite shortcomings of the first charge exchange model, charge exchange seems to be sufficient for explaining the experimental results, being confirmed by the own development of intensive computer simulations, which are presented below. A possible alternative to charge *exchange* could be a time-dependent so-called dynamical *screening* of the ion's charge state. Such a screening can occur by momentary continuum scattering states of target electrons. Thus, if the screening of the ion's charge is different between approaching and leaving a string of crystal atoms, then an irreversible change of transverse energy may arise. However, this possibility seems to be ruled out by the experimental finding that fully stripped ions do not show the effect of cooling/heating, despite the possibility that their charge states could still be strongly dynamically screened by the *target* electrons. Another critical point about this alternative is the fast response of the target electrons, which can be estimated by the plasma frequency to be in the range of 10^{-16}s. Such a time scale is relatively short in comparison to the time period of a half-oscillation in the order of about 10^{-15}s. That is, even though the target response is too slow in order to completely neutralize the passing ion, it is on the other hand fast enough for preventing long-range time asymmetries. Besides, there cannot be any asymmetry expected in the behavior of the target electrons, thus the dynamical screening should be the same during approaching and leaving a string. In contrast, if the *ion* is considered as the source for asymmetry, one does not encounter the same problem as with the target electrons. The ion charge state depends on past capture and loss events, and could indeed exhibit an asymmetry in respect to approaching vs. leaving a string, if there is a "memory" effect present: the ion's charge state is determined by past charge exchange events, but not by future ones. From this follows that it is most likely the state of the *ion* which may provide an effective time asymmetry leading to the violation of reversibility. Besides the ion's *charge* state it could also be its *excitation* state for playing a certain role, because the ion-crystal potential is also changed if the screening of the ion's nuclear charge by its bound electrons is altered due to excitation (excited electrons screen the nuclear charge less because of their greater binding radius). However, since in case of multiple charge exchange the state of excitation is determined by charge exchange itself, it is therefore reasonable to focus on charge exchange first. Therefore, this is the main topic in the theoretical approach towards an understanding of cooling and heating.

4.1 Weak Violation of Reversibility due to Energy Loss

The derivation of the rule of reversibility was based upon a time-independent situation, because any energy loss violates the basic symmetry of the scattering function in Eqn. (2.18), as will be discussed now. This means that the rule is actually only applicable when energy loss is negligible, which is by no means the case in the experiments, because there energy losses up to 30 % occurred due to the thickness of the crystals. Thus, the question arises whether the rule of reversibility is violated in the appearance of cooling and heating just because of the energy loss involved in the measurements. Therefore, it is necessary to estimate the degree of the violation due to inelastic scattering, which occurs by target excitation and ionization.
The fundamental result as stated by the rule of reversibility is a detailed balance, that is, the transition from any transverse energy $E_\perp$ to any other transverse energy $E'_\perp$ has the same probability as the reversed transition, but weighted by the accessible areas of each transverse energy. This symmetry is broken if inelastic scattering takes place. The reason is that all scattering events in channeling are pure Coulomb scattering, obeying the law of Rutherford, or scattering on a screened Coulomb potential, respectively. It is well known that the cross section for Coulomb scattering decreases when the ion energy is increased. Furthermore, measurements of other groups [12] as well as from our group have demonstrated that the energy loss due to inelastic scattering is decreased for channeled ions. The reason lies in the fact that channeled ions undergo less or weaker interactions with the crystal atoms than random ions, because the first are confined to larger impact parameters.
Due to the difference in the suffered energy loss channeled ions traverse a crystal with a higher energy than random ions. Therefore, according to the Rutherford cross section channeled ions are less likely to be scattered to larger transverse energy. Thus, the symmetry in the transitions above is broken due to energy loss. The upper limit of the degree to which it is broken can be estimated by the difference in Rutherford scattering cross section of channeled vs. random ions. Measurements of our group in cooling and heating regimes showed that the energy of channeled ions is by the order of about 10 % larger than the energy of random ions [32], see also Fig. 3.18. Hence, the cross section of channeled ions to be scattered to larger transverse energies cannot be larger than these 10 % when compared to the reversed scattering form larger transverse energy to best channeled ions. Since this amount is the upper limit that one can possibly expect, it is made clear that the violation of the rule of reversibility due to inelastic scattering cannot be stronger than about 10 %. However, most observed angular flux redistributions are much stronger, even as strong as 400-500 % (see Fig. 2.3), and, therefore, the violation of reversibility due to energy loss is called a "*weak* violation", whereas the observations of cooling and heating are called "*strong* violation".
The estimate given above points to the fact that the observed violation of the rule of reversibility must have another origin than mere inelastic scattering. Hence, in order to achieve a strong violation of reversibility a new mechanism within the ion-crystal

interaction has to be found, which is not yet entailed in the standard channeling theory so far. Charge exchange is such a mechanism and is discussed in detail in the next section.
It must be noted here that also the finding of the disappearance of cooling for fully stripped ions points rather to charge exchange than to violations due to energy loss. Channeled protons, for instance, suffer about half of the energy loss as compared to protons in random directions [12], but yet their cooling strength disappears when their mean charge states go over into their nuclear charge. The same was seen for all other tested ions, see. Tab. 3.1. Thus, from the simple estimates above about Rutherford scattering one would even expect a flux redistribution in case of fully stripped ions, which is in clear contradiction to the experiment. It is thus concluded that violations of reversibility only by energy loss can indeed be regarded as very "weak", that is, even weaker than the difference in energy loss of channeled vs. non-channeled ions.

4.2 Charge Exchange

All experiments performed for cooling and heating with heavy ions around the maximum of the stopping power at about 1 MeV/nucleon cannot be described by perturbation theory. The strength of the ion-crystal interaction is so large that the target electron system is ionized to a large degree, thus ultimately altering the ion-crystal potential. The majority of undertaken measurements for cooling and heating occurred in exactly this region of strong perturbation. In the literature one can only find theories that are applicable either at very high energy or for light ions only, where perturbative treatments are valid. Especially the capture process is difficult to describe due to its requirement of involving three particles for momentum and energy conservation. Solutions to the non-perturbative three-body problem cannot be explicitly given. This difficult situation is also reflected by the fact that all up to date theories for energy loss of heavy ions in solids do not explicitly treat charge exchange, despite the fact that the ion charge is the source for the ion-solid interaction leading to energy loss [24]. Instead all such theories must take the corresponding charge states either from estimates or from measured values. There are a few perturbative capture theories, such as Oppenheimer-Brinkman-Kramer [33], the so-called Strong Potential Born Approximation (SPBA) [34], or even a computer code named ETACHA, which uses perturbative capture cross sections for hydrogen-like ions and just utilizes a scaling procedure for heavier ions [35]. However, all these theories cannot be applied to the many-body, strongly perturbed ion-atom interactions within a crystal, which requires furthermore *impact parameter dependent* electron capture and loss cross sections. Another consequence of the strength of the ion-solid interaction is multiple charge exchange, which leads to large projectile and target ionization and, thus, to non-stationary screening, and finally time-dependent projectile-target potentials. Thus, one cannot just simply scale the cross sections of the relevant processes from known values given for protons to the case of heavy ions.
Quantum mechanical approaches from first principles are practically impossible due

to the necessary treatment of a dynamical, time dependent many-body system with strong perturbations. Due to this lack of available theories in the experimentally studied ion and energy range, in this work a classical approach was chosen and significantly extended to the application for cooling and heating. Before getting into details in the next section, the very first model for charge exchange in context of cooling and heating [3] is shortly presented. This model was published by our group before the transition from cooling to heating was observed. This is one reason why this model can only be regarded as the very first theoretical approach in rather qualitative terms. Therefore, no details on the quantitative sides are given, as it turned out later that they are in severe contradiction to the transition of cooling to heating (for instance, from its scaling one would expect cooling at low and heating at high energy, in contrast to the experimental findings). But the merit of this first model is to give qualitative insights into the possible mechanism of charge exchange as the source for violation of reversibility.

The basic idea was that the impact parameter dependence is different for electron capture as compared to electron loss. There are two strong arguments supporting this starting point. On one side, experiments that showed different charge state distributions of channeled vs. non-channeled ions clearly point to such a difference [26, 27, 32]. On the other side, electron capture and loss are not each other's time reversal as they depend on different mechanisms: *bound* electrons are captured, but lost to the *continuum*; furthermore, continuum electrons can only be captured by emission of a photon (the so-called radiative electron capture, REC), or by excitation or ionization of a bound projectile electron (the so-called dielectronic recombination, DR). Therefore, it is quite conceivable that capture and loss have a different dependence on the impact parameter. In the original model this difference was estimated by simple approximations of the mean capture and loss radius. The mean capture radius was determined from the distance between ion and electron where the Coulomb force from the ion equals the atomic binding force. This gives the so-called "release" radius R. The second relevant radius R' is determined by the distance below which the released electron is bound in the ion potential. Since both conditions must be fulfilled for electron capture, the actual capture radius R_c is the smaller one of the two, $R_c = min(R, R')$. The mean loss radius was determined from Thomson cross section for the energy transfer from an ion to an electron at rest. If the transferred energy exceeds the binding energy of a projectile electron, this electron is lost, and from the Thomson estimate one gets the mean loss radius R_l. It is quite clear that both estimates R_c and R_l are too crude for the present situation of many-electron ions around the maximum of the stopping power, indicating the situation of strong ion-crystal interactions. However, in the following the qualitative aspects are presented as an introduction of reversibility violation due to charge exchange.

Fig. 4.1 shows the basic principle of a cycle of electron capture and loss leading to an irreversible change of transverse energy. The ions are described as point charges and it is supposed that the transverse potential $U(r)$ depends linearly on the ion charge state Q, thus $U(r) = Q \cdot U_p(r)$, where $U_p(r)$ is the transverse potential of a proton. If the ion captures an electron at a distance r_c, its new charge state is $Q - 1$, thus it loses

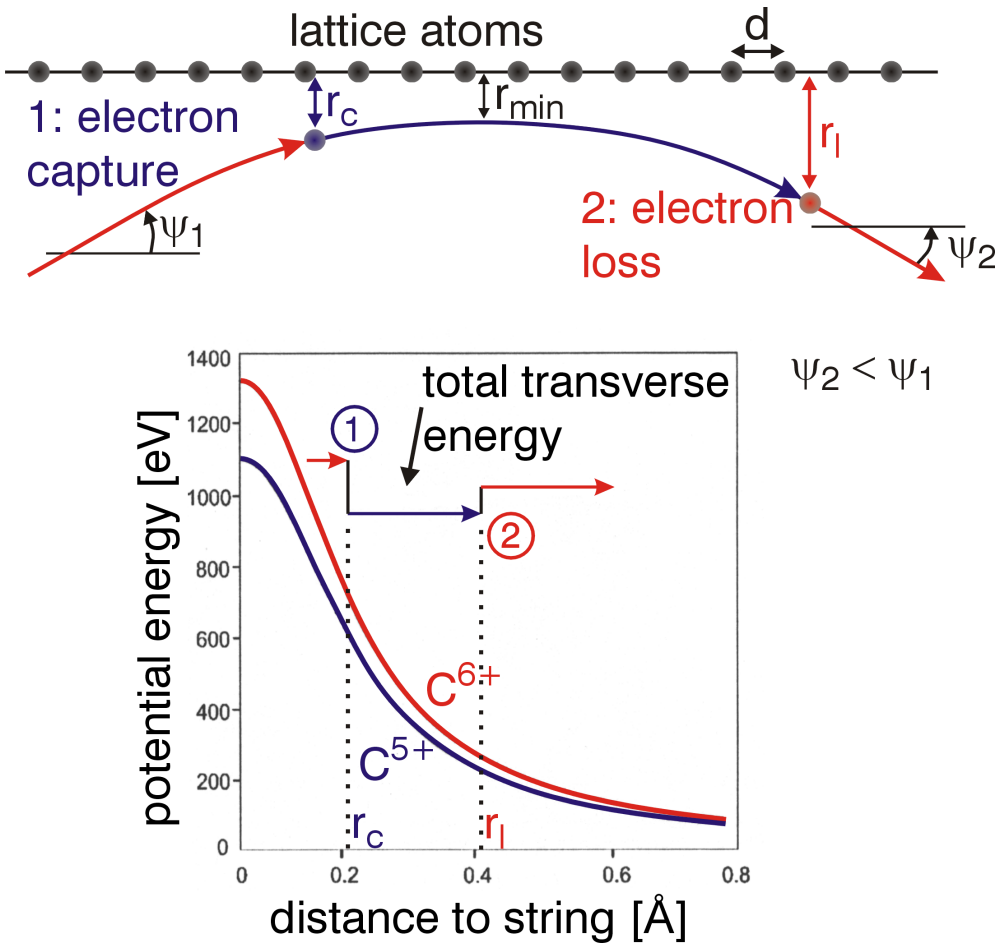

Figure 4.1: Basic principle of one cycle of charge exchange leading to an irreversible loss of transverse energy, hence cooling. If the initially bare C^{6+} ion captures an electron at distance r_c from the string, then its potential energy is reduced due to its correspondingly lowered charge state C^{5+}. It gains transverse energy by losing this electron at a distance r_l. As can be seen from the potential curves below, this regain of transverse energy is smaller then the previous loss, thus, in total, the transverse energy of the ion is reduced. The reversed condition $r_c > r_l$ would then lead to an increase of transverse energy, hence heating, because the charge exchange cycle would be run through in the opposite direction.

some transverse energy. If subsequently the ion loses this electron at a distance r_l, it regains transverse energy. However, as can be seen by the transverse potential curves, the later regain is smaller than the former loss of transverse energy, hence, in total transverse energy is lost. If the mean capture radius $\langle r_c \rangle$ is on the average smaller than the mean loss radius $\langle r_l \rangle$, the ion runs through the charge exchange cycle as shown in the figure. Thus, under this condition of $\langle r_c \rangle < \langle r_l \rangle$ the ion's transverse energy is reduced. And since capture and loss are irreversible processes, because they are not each

other's time reversal, this loss of transverse energy is irreversible. This immediately leads to a violation of the rule of reversibility, Eqn. (2.20), because transitions from larger to smaller transverse energies are enhanced. If, on the opposite, the condition of the mean radii is reversed, that is, $\langle r_c \rangle > \langle r_l \rangle$, then a net gain of transverse energy appears, thus again a violation of reversibility. In the first case cooling is expected due to the enrichment of states with less transverse energy, and in the latter case heating occurs, respectively.
It is quite essential here to note that such charge exchange cycles are effective for cooling/heating only, if the number of charge exchanges is so small that no local charge state equilibrium can be reached. Otherwise the transverse potential would not exhibit a time dependence, but just depend on r, thus having only $U = U(r)$, because $Q = Q(r)$. But if there is no local charge state equilibrium $Q(r)$, then one has a time-dependent potential, namely $U(r, t)$, which is necessary for breaking reversibility.
The merit of this simple charge exchange model lies in the offer for an explanation of heating. While cooling could have been expected in terms of a weak violation of reversibility due to energy loss, heating is definitely not to be explained in such terms. As mentioned above, this model was published before the discovery of the fact that the appearance of cooling and heating is mainly a question of the ion energy and not of the ion nuclear charge. The experiments present at the time of the publication of this simple model could indeed be qualitatively explained by the two relations about the mean capture and loss radii with their estimates as described above. However, with more experimental data at hand it was soon clear that the quantitative part of the model failed completely in describing cooling and heating. The most prominent example for this failure is the experimentally found fast transition from cooling to heating within a relative velocity change of only about 15%. The velocity scaling of the estimated capture and loss radii R_c and R_l could never reproduce such a rapid transition. Even worse, according to their scaling, cooling would have been expected at low and heating at high energies, in contrast to the experiments. But the qualitative aspect, that is, the irreversible change of transverse energy by charge exchange, remained as the basic source for a violation of the rule of reversibility. In the following section a much more quantitative and successful method is discussed in detail.

4.3 Classical Trajectory Monte-Carlo: CTMC Simulation

Due to the lack of suitable theories of impact parameter dependent charge exchange in the case of swift heavy ions in solids, an own approach was undertaken that is based upon a classical procedure. About 40 years ago the so-called Classical Trajectory Monte-Carlo (CTMC) method was developed [9]. The original work was mostly aimed at describing ionization cross sections of light ions in gases. Taking into account the available computer power back then it is not surprising that many CTMC simulations could only treat one active electron moving in an effective atomic potential,

thus implicitly entailing screening effects by the other electrons that were not explicitly calculated. A further extension to heavy ions with many active electrons was called "n-body CTMC" (nCTMC) [10]. All CTMC methods treat the system under consideration as a classical many-body system, in which the trajectory of each particle is calculated according to classical physics. Only the possible initial conditions are taken from quantum mechanics. The basic assumption underlying this method is the validity of classical mechanics for the energy region in which the systems are studied. There is a rather simple argument derived by Lindhard [1] giving an estimate of the valid energy region for a description on a classical basis. The basic condition is that the distance of closest approach p of two collision partners must be significantly larger than the de-Broglie wavelengths λ of the particles, that is, $p \gg \lambda$. From this condition follows the validity for applying classical physics if (in atomic units) $p/\lambda = (2Z_1Z_2/v) \gg 1$. Therefore, in case of swift heavy ions around the maximum of the sopping power at 1 MeV/nucleon ($v \approx 6 - 7$) the classical approach is valid. Thus, it is sufficient to calculate a large statistical ensemble according to the allowed initial conditions and to deduce the classical mean values, assuming that they are close to the ones from a full quantum mechanical approach. Of course, despite Lindhard's estimate of the valid region for classical descriptions, there are effects originating from the nature of quantum mechanics which are not entailed in any classical description. Among them there are: suppression of small energy transfers below the smallest possible excitation/ionization energy in quantum mechanical systems, electron promotion due to the Pauli exclusion principle, radiative deexcitation (a bound electron jumps onto a lower lying state by emitting a photon), radiative electron capture (a free electron is captured by the simultaneous emission of a photon for conserving momentum and energy), or tunneling effects (electron is captured by tunneling through the potential barrier between atom and ion). However, there are good reasons why these restrictions are expected to only play a minor role, as explained in the following.

Quantum mechanical suppression of small energy transfers can be neglected, because they are dominant only at impact parameters that are much larger than the ones used in the channeling simulations described in the next section. In that sense only inelastic ion-atom collisions are considered. Another typical quantum mechanical feature is electron promotion, which takes place, when an ion or atom approaches another atom in a way that, for instance, all four K electrons of both nuclei would be distributed on the 1s level of the "compound" nucleus, or molecule. Since such a setting is prohibited by the Pauli exclusion the two K electrons of the lighter collision partner are brought to a higher level, thus this is called electron promotion. It is expected that such a promotion enhances the probability for target ionization, but also for electron capture, as it decreases the relevant impact parameter [36]. However, this promotion is expected at collision velocities much smaller than the orbital velocity of the target electrons, in order for the electron system to adiabatically adjust to the new situation. Our experimental velocities were orders of magnitude larger.

Radiative deexcitation can be neglected due to the high collision frequency in a solid,

which is of the order of $10^{-17}s$. According to Bohr the estimated time for dipole transitions in hydrogenic ions reads [8]

$$\tau = 0.9 \cdot 10^{-10} \frac{n^5}{q^4} s, \tag{4.1}$$

where n is the quantum number of the outer most still occupied level and q is the charge state of the ion. Thus, typical transition times are of the order of $10^{-14} - 10^{-13}s$, which is clearly orders of magnitudes longer than the collision frequency.
Radiative electron capture (REC) is effective only at velocities that are significantly higher than the velocities in our experiments. This can be seen from measurements of REC cross sections [37] and capture cross sections at relatively large impact parameters compared with nCTMC simulations [10]. Thus, in all experiments here the dominant electron capture process is the so-called mechanical electron capture (MEC), where an electron is captured under conservation of energy and momentum due to (at least) a third collision partner. MEC is even effective at large channeling impact parameters due to the long range of the (possibly screened) Coulomb interaction. Another form of capture process is the so-called dielectronic recombination (DR), whereby an electron is captured by excitation or ionization of another bound projectile electron [38]. Such a process is entailed within a classical simulation as long as projectile electrons interact with each other, which is the case within the simulations as described in detail in section 4.4.2 below.
Electron capture by tunnelling is important only at those ion velocities that are smaller than or equal to the mean orbital velocities of the target electrons, and can thus also be neglected in the studied energy range [39].
Summing up, all deviations of classical approaches from the results of full quantum mechanical calculations are found to be important only at lower ion velocities when they come close to the orbital velocities.

The basic initial condition from which all CTMC methods start is a microcanonical distribution according to classical physics. However, in contrast to quantum mechanics, this classical distribution cannot fulfill both the correct momentum and the correct position distribution, but only one of them. Since the classical simulations developed in this work were aimed at channeling with its confinement to certain impact parameters, the priority here was set upon a correct position distribution, rather than a correct momentum distribution, of the target electrons. The corresponding method for initialization in this case is described in detail in the next section. Within any CTMC simulation, once the momentum and position ensembles, that each classical particle may take on, are chosen, the initial conditions for each run are selected with the help of random number generators. Thus, this Monte-Carlo method probes randomly the ensemble of all possible initial conditions.
For nCTMC, i.e. when using more than just one active electron, all electrons are put on orbits according to the microcanonical ensemble with an *effective* interaction charge $Z_b Z_i$ ($Z_i = -1$), whereby the screened nuclear charge Z_b is determined by the sequen-

tial ionization energies U_i of the i-th target electron with quantum number n_i [10], i.e.

$$Z_b Z_i = n_i \mid 2U_i \mid^{\frac{1}{2}} . \tag{4.2}$$

This procedure is quite essential for *all* classical treatments of atoms with many electrons, because a classical atom is instable by autoionization due to the intra-atomic electron-electron interaction, which must therefore be switched off. The presence of the other atomic bound electrons is just implicitly taken into account by the fact that the charge of the atomic nucleus as seen by the i-th electron is screened according to Eqn. (4.2). During the collision these effective screened charges should be continuously adjusted due to the ion induced perturbation on the atomic electron system. In the literature there exists one variant of CTMC with such a continuous, or "dynamical", adjustment, called "dCTMC" [40]. However, this CTMC version was only applied for He atoms with two active electrons ($n = 2$), whereby the effective screened charges are determined by the spatial distribution of the two electrons. It is, however, not published how to apply dCTMC for many electron systems, because dCTMC needs quantum mechanical wave functions, and these are unknown in many electron systems under great perturbations.

For calculating the temporal evolution of the many-body system with N particles there are basically two equivalent possibilities: either one applies the Newtonian or the Hamiltonian formalism. The Newtonian method is used in this work and discussed in more details below. The difference between both methods lies mostly in respect to the number and type of equations. For the Hamiltonian way, in three dimensions $6N$ coupled first order differential equations must be solved, while there are $3N$ linear plus $3N$ quadratic equations in case of the Newtonian method. Both methods suffer from numerical instabilities when calculated on computers. This problem is taken into account with a special correction as described in the next section. Eventually, the choice between Hamiltonian or Newtonian method is a rather subjective one, especially because the computation time is determined mostly by the numerical inaccuracy problems than the number and type of basic equations to be solved.

The main use of nCTMC in respect to the simulations developed for cooling and heating has to be seen in providing good agreements with measurements performed in about the ion energy and ion mass region that our experiments took place. However, nCTMC can only be applied for the *single* collision between an ion with one atom, thus the situation within a dilute gas. In contrast, for the detailed channeling simulations required for reproducing cooling and heating the condition within a solid must be taken into account. Due to the long range of the ion-atom interaction the ion's effective "interaction sphere" contains at each time *several* crystal atoms with which the ion simultaneously interacts. The extension to simulations of ions with *solids* is the main part of the theoretical approach done in this work, and is also discussed below.

A typical study where nCTMC was applied is the collision of 333 MeV U^{32+} ions with Ne gas atoms under the condition of single collisions [10]. The cited work shows remarkable agreements with measured momentum distributions of the ion and atomic recoil as well as of the ionized electrons. The most important result in context of cooling and heating is the collision dynamics, which significantly differs from a pure

Rutherford scattering due to time dependent screening effects induced on the target electron system by the ion. However, these studies did not look at impact parameter dependent probabilities for electron capture, but only total cross sections. Besides, these cross sections only refer to gases, and there may be a difference between gases and solids due to the interaction of the ion with effectively several atoms at each time, which was indeed found as discussed below.

4.4 nN-CTMC Simulation: Development and Results

The main purpose of the theoretical approach in this work is the extension of the successful nCTMC method, where the ion interacts with only one atom carrying n electrons, resembling the situation of dilute gases, to an "nN-CTMC" method with the ion *simultaneously* interacting with N atoms each carrying n electrons, thus being able to simulate the ion's interaction with a solid. The essential physical difference hereby is that in case of dilute gases the ion is always in ground state before the next collision, because the time scale for radiative deexcitation is much smaller than the collision frequency. In contrast, these time scales are reversed in case of solids, therefore the ions are highly excited therein. And because of the increased ionization cross section of highly excited ions in solids their charge state is higher than in gases [8]. Thus, a detailed simulation of ion channeling makes the extension from nCTMC to nN-CTMC necessary.
However, this extension is not just a multiplication of the number of target atoms, because additional concepts must be introduced. The main reason for this is the fact that within classical atoms atomic bound electrons must not interact with each other, else such an atom would instantly decay by autoionization. However, if this restriction of interaction partners would be kept throughout the simulation, one would totally neglect the possibility of electron impact ionization of electrons that have been captured from a target atom into the ion, as this ionization process occurs by the interaction of projectile electrons with target electrons. This electron-electron scattering, or so-called "anti-screening", is the dominant ionization process for a projectile at large impact parameters, where the contribution from target nuclei to projectile ionization is largely reduced. From this follows the necessity of "retyping" all target electrons that are captured by the ion. This new concept is not necessary for the nCTMC method, because there simply is no successive collision with further target electrons except the ones of the single target atom. Another new feature must be found in order to allow for simulations of macroscopically long channels, despite the fact that due to limits of available computation power the ion can only interact with a reasonably small number of target atoms.
In the following sections the basic properties of the newly developed simulation and all new concepts are addressed, before validity checks and essential results are discussed.

After that the mechanism for violating the rule of reversibility is studied, together with new insights into the charge exchange of swift heavy ions in solids.

4.4.1 Basic Properties

Before going into details of basic properties a specific difference to all previous CTMC codes in respect to the initial distribution of target electrons must be treated first. All other CTMC simulations use a microcanonical ensemble. Such classical ensembles either allow for a correct momentum or a correct spatial distribution, but cannot meet both conditions as in quantum mechanics. But since the main subject of this work has to do with channeling, special care has to be taken in order to simulate the best possible electron density in the channel. In other words, here the attention is turned to the local electron distribution at the cost of the correct momentum distribution. Therefore, not a microcanonical ensemble is taken, but instead all target electrons are distributed homogenously over spheres centered at the atomic nucleus with radii according to tabulated values of mean binding radii from Hartree-Fock calculations [41]. The corresponding momentum values are taken according to the Virial theorem. The initial velocity vectors are all perpendicular to the normal of the orbital spheres. The procedure with the Virial theorem yields at the same time *effective screened* nuclear charges with which each electron interacts. Thus, the intra-atomic electron-electron interaction is only implicitly taken into account, thus allowing stable classical atoms. Tab. 4.1 gives an overlook of the atomic data yielded by Hartree-Fock calculations.

Shell	Binding energy	Binding radius	Orbital velocity	Screened nuclear charge
	[eV]	[Å]	$[10^7 m/s]$	[e]
K	1834	0.04	2.54	10.2
L_I	151	0.20	0.73	4.2
$L_{II,III}$	109	0.21	0.62	3.2
M_I	13.8	0.80	0.22	1.5
$M_{II,III}$	7.3	1.04	0.16	1.1

Table 4.1: Atomic data from Hartree-Fock calculations [41] and application of Virial theorem used for modeling the Si atoms.

Each crystal atom is prepared according to the conditions stated above, thus neglecting any solid state effects. In this sense the crystal atoms are modeled as a gas with the density of a solid. The small differences in binding energies of valence electrons in a solid as compared to the ones of the isolated atom do not play an essential role here, because the average energy transferred from the ion to the target electrons is much larger.
Having in mind the dynamical "dCTMC" method mentioned above, one may expect that the screened nuclear charges should be adjusted from time to time as the atomic internal state is constantly changing under the influence of the ion, e.g. due to ioniza-

tion and excitation. However, it turned out that such a correction is not necessary. One reason is most likely the strength of the ion-atom interaction leading to a high rate of ionization, which leads also to the "retyping" procedure, discussed below, after which the formerly atomically bound electrons start interacting with each other, thus turning the implicit presence of other electrons into an explicit electron-electron interaction

In order to calculate the many-particle dynamics nN-CTMC uses Newtonian mechanics. Thus, for each particle the total force resulting from its interaction with other particles is calculated for each time step. According to Newton's Law of Motion, Eqn. (4.3), the following basic equations are applied for each particle i from the set of all M particles of the simulation, i.e. the ion and atomic nuclei, as well as all projectile and target electrons ($M = 1 + N + N \cdot n$). The position of the i-th particle in three dimensions is x_i^k, with $k = 1, 2, 3$, and $k = 2$ being the forward beam direction. F_{ij}^k is the force acting on particle i along direction k due to its interaction with particle j in a distance of r_{ij}. It is assumed that within the time interval Δt all forces do not significantly change, thus the law of motion is just integrated under the condition of constant forces:

$$m_i \ddot{x}_i^k = \sum_{j \neq i}^{M} F_{ij}^k \tag{4.3}$$

$$F_{ij}^k = \frac{q_i^* \; q_j^* \; e^2}{4\pi\epsilon_0} \cdot \frac{x_i^k - x_j^k}{r_{ij}^3} \tag{4.4}$$

$$F_{ji}^k = -F_{ij}^k \tag{4.5}$$

$$\dot{x}_{i,t+\Delta t}^k = \dot{x}_{i,t}^k + \ddot{x}_{i,t}^k \cdot \Delta t \tag{4.6}$$

$$x_{i,t+\Delta t}^k = x_{i,t}^k + \dot{x}_{i,t}^k \cdot \Delta t + \frac{1}{2} \ddot{x}_{i,t}^k \cdot \Delta t^2 \tag{4.7}$$

The second equation is the Coulomb force acting between any two particles with charges q_i^* and q_j^*. This formalism entails the possibility that the charge q^* that an electron is interacting with may be a screened charge, like in case of its corresponding atomic nucleus, or an unscreened charge, as in case of the projectile nucleus. The forces between any two bound electrons within all target atoms are set to zero, while projectile electrons interact with each other and with all target electrons. Eqn. (4.5) allows to cut the number of interactions in half due to "actio=reactio".

There remains one parameter undetermined so far in the last two equations, namely the time step variable Δt. Two conditions must be fulfilled for the setting of its value, namely minimization of computation time on one side and guaranteeing numerical stability on the other side. The latter criterion was studied by simply simulating the internal dynamics of one atom without the influence of the ion over the typical time length of an ion's passage. It was found that if Δt is set to $10^{-21} s$ the change in the binding energy of the L electrons in a Si atom is smaller than 5%, and thus regarded as a fair lower limit for Δt. However, this would not be enough in order to also keep the strongly bound Si K-electrons on numerically stable orbits. Therefore, the distance of these two electrons to their atomic nucleus is kept fixed to the value of the mean

binding radius as given in Tab. 4.1. Of course, this condition prevents any excitation or ionization. But this restriction is justified by the fact that within the energy regime of our experiments the capture cross section for K electrons is negligible [42], because their orbital velocity exceeds even the one of our fastest ions, and furthermore, their binding radius is much smaller than the mean distance of closest approach in channeling, thus the accessible impact parameters are too large for an effective capture.
At each time step all equations above are calculated yielding the new positions and velocities for all particles at time $t+\Delta t$. Since Δt is so small, the ions travel in forward direction along a step length of the order of 10^{-4}Å, which is four orders of magnitude less than interatomic distances. Therefore, for each ion trajectory an immense number of single iteration steps with the corresponding number of equations must be solved. The total number of these basic calculations is in the order of about $10^{11}...10^{12}$. This raises immediately problems in respect to numerical inaccuracies due to the finiteness of the internal number representation in computers. In order to account for that a special correction routine must be applied, as described below.
Before continuing the iteration after each time step, the simulation must perform some checks in respect to the possible occurrence of special events as defined by the necessary concepts discussed in the next section.

4.4.2 New Concepts

The condition of interacting with several atoms at the density of a solid requires to extend the nCTMC method by new concepts. Their physical function is to allow for the correct simulation of charge exchange, and are called "retyping", "resetting", and "replacing". The correction for allowing numerical stability is called "re-gridding". All these concepts are discussed in the following.

(a) Retyping

Within nN-CTMC any bound target electron has only the following interaction partners: its corresponding target nucleus, which is screened by the implicit presence of the other bound electrons of this atom, the projectile nucleus, and all bound projectile and free electrons. The latter are electrons that are neither bound in any atom nor in the ion. If a bound target electron is captured by the ion, it must interact with all other present particles, especially with all target electrons in order to allow for projectile ionization by electron-electron scattering, as mentioned above. This change in the set of interaction partners is called "retyping", meaning the change of the type from "bound target" to a "free or bound projectile" electron. There exist three possibilities for this retyping procedure: it could happen in the moment where the electron in question is ionized, i.e. when its total energy in the atomic frame is positive, or when the electron is bound in the ion, i.e. when its total energy in the ion frame is negative, or when these two conditions are both fulfilled. The disadvantage of the first possibility is the fact that many electrons are just ionized from the atom without being captured by the

ion and leaving the subsequent motion of the ion essentially unchanged. If one would also retype such electrons, then the number of pair wise interacting particles would increase drastically, thus enormously increasing computation time. Another criterion for the best choice of retyping conditions is the "smoothness" of the induced change as explained in the following. Within the second possibility most electrons are still bound in the atom. If one or more electrons are retyped while still being bound in the atom, they would at once start interacting with all other electrons. This sudden switching on of interactions increases the probability for distortions within the atom due to autoionization. Therefore, the third possibility was chosen for retyping, i.e. when the electron is both ionized from the atom and bound to the ion. Whatever condition comes last, determines thus the time at which the electron is retyped.

(b) Resetting and Replacing

The next new concept necessary for an nN-CTMC simulation is called "resetting". It allows to simulate an arbitrarily long channel while keeping the number of interaction particles constant. The ion moves along two strings of atoms, thus resembling axial channeling along two parallel strings of atoms. These two strings are separated by a distance δ_1, where all atoms of each string have an interatomic distance of δ_2. The third distance δ_{displ} gives the displacement of the second string in relation to the first along the x_2-direction (beam direction). All simulations refer to channeling along the $\langle 100 \rangle$ axial direction in a Si crystal. Thus, the three distances above are $\delta_1 = 1.92$ Å, $\delta_2 = 5.43$ Å, and $\delta_{displ} = 1.36$ Å.
In order to simulate macroscopically long channels, the "resetting" procedure removes each time that the ion passes the third atom of the closest string both atoms at the back end and places new atoms at the two front positions. Therefore, the ion is always surrounded by a fixed number of crystal atoms. This number must be small enough to keep the overall computation time as low as possible and large enough in order to avoid a "sudden shock" for the target system. This last point would happen, if the new atoms are put too close to the moving ion, because in this case the influence of the ion would not rise slowly, but rather like a sudden shock due to the immediately present ion potential. Taking 8 Si atoms in total, that is, four atoms per string, the above conditions are well satisfied. The potential energy of an electron in the field of a point charge $Q = 20^+$ in a distance of 10 Å is about 29 eV, which is small enough compared with the binding energy of the Si L-electrons according to Tab. 4.1.
By taking only two strings of crystal atoms one has to deal with the fact that in such cases the ions would slowly move away from the plane spanned by the two strings, because in total there is a repulsive force pushing the ion away from this plane. One possibility would be to make a full 3-dimensional simulation. However, such a simulation would have a much greater phase space, thus requiring a much larger statistical ensemble, that is, unrealistically long computation times. On the other hand, since the main purpose is looking for a violation of reversibility, the corresponding rates of de- and re-channeling can also be studied, if the ion is kept in a plane at a fixed distance

to the parallel plane spanned by the two strings. However, this does not mean planar channeling, because the ion finds itself in a potential being the sum of the two string potentials. The fact that the ion is fixed to moving within a plane has only the effect that its vertical position (x_3-direction) is kept constant during its motion along the two string potentials. In this simplified model one has a definite situation of transverse and longitudinal momentum vectors and corresponding energies, and de- and re-channeling can be easily detected. If the transverse energy of an ion is too little, it is only able to oscillate between the two strings, thus being channeled. If, on the other hand, its transverse energy is large enough, it can cross the strings, hence being non-channeled. In such a case of crossing one string, the other string is mirrored on the crossed string, so that the ion is always surrounded by two strings of crystals atoms.
Since the ions are simulated as initially bare point charges the number of all particles is therefore $M = 1 + 8 + 8 \cdot 14 = 121$. The total number of interactions is smaller than one would expect from $\frac{M^2-M}{2} = 14641$, because the majority of particles, that is, the bound target electrons do not directly interact with each other until they are retyped. Thus, typical "effective" values for M are in the order of about 300. Still the required computation power is very large, and was only manageable with the help of a special computer cluster consisting in the meanwhile of 48 single 1.8 GHz AMD processors. Typical calculation times are given below when discussing the results of the simulations.

The "resetting" procedure was aimed at keeping the number of all particles constant. Thus, if the two atoms at the back end are to be removed, this removal applies also to all those electrons that were initially bound in one of these two atoms. This, however, entails in connection with capture events a pitfall: suppose that an electron of one of those atoms was captured that are to be removed by resetting. If the resetting procedure would be applied as described so far, then the charge state of the ion and its internal state would be suddenly changed by the removal of the corresponding electron. Therefore, a third concept is to be introduced, which is called "replacing": this procedure checks whether an electron to be removed by resetting is bound in the ion. If such a case happens, then this electron is to be replaced by another electron, preferably a free electron. It should be mentioned that this replacement happens very often, especially at low velocities where a lot of target electrons are captured and remain bound in the ion. But at the same time there are a lot of ionized, free electrons far away from the ion that can be taken instead.

(c) "Re-Gridding"

As mentioned above the number of total basic calculation steps lies in the order of $10^{11}...10^{12}$. Keeping in mind that each basic calculation consists of several mathematical operations, such as multiplication and summation, it is to be expected that due to the finiteness of internal number representations in a computer the numerical stability cannot be guaranteed for the entire length of a trajectory. The main source for numerical inaccuracy is the necessity for rounding all numbers used in the calculation,

plus computer conditioned errors in calculating the square root (which is inevitable for determining the distance between any two particles, which is required for both the Hamiltonian and Newtonian method).
At each time step the computer is supposed to calculate the "movement vector" $\Delta\vec{x}_i$ that each particle has to travel along during one iteration step. However, due to numerical inaccuracies the computer actually yields $\Delta\vec{x}_i + \delta x_i$, whereby δx_i refers to the numerical errors. Due to the iterations such errors can increase in an exponential way, and sooner or later they distort the entire particle dynamics. It was shown that without any correction ion trajectories calculated on different computers with different CPU's, that is, different internal number representations, and different compilers as well as different compiler options (for instance, some compilers make computer programs run faster, but at the cost of numerical accuracy), were significantly different in the order of the smearing out due to multiple scattering on the target electrons.
In order to resolve this situation, a procedure was introduced for keeping the numerical errors δx_i from increasing. The idea hereby was to restrict the calculation onto a "grid", that is, all position and velocity vectors were rounded to the nearest intersection points on a 3-dimensional grid with a mesh size of $\delta\epsilon$. This mesh size has to be chosen in a way such that $\delta\epsilon \gg \delta x_i$ and $\delta\epsilon \ll \Delta x_i$. This choice enables to both suppress the influence of δx_i on Δx_i and also not to interfere too strongly with the correct Δx_i. The same argument has to be fulfilled in case of the velocity vectors. Detailed test simulations yielded the following values for $\delta\epsilon_{\vec{x}}$ in case of the position vectors and $\delta\epsilon_{\vec{v}}$ in case of the velocity vectors:
$\delta\epsilon_{\vec{x}} = 10^{-11}$Å and $\delta\epsilon_{\vec{v}} = 10^{-4} m/s$. For comparison, maximal $\mid \Delta\vec{x} \mid$ values are in the order of 10^{-4} Å and even transverse velocities are in the order of at least meters per second (mostly around $10^3 ... 10^4$m/s). With this choice the ion trajectories became independent on the computer/compiler with which the simulations were run.

4.4.3 Validity

Since these new simulations are supposed to help finding the mechanism for this only recently discovered phenomenon of cooling and heating, it seems appropriate to first check the simulation against well known data. Possible candidates are measured energy losses and charge state distributions, as well as critical angles. However, it appears questionable of whether or not energy losses can be suitably simulated when the ion is additionally kept in a fixed vertical distance to the plane spanned by the two strings. But the simulation can, of course, also be checked under the geometry of amorphous solids. For doing so the target atoms are not aligned along two strings, but homogenously distributed in a cylinder with macroscopic length like a gas with the density of a solid. Since there are very accurate data available, even for charge state dependent energy loss, [43], the test case was selected to be for 60 MeV Ni ions in a thin carbon foil. The results were very promising, because nN-CTMC reproduced both the measured energy loss within an error of only 5 %, and within the *same* calculation also the charge state distributions behind carbon foils within a few percent. This finding is very remarkable in relation to all theoretical approaches up to now in the field of

energy loss and charge exchange.
It must be pointed out here that, in order to reproduce measured mean charge states, the ions are simulated as initially bare point charges with a "core charge" that differs from the value of the ion's nuclear charge. This core charge was set to 22, which is lower by six charge units as compared with the nuclear charge of Ni ions (Z_1=28). Such a necessary difference by 6-7 electrons was found to be constant for all tested ions from Ti (Z_1=22) up to Y (Z_1=39), whereby in the last case this was confirmed by taking two different energies (72 MeV and 185 MeV), where the corresponding measured charge states are certainly not the same. The choice of setting the core charge lower by 6-7 charge units as compared to the nuclear charge is justified by the following two arguments, and must thus not be confused with a free parameter. First of all, the two K electrons cannot be explicitly taken into account due to their high orbital velocity, which would require the time step variable Δt to be smaller by at least one order of magnitude in order to allow for stable orbits. However, on the other hand, it is not necessary to explicitly calculate the two K electrons, because their excitation or ionization probability is drastically reduced as compared to the ones of the L electrons, not only due to their high orbital velocity, but also due to their small binding radius which would require very small impact parameters. This explains a difference by 2 charge units. The rest, that is, 4-5 charge units, can be justified directly by further calculations, where bare nuclear charges are simulated and their mean equilibrium charge states are compared with measured or tabulated values. It is found that these values are reproduced, if $Q_{core} = Z_1 - 6$ in case of Ti, Fe, and Ni ions, and $Q_{core} = Z_1 - 7$ for Y ions. The latter case is interesting, not just because it is the actual case for the channeling simulations, but also because it was tested at two different energies, 72 MeV and 185 MeV, where the tabulated charge states differ by 7 charge units due to their energy dependence [23]. Under the *same* setting of the core charge by $Q_{core} = Z_1 - 7$ for *both* energies, the simulated charge states reproduced quite well the tabulated ones, whereby it must be pointed out that at the lower energy in the mean 13 electrons are bound in the ion and 6 electrons at the higher energy. With this core charge it is possible to not only reproduce correctly the different mean charge states at different energies, but also the widths of the corresponding charge state distributions, and, as said above, to achieve a very good agreement with energy loss measurements. The reason for the necessity of using such a core charge instead of the real ion nuclear charge within a classical simulation comes from the lack of purely quantum mechanical features. Due to Heisenberg's uncertainty relation and quantization of atomic states, quantum mechanical ions can arrange bound electrons in such a way that the perturbation by the electron-electron interaction is minimized, hence there can be more bound electrons. This has to be taken into account when doing a classical simulation of charge exchange. And since the difference between core charge and nuclear charge is about constant over a relatively wide range of ions and energies, it must not be confused with a fitting parameter, but is rather a "technical constant" of the simulation.
A third test to check its validity was the comparison of simulated critical angles with the Lindhard angles. The latter are only given for ions with zero impact parameter in respect to the string, as given by Eqn. (2.2). Within the simulations one can figure

out the critical angle by increasing the initial angle of ions starting in the middle of the channel up to the value where half of the ions are channeled and the other half is non-channeled. In order to allow for non-channeled motion this was done with a distance of 0.1 Å between the plane in which the motion of the ion is kept and the string plane. Tab. 4.2 shows the results for Y ions along the Si-⟨100⟩ channel, which are in good agreement with Lindhard's estimates, taking into account that they are actually suitable only for zero distance between the plane of motion and the string plane and actually valid only in the sense of a perturbative approximation, were both the target atoms and the projectile are in their ground states (in fact, even the ion projectile was assumed to be an atom). This result is not only important in the sense of a validity

Energy [MeV]	$\psi_{1,Lindhard}$	$\psi_{1,Simulation}$
185	0.23	0.27
72	0.36	0.39

Table 4.2: Comparison of Lindhard angles according to Eqn. (2.2) and simulated critical angles.

check, but it also allows a deeper insight into the dynamics of a channeling ion. Besides nearly coinciding with the Lindhard critical angles, it was found that the simulated channeling trajectories looked very much like those obtained from simple estimates of particle oscillations within the stationary continuum potential, despite the fact that nN-CTMC calculated the particle dynamics in detail, including highly excited target and projectile ions, as well as charge exchange. This means that *angular* scattering is nearly unchanged by the additional processes included in nN-CTMC at least at impact parameters responsible for channeling. Thus, it looks like that violations of the rule of reversibility can be expected to manifest themselves in the *statistical* behavior, such as de- and rechanneling probabilities, but not in drastic changes of individual trajectories.

4.4.4 Results

In contrast to lighter ions, experiments with Y ions transmitted through Si crystals showed not only clear cooling, but also pure heating patterns, so it is this case that was chosen for the very time consuming simulation of cooling and heating and the transition thereof. The only different experimental parameter separating cooling and heating is the energy. This means that all other parameters in the simulations are the same, except for the entrance energy. The goal of these simulations consisted of two parts: first to see whether one can reproduce the effect of cooling and heating, and if so, secondly to find the mechanism. In order to fulfill the first part, it must be studied what signatures can be searched for in the simulations in order to deduce a possible appearance of cooling or heating. It is clear that due to the requirement of an enormous computation power it is by no means possible to simulate an isotropic beam and to directly look for redistributions in the outgoing angular flux. However, since

the transition from channeled to non-channeled motion will most likely appear among the ions which move around the critical angle, it is in first approximation sufficient to only simulate a few hundred ions slightly below and above the critical angle. Thus, the signatures of cooling and heating are sought in the inequality of de- and re-channeling probabilities, which would directly indicate the violation of the rule of reversibility. A second independent test is to look for an asymmetry in the transitions from one angle to another, because if reversibility is violated, one of the two angles will be depopulated at the cost of the other one.
The next section deals in details with the found results in terms of de- and re-channeling probabilities, while in the subsequent section the mechanism for the first results is discussed in terms of asymmetrical charge states.

4.4.4.1 De- and Rechanneling

All reported simulations in this section consisted of the following system: Y ions transmitted along two strings with 8 Si atoms at each time (resetting procedure as described above). The Y ions started initially as bare point charges with this "core charge" being 32. The geometry of the strings was given above. All ions started in a distance of 20 Å away from the first atom of the strings in order to have a slow increase of the interaction strength between ion and the "crystal". For all simulations the distance (along the x_3-direction) between the plane in which the ion was kept to move and the plane spanned by the two strings was set to 0.3 Å. This choice allows both to study also non-channeled motion and to keep the string potential still strong enough. Note that the critical angle significantly depends on this distance, while the Lindhard angle is defined for a motion in the plane of the two strings. However, for such a motion no de- or rechanneling events could happen, because ions would never break through strings, but would just be deflected (except for very large impact angles close to a completely perpendicular motion). When the ions passed the first atom in the strings, they were at the same time exactly in the middle of the channel. Before the actual long runs, a few trials had to be simulated in order to find the corresponding critical angles under the condition of the distance of 0.3 Å between the plane of motion and the string plane. Finally three groups of ions were simulated for each energy, namely two groups were slightly below and above the critical angle and the third group almost exactly at the critical angle.
The motion of a few ions around the critical angle is shown in Fig. 4.2. One can clearly see the variety of different types of trajectories in terms of channeled or non-channeled motion. Since all these simulations used the fixed motion of the ions within a plane parallel to the plane of the strings, one can easily define the criterion for channeled vs. non-channeled motion: an ion is channeled, if it does not cross a string, but is "reflected" instead. Hence, an ion is recognized as being non-channeled, if it crosses a string. These simple definitions also allow to give a well-defined meaning to the terms de- and re-channeling: an ion is dechanneled at a certain string, if it crosses this string, but did not show a crossing at the string that was encountered before. Thus, an ion is said to be rechanneled, if it crossed the last string but is reflected at the encounter of

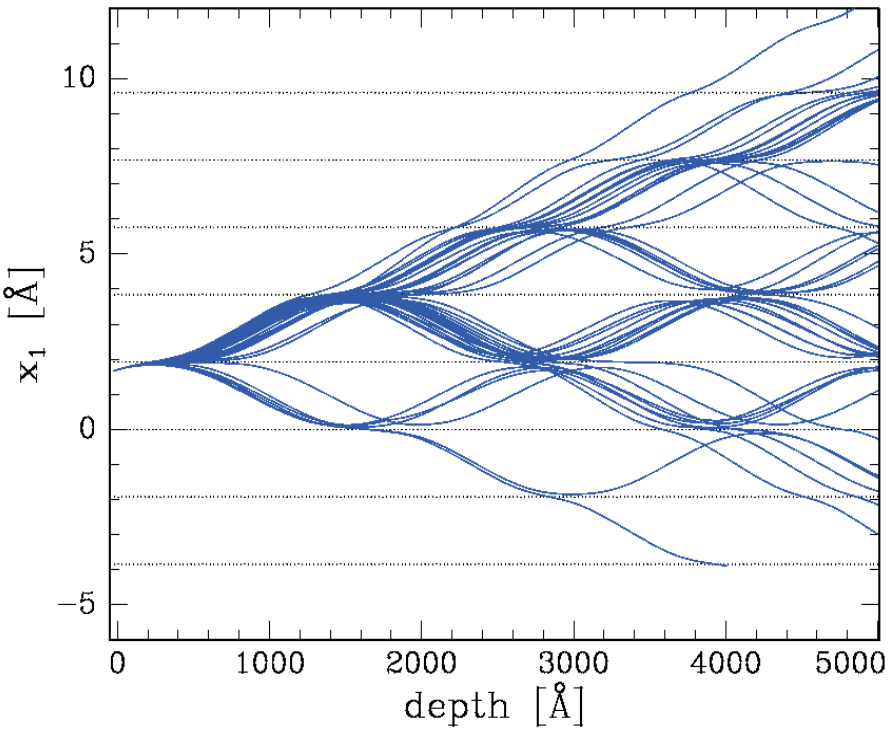

Figure 4.2: Typical ion trajectories along the strings of crystal atoms, whereby at each time only two strings are explicitly taken into account ("resetting" procedure). One can clearly distinguish channeled from non-channeled motion in terms of "being reflected from a string" and "crossing a string".

the subsequent string.
Of course, these definitions must be differed from the definitions as given in the theory of channeling. In the latter case channeling is defined as a motion confined to a certain region of impact parameters that prevents large angle scattering [1]. The main difference between this definition and the one used for the simulations is the fact that in real 3-dimensional channeling axially channeled ions can jump from one channel into the neighbored one if the ion's transverse energy is high enough to get over the corresponding potential separating the two axial channels - note that in case of planar channeling such changing of channels is not possible [12]. However, within the simulations there is only a two-dimensional motion of the ion within a fixed distance along the vertical x_3-direction. This feature allows the well-defined concept of channeled vs. non-channeled motion in terms of "reflected by a string" vs. "crossing a string". In this sense only is the term channeling to be understood within the presented simulations.
In order to simulate one cooling and one heating regime, the corresponding energies were taken along the experimental values as in Fig. 3.7, that is, 185 MeV for cooling and 72 MeV for heating. The lengths of the simulated channels were chosen individually for the two energies due to the differences in critical angle, ion velocities and

strength of the transverse potentials. A stronger potential yields a higher rate of oscillation and thus a smaller channel length for the same number of oscillations. In order to ensure 7 complete single encounters with strings for both cases, the channel length in case of cooling was set to 8500 Å (0.85μm) and 5000 Å (0.50μm) for heating. Nevertheless, the heating calculations took longer, because more ionization and capture events ("retyping") occurred, thus leading to a larger number of total interactions and hence longer computation time.
For these simulations 6 different runs according to two different energies with each three different entrance angles were calculated. A single run took about one day on a single processor of the cluster. In order to achieve a satisfying statistics, about 500 single runs for each of the six different cases was simulated.
After all these runs all data were analyzed by another computer program that counted all events of de- and rechanneling, thus finally yielding the sought probabilities for these two processes. Besides these probabilities the analysis included a further parameter indicating the change of flux along the channel. This parameter is called λ_i and is defined for the i-th string encounter on the way of the ions along the simulated channel as follows:

$$\lambda_i = \frac{N_{cross,i} - N_{refl,i}}{N_{cross,i} + N_{refl,i}}, \tag{4.8}$$

where $N_{cross,i}$ is the total number of ions that cross the string at the i-th string encounter, while $N_{refl,i}$ is the total number of ions that were reflected at the i-th string encounter. Thus, if $\lambda_i = -1$ all ions are reflected, while $\lambda_i = +1$ indicates that all ions cross the corresponding string. λ_1 is the measure of the initial conditions in respect to the critical angle, and $\lambda_1 = 0$ indicates that the ions move exactly with the critical angle, because at the first string encounter half of them are reflected, while the other half crosses the string. Tab. 4.3 shows the flux development according to the λ-measure between first and last string encounter, that is, λ_1 and λ_7. It must be

Energy [MeV]	Regime	$\psi_{entrance}$	λ_1	λ_7
185	cooling	0.12°	-0.98 ± 0.04	-0.71 ± 0.03
185	cooling	0.13°	-0.73 ± 0.03	-0.39 ± 0.02
185	cooling	0.14°	0.86 ± 0.04	0.09 ± 0.01
72	heating	0.23°	-0.92 ± 0.04	-0.16 ± 0.01
72	heating	0.25°	0.12 ± 0.01	0.06 ± 0.01
72	heating	0.27°	0.89 ± 0.04	0.42 ± 0.02

Table 4.3: List of all simulated flux developments according to the λ measure, Eqn. (4.8) of channeled vs. non-channeled flux. In case of high (low) energy the trend goes towards more negative (positive) values. The critical angles turn out to about 0.135° for cooling and 0.25° for heating.

pointed out that even for a heating case one would expect that if λ_1 is close to 1, λ_7 will be significantly lower than 1, but not as low as in a cooling case. This expectation

takes into account that the flux is initially not in equilibrium in terms of a model with two states corresponding to channeled and non-channeled ions. For instance, the state of channeled ions may not be populated in the beginning, but the flux will approach a dynamical equilibrium of constant populations of the two states that are determined by the actual probabilities for de- and rechanneling. Thus, Tab. 4.3 gives first indications of a substantial difference in the flux developments in the two cases, which is best seen when comparing λ_7 values that correspond to about equal λ_1 values. In case of cooling, the flux tends to stabilize towards negative values of λ, while in case of heating the opposite trend is seen.
This first impression is clearly confirmed by the actual numbers of de- and rechanneling probabilities. For any string encounter one can define de- and rechanneling probabilities as follows. For each ion and each string encounter it is tested whether a dechanneling or rechanneling event took place, as defined above. Of course, if a non-channeled ion remains non-channeled, none of the two events occurred, the same applies for channeled ions that remain channeled. If at the i-th string encounter $N_{de,i}$ is the number of all ions that underwent a dechanneling event, then the corresponding dechanneling probability for this string is simply $p_{de,i} = N_{de,i}/N_{ions,i}$, whereby $N_{ions,i}$ is the number of all ions that passed the i-th string encounter. The rechanneling probability is determined analogously. The results are given in Tab. 4.4, where the mean de- and rechanneling probabilities are averaged over the last 6 string encounters (of course, the first string encounter does not allow to define a de- or rechanneling event). If the

Energy [MeV]	Regime	$\psi_{1,in}$	$\langle p_{de} \rangle$	$\langle p_{re} \rangle$
185	cooling	0.14	0.18 ± 0.01	0.17 ± 0.01
185	cooling	0.13	0.11 ± 0.01	0.22 ± 0.02
185	cooling	0.12	0.04 ± 0.01	0.19 ± 0.03
72	heating	0.27	0.29 ± 0.02	0.12 ± 0.01
72	heating	0.25	0.24 ± 0.01	0.21 ± 0.01
72	heating	0.23	0.14 ± 0.01	0.17 ± 0.02

Table 4.4: De- and rechanneling probabilities, $\langle p_{de} \rangle$ and $\langle p_{re} \rangle$, averaged over the last six string encounters. While at high energy rechanneling probabilities are larger than dechanneling probabilities, at low energy this relation is reversed. However, this difference is at high energy larger for channeled ions, and at low energy larger for non-channeled ions.

probability for dechanneling is larger than for rechanneling, a net flux outwards of the channel to non-channeled motion occurs in case of isotropic beams. If this condition is reversed, a net flux into the channels happens. When looking at the numbers as given in the table above one can clearly see essential differences between the two simulated regimes - keeping in mind that the only difference of the simulation parameters was the ion energy (and accordingly different entrance angles). In case of the low energy, i.e. the experimental heating regime, the dechanneling probability is for the ions above the critical angle about twice as large as the rechanneling probability, hence clearly

indicating a net flux outwards the channel. The corresponding group in case of the high energy shows practically no difference in the two probabilities, indicating the absence of a redistribution of the flux slightly above the critical angle. However, in reality this group will be fed due to multiple scattering on target nuclei and electrons by ions with even larger angles, hence populating this level. On the other hand, the dechanneling of the group of ions with smaller angles is strongly suppressed, as is shown by the much stronger probabilities for rechanneling than dechanneling for the other two groups. Therefore, one can expect an overall net flux inwards the channel, indicating cooling. In case of the low ion energy (heating regime) there is for the group around the critical angle still a slight outward flux seen, whereas for the ions below the critical angle the rechanneling probability is a bit larger than the one for dechanneling. This finding may point to a slight increase of best channeled ions even in case of heating, as was also seen in many experiments where the flux of the best channeled ions was less reduced than the rest in case of heating (see section 3.1.2.2).

These results were further supported by a second independent method of looking for the redistribution of the angular flux. Suppose that the detailed balance as proposed by the rule of reversibility would be valid. Then the net flux from one transverse energy $E_{\perp,i}$ into another energy $E_{\perp,j}$ must be the same as in the other direction. However, within such a many-body simulation it is quite complicated to determine the transverse energy due to its potential part, whose calculation would require to solve the Poisson equation for the spatial distribution of all particles. Nevertheless, a much faster way is to take the angle of motion ψ along the string direction. In order to warrant definite conditions for all ions independent on their momentary positions, these angles must be chosen as the angles of motion when the ions cross the middle of the channel, because in such a case the contributions to the potential part of $E_\perp$ from both strings cancel out each other, and thus only the kinetic energy must be calculated. While all entrance angle distributions are delta functions, the distributions of the angles inside the channel will be smeared out by angular straggling, caused by the scattering on the target electrons. Therefore, in order to study the transitions from one angle to another, one must perform the following comparison. Let us take two angles, ψ_i and ψ_j, that were both used in the simulations as *entrance* angles. Then one measures the probability $p_{i\to j}$ for ions that enter the strings with the entrance angle ψ_i and reach the last crossing of the channel middle within an *interval* of angles $[\psi_j]$ which is centered around the angle ψ_j which is chosen as entrance angle in the other simulation run. This probability $p_{i\to j}$ is then to be compared with the corresponding reversal, that is, one just reverses $i \leftrightarrow j$. The results are shown in Tab. 4.5. One can clearly see that in case of high energy the net flux goes from higher to lower angles, while this is reversed in case of low energy. This result clearly demonstrates the violation of detailed balance, and is in agreement with the results in respect to different de- and rechanneling probabilities.

The main result of the above analysis is the presentation of very strong evidences for cooling and heating in dependence of the ion energy, and thus also for the transition between these two regimes. Hence, the first goal of the simulations is reached, but the

Energy [MeV]	Regime	ψ_i	$[\psi_j]$	$p_{i\to j}$
185	cooling	0.12	0.135-0.145	0.03
185	cooling	0.14	0.115-0.125	0.08
72	heating	0.23	0.265-0.275	0.05
72	heating	0.27	0.225-0.235	0.03

Table 4.5: Study of detailed balance of the transition probability $p_{i\to j}$ from one initial mid-channel angle ψ_i to an *interval* $[\psi_j]$ of angles at the last mid-channel crossings centered around the entrance angle ψ_j of the corresponding reversed case. For instance, the interval $[\psi_j]$ in the first row is centered around the entrance angle in the second row. It is seen that the found transitions clearly violate the detailed balance of the rule of reversibility. At high energy the smaller angles are more probably populated, and vice versa at low energy.

still open question remains of how to explain this effect. The next section treats the detailed search for the underlying mechanism within nN-CTMC.

4.4.4.2 Time Asymmetry in Charge States

As it was discussed above, the expected mechanism responsible for cooling and heating is charge exchange. Therefore, it is reasonable to study the charge states of the ions in detail. Since within nN-CTMC all parameters of interest can be stored along each ion's trajectory, it is very easy to study the impact parameter dependent charge state of the ions on their passage of the two strings. This feature of nN-CTMC is a clear example of the exclusive accessibility of an important parameter by simulation, whereas it is inaccessible by experiment.

(a) Channeling vs. Random Charge States

Every time an ion has traveled 1 Å in forward direction, its longitudinal and transverse velocities as well as its charge state are stored. The charge state is defined through the total number of all such electrons whose total energy is negative in the ion frame. Furthermore, the simulation also stores data about mean binding radii and energies of these bound electrons, yielding an insight into the population of excited states. Fig. 4.3 shows the result of the mean charge states of channeled ions plotted against their position in between the two strings for the same ion energies as above. One can see two important features: the simulation reproduces both measured charge states in case of random ions, and, even more importantly, the experimentally observed shifts in the charge state distributions of channeled vs. non-channeled ions (see section 3.2.2.1) [22]. A non-channeled, or random, ion probes all impact parameters equally, while channeled ions are confined to a certain region of impact parameters centered around the middle of the channel. Furthermore, the impact parameters tested by channeled ions are not

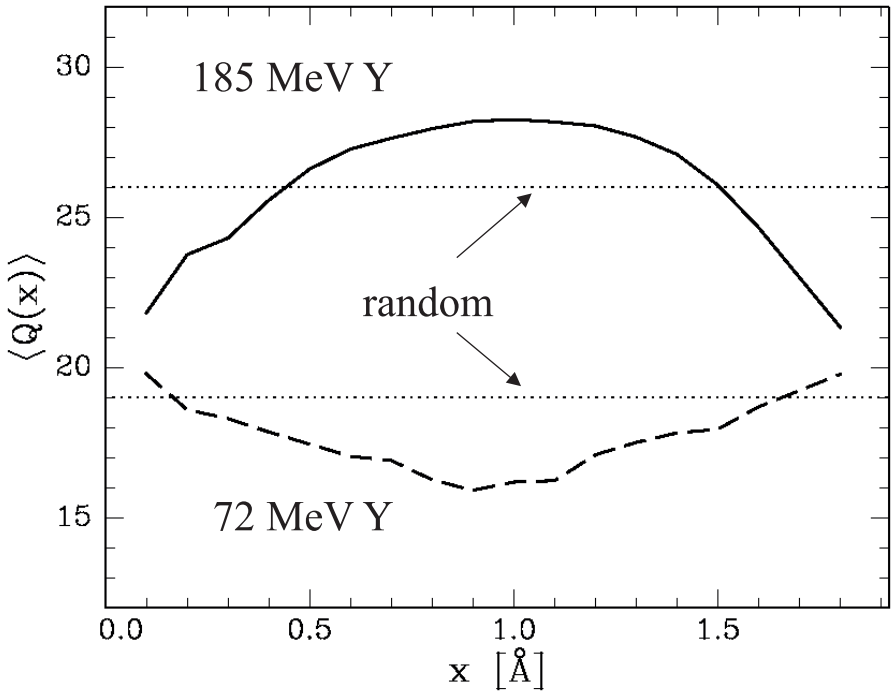

Figure 4.3: Simulated mean charge states of Y ions as a function of the transverse position x between the two strings, located at $x = 0$ and $x = 1.92$ Å, at two different energies: 185 MeV and 72 MeV. In correspondence to the charge state measurements, see Tab. 3.2, the charge state of ions channeling around the middle of the channel at $x = 0.96$ Å is shifted to higher (lower) values as compared to the random value, when the ion energy is high (low). The indicated random values [23] refer to C foils, while the corresponding values for Si can be expected to be lower by one charge unit [25].

equally distributed, as more channeled ions are found in the middle of the channel (the so-called "flux peaking" effect [12]). The effect is, therefore, that according to the figure the mean charge state of channeled ions is higher (lower) in case of high (low) ion energy, i.e. cooling (heating) - in accordance to the experimental results in Tab. 3.2.

(b) "Hysteresis" of Charge States

The finding above encourages to look for possible time asymmetries of the ion's charge states when approaching and when leaving a string. The results are plotted in Fig. 4.4. In case of cooling, a clear asymmetry over the entire impact parameter region is seen in the charge state between the ion's approaching of a string and its leaving a string. In that sense one could also speak of a "memory" effect: the ion "remembers" its motion at smaller impact parameters, where it has captured electrons that are not

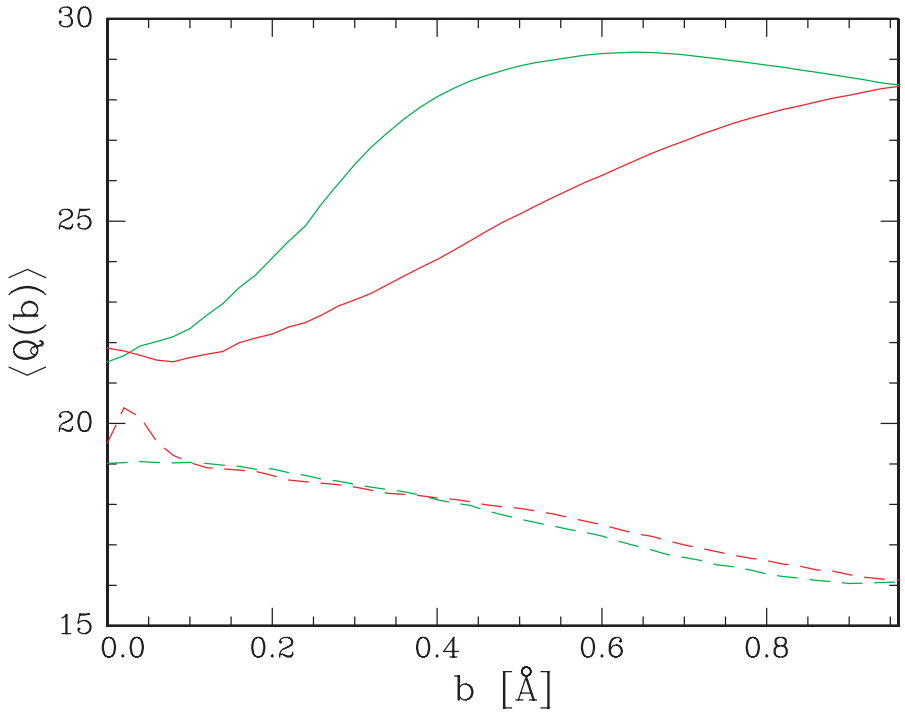

Figure 4.4: Mean simulated charge states in dependence on the impact parameter b for high energy (cooling, solid lines) and low energy (heating, dashed lines), distinguished between approaching the string (green lines) and leaving (red lines). In both cases a "hysteresis" behavior is seen, which extends over the entire impact parameter range in case of cooling, but which is effectively restricted to small impact parameters in case of heating. Most importantly, in cooling the ion approaches the string with a higher charge state and leaves with a lower charge state, whereas this is reversed for heating.

all lost yet when returning to larger impact parameters. In case of heating, this asymmetry is much smaller, almost insignificant, for best channeled ions, but clearly seen for those ions that are crossing strings (in the figure at "zero" distance b to the string - note that b is the value in the transverse x_1-direction, thus a string crossing happens at "$b = 0$". The region of string crossings is characterized as the region of most violent collisions due to reaching the closest distance to crystal atoms. This impact parameter dependent behavior of the charge state in the heating regime reflects quite well the experimental finding that heating starts its angular flux reduction around the critical angle, and then proceeds down to the best channeled ions when the ion energy is decreased. The simulations suggest the following scenario: heating happens around the critical angle, but there is some feeding process by ions with lower transverse energy due to diffusion to higher transverse energies by multiple electron scattering, while cooling occurs best at smaller angles than the critical one, but there is also some feeding by ions with larger angles due to multiple scattering. The latter case means that once an ion became channeled it is more likely kept there and cannot escape again as

one would expect from the rule of reversibility.
The results in Fig. 4.4 also show a clear difference between cooling and heating in respect to the impact parameter dependent amount of asymmetry, which is much larger for cooling. This reflects the findings given in Tab. 4.4, where one could see that in case of heating especially ions at or above the critical angle have a large difference between de- and rechanneling probability, while in case of cooling the larger differences are seen for ions moving below the critical angle.

(c) Adiabatic Charge States

So far there is a strong correlation found between charge state asymmetries in terms of the hysteresis behavior on one side and different probabilities for de- and rechanneling on the other side. The next step is to figure out the mechanism for both the shifts in the charge states and their asymmetry in respect to the transverse motion. In order to keep things as simple and definite as possible, the following simulations were done at *fixed* impact parameters. This procedure allows one to calculate the mean charge state that any ion would take on, if it spent an infinite amount of time at a certain impact parameter. Therefore, these charge states are called *adiabatic* charge states. In channeling, every ion can only spend a finite amount of time at each accessible impact parameter, hence if the transverse ion velocity is high enough, there is not sufficient time to reach the corresponding adiabatic charge states. Therefore, any ion tries to reach the impact parameter dependent adiabatic charge states, but will at high transverse velocity never reach them as it has already moved on to the next impact parameter with another adiabatic charge state. In order to get these impact parameter dependent adiabatic charge states, all ions are kept fixed at their entrance impact parameters in respect to one of the two strings. The results are shown in Fig. 4.5. It is seen that for the *same* initial charge states the case of high velocity requires much longer channel lengths for reaching each impact parameter dependent charge state than in case of low velocity. This difference explains at once the difference in the amount of asymmetries as described above: at low velocity the actual ion charge states reaches almost perfectly its adiabatic charge state, whereas at high velocity the adjustment time for the ions is too short. This kind of "hysteresis" behavior is shown in Fig. 4.6, where the actual channeling charge states are compared with the adiabatic ones for each impact parameter. These findings may also explain the energy dependence (see section 3.1.2.4), because it seems realistic to expect that the amount of charge state asymmetry increases with increasing velocity, because this leaves the ions less time for adjusting their charge states towards the adiabatic ones. On the other hand, at very high velocities towards the one for fully stripped ions, the charge state asymmetry should decrease again, because if the ions move too fast for effective electron capture, they will reach practically impact parameter independent charge states, thus losing any asymmetry between approaching and leaving a string. Such an expectation would be in accordance to the experimental finding of an optimal ion energy for maximum cooling strength.

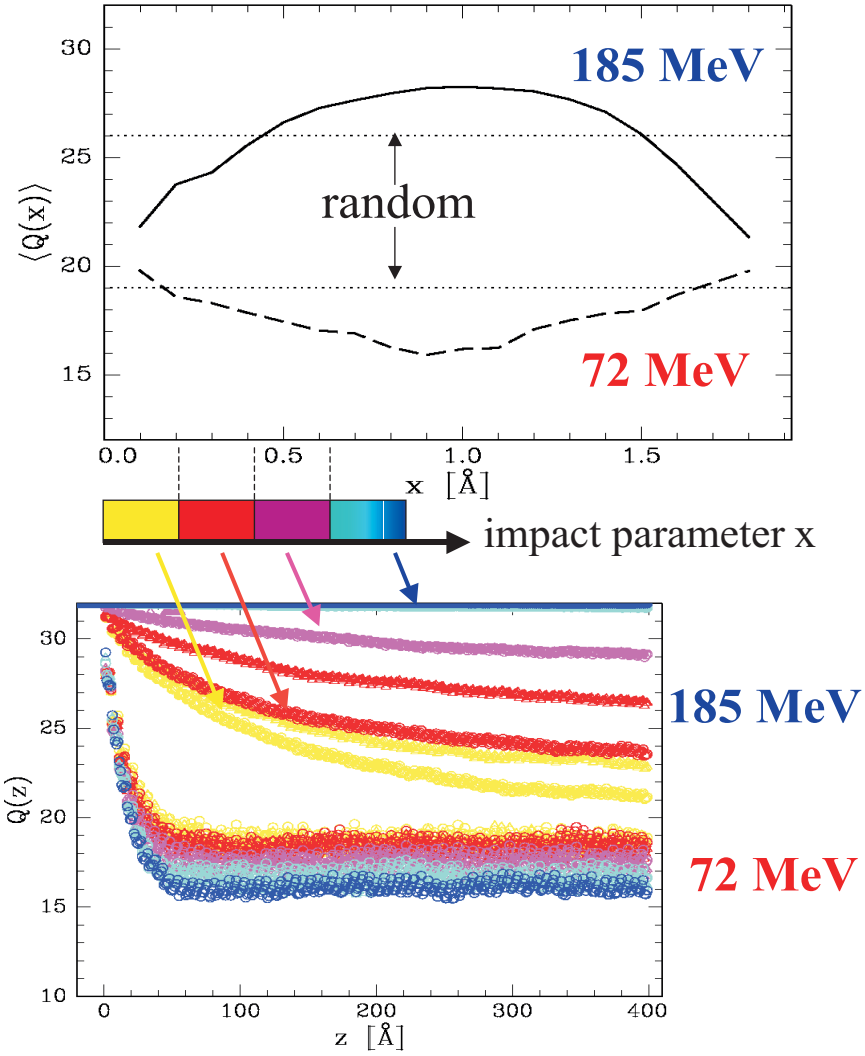

Figure 4.5: Impact parameter dependent *adiabatic* charge states (bottom part), compared with channeling charge states from Fig. 4.3 (top part). The colors indicating each impact parameter range are given by the inset. In case of high energy (cooling) the ions must travel a larger depth z in order to reach the adiabatic charge states, while this occurs much faster for low energy (heating). It is essential that the adiabatic charge states increase with increasing impact parameter in case of cooling, whereas this is reversed for heating, in accordance with the top part of the figure.

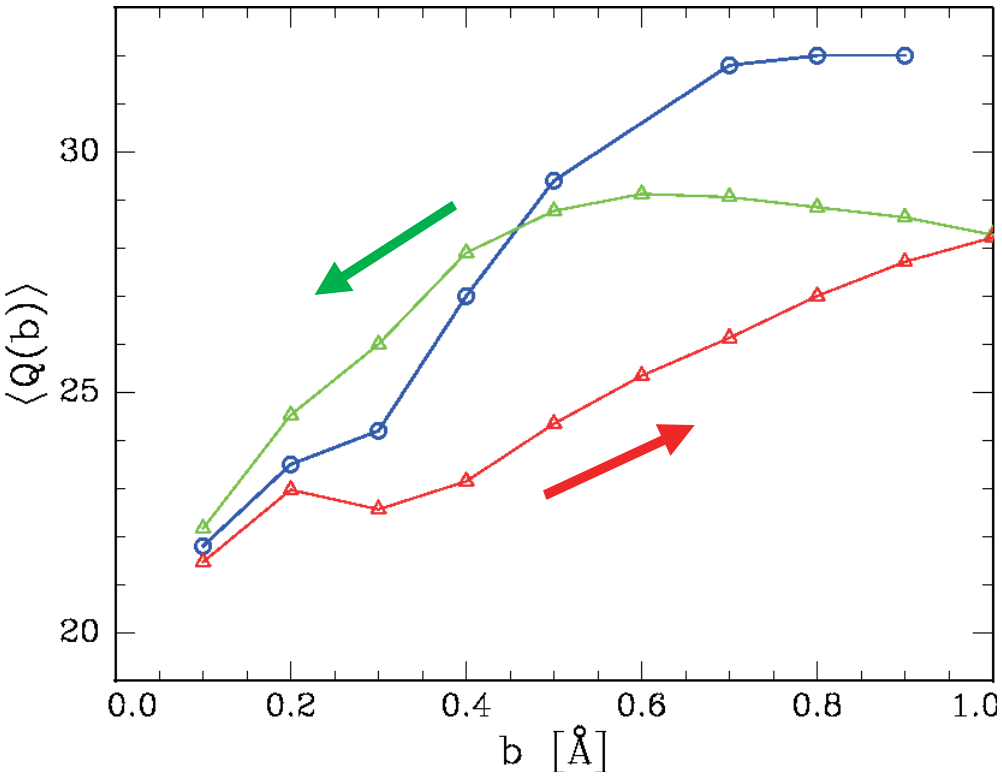

Figure 4.6: Channeling charge states in case of cooling (green curves for string approaching and red curve for string leaving) compared with the adiabatic charge states (blue curve) plotted against impact parameter. One can see that the channeling charge states never reach the adiabatic ones towards which they move. The ion approaches the string with a higher charge state and leaves it with a lower one. The channeling charge state at the middle of the channel is lower than the corresponding adiabatic one, because when probing all impact parameters the ion can capture a few electrons at small impact parameters and does not lose all of them until it reaches the middle of the channel.

The most essential finding here is the fact that while at high velocity the mean charge states of ions moving with larger impact parameter are higher than the one at smaller impact parameters, this behavior is reversed in case of low velocity. Even more surprising is that this reversal happens in a very narrow velocity region, which is pretty close to the observed transition region from cooling to heating. This is shown in Fig. 4.7. The shifts in charge states in respect to the impact parameter region occur in between $v_{ion} = 1.54 \cdot 10^7 m/s$ and $v_{ion} = 1.37 \cdot 10^7 m/s$, while the experimentally deduced transition velocity is about $v_{ion} = 1.59 \cdot 10^7 m/s$. One must keep in mind here that the definition of the experimental transition energies is not absolutely unique, as discussed in section 3.1.2.2.

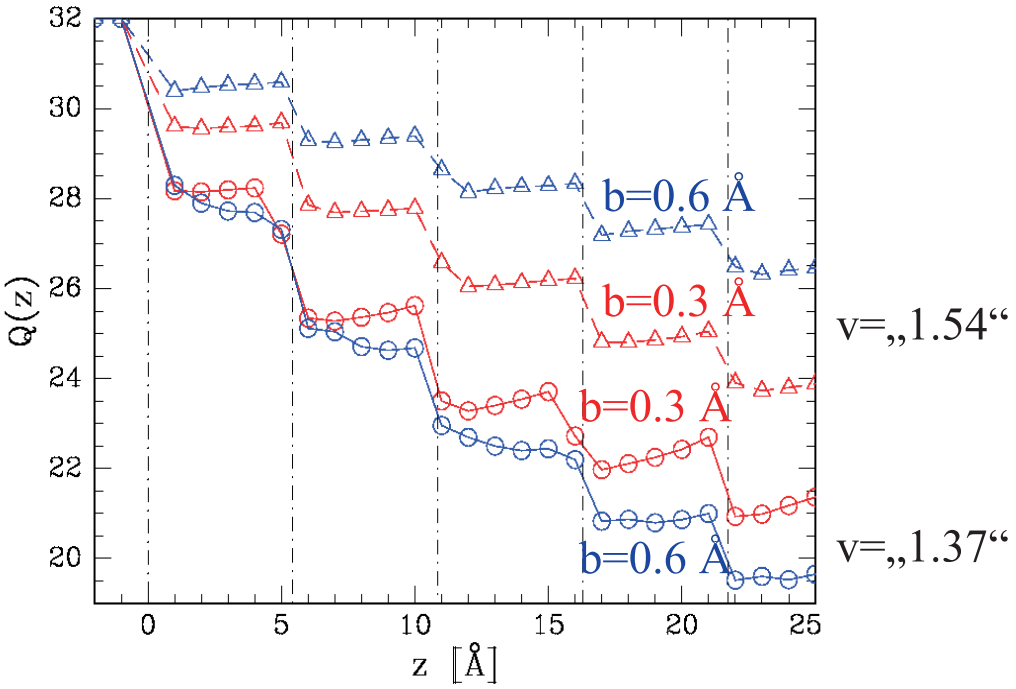

Figure 4.7: Same as in bottom part of Fig. 4.5, but here for the first 25 Å only, two impact parameters, $b = 0.3$ Å (red symbols) and $b = 0.6$ Å (blue symbols), and two relatively close velocities ($1.54 \cdot 10^7$m/s, indicated by triangles, and $1.37 \cdot 10^7$m/s, circles). The positions of the crystal atoms are marked by vertical lines. For the higher velocity the ion charge state is higher at the larger impact parameter, whereas this is just reversed in case of the slightly lower ion velocity. This rapid transition occurs close to the experimentally determined transition velocity from cooling to heating at $v_t = 1.59 \cdot 10^7 m/s$.

(d) Impact Parameter Regions for Effective Electron Capture

The remarkable feature of the shifts above can be explained by the following considerations. In Fig. 4.7 one can see that at the higher velocity the ion charge state is decreased from its initial value at each passage of an atom and remains constant in the space in between. The smaller the impact parameter, the larger the amount of captured ions. This picture is what one would expect from considerations of any theory of electron capture. In order to capture an electron by mechanical electron capture (MEC) the ion must transfer sufficient momentum to a target electron in order to release it from the atom and to accelerate it up to the ion velocity. It is expected that the probability for electron capture is larger the smaller the impact parameter and the smaller the difference in the relative velocity. This explains the results found at higher velocity, but it fails to explain the case of lower velocity. The figure above

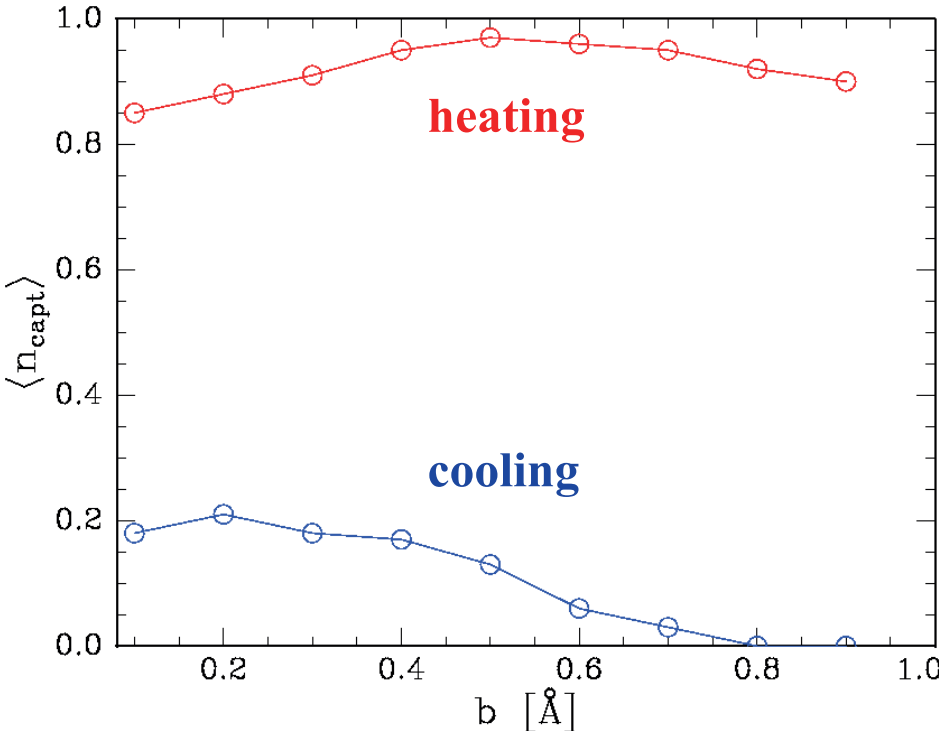

Figure 4.8: Mean number of "retyped" electrons, resembling the number of captured electrons without distortion due to subsequent electron loss, plotted against the impact parameter for 185 MeV (cooling, blue line) and 72 MeV (heating, red line). There is a significant difference in the range of the impact parameter region for *effective* electron capture. While capture is almost constant over the whole range of impact parameters up to the middle of the channel in case of heating, only a relatively small impact parameter interval is effective for electron capture in case of cooling.

clearly shows that in the latter case the ion's charge state makes indeed within the first collision with a target atom the same step downward in its charge states independent on the impact parameter, but the smaller the impact parameter, the more increase of charge state *after* passing the target atom appears. This effect can be understood by Fig. 4.8, in which the number of *retyped* electrons is plotted against the impact parameter. Note that this number is more suitable than the number of captured electrons, because any retyped electron is captured, but could be ionized in the subsequent events, thus distorting the ion's capability of capturing electrons by subsequent electron loss. Furthermore, when taking the number of captured electrons instead, one must decide the point in time at which one counts the number of bound electrons, under the risk that in the meanwhile some charge exchange took place. The displayed result is very clear in respect to the different "effective" impact parameter regions in which electrons are captured in reasonably large amounts: at high velocity this region is confined to small impact parameters, as one would expect from any simple consideration; at low velocity, however, there is almost no dependence on the impact parameter up to the

middle of the channel. It was seen by further studies that the maximum seen at low velocity results from electron capture events in which electrons are captured from the *second* string, which has an even larger impact parameter.
Now, if there is no more an impact parameter dependence for electron capture, then the impact parameter dependent charge state is fully determined by electron *loss*. It is evident that the probability for electron loss is smaller in the middle of the channel. One reason thereof is the reduced ionization by the (screened) target nuclei-electron interaction due to the larger impact parameters. The other reason is that in the middle of the channel the electron density is smaller and, therefore, the probability for electron impact ionization of the ion is reduced. In contrast, when moving close to strings, electron-electron and target nuclei-electron scattering is much stronger. From this it follows that at low velocity the ion captures at larger impact parameters indeed as many electrons as at smaller impact parameters, but at the same time it loses less of them by electron impact ionization and Coulomb ionization by the target nuclei. Hence, its charge state is smaller in the middle of the channel as compared to the regions close to the strings. At high velocity, the ion's charge state is primarily determined by electron capture, because for instance in the middle of the channel there is no electron capture and thus electron loss does not take place.

(e) Complex Features of Electron Capture

At this stage the chain of explanations of the found differences in de- and rechanneling probabilities seemed to be reduced to the final question of why the effective impact parameter region for electron capture changes so drastically in exactly the velocity interval as seen above, being very close to the transition velocity. The hope was to find a rather simple physical argument that would allow a final explanation of the findings presented above. The first step was to further reduce the simulation onto one-electron-atoms only, thus removing any possible many-particle aspects and just treating the three-body dynamics of the projectile and target nuclei and the one electron to be captured. For these simulations the conditions for this single electron were the same as in a full many-electron Si atom, that is, the target nucleus charge, the corresponding electron orbital velocity and radius were taken as given in Tab. 4.1.
Unfortunately, the complexity of three-body dynamics prevents any simple analytical expression. According to other works, for instance [44], the three-body Coulomb system is considered having "chaotic" features. Tab. 4.6 summarizes the complex dependence of capture probabilities p at high and low velocity at different impact parameters b and different ion charge states Q, indicating that simple explanations may not be expected. At low velocity and small impact parameter there is almost no dependence on the charge state, and a linear dependence at large impact parameter. In contrast, at high velocity and small impact parameter the probability scales with about the second power of the charge state, while at large impact parameter an exponential increase with charge state is seen. This non-trivial behavior is confirmed by Fig. 4.9 which shows the two dimensional map of the two angles θ_0 and ϕ_0 for the spherical coordinates which

b [Å]	Q	p_{low}	p_{high}
0.2	26	0.92	0.23
0.2	20	0.92	0.15
0.2	18	0.89	0.08
0.6	26	0.81	0.002
0.6	20	0.63	<0.0001
0.6	18	0.58	–

Table 4.6: Capture probabilities p_{high} and p_{low} at high/low velocity in dependence on impact parameter b and ion bare core charge Q. No trivial overall result was found, ranging from invariance on charge states over linear and quadratic until exponential dependence.

define the initial position of the one electron on the sphere around its atomic nucleus at the beginning of each run. The figure demonstrates the complexity of the three-body capture dynamics, and it is finally concluded that a simple and analytical expression cannot be given. With this result it is also understandable why such an expression can now less than ever be expected for the cases of many-electron systems.
Furthermore, some other properties of this three-body system were studied. For instance, the amount of transferred momentum in forward direction from the ion upon the target electron. Despite of finding the expectable trend in terms of increasing momentum transfer with decreasing ion velocity, there was no systematic pattern which could have given a simple explanation for the drastic impact parameter dependence as stated above. A significant difference between electron capture in case of low velocities as compared to high velocities was found in the relative position of ion, atom, and electron at the point of retyping: at low velocity the electron was in between the ion and atom, while at high velocity the ion has always already past the atom and the electron when finally the capture event took place. Certainly, these findings are directly correlated with the amount of transferred forward momentum, but again no simple expression could be found. Another study was about so-called "molecular" states, that is, short periods in time where the electron is bound both in the atomic and ionic frame (and thus not retyped yet). The result was that at low ion velocity there are indeed such states, but out of all states leading to capture events they did not play the dominant role. Moreover, these states totally vanished at higher velocities above the transition velocity. Note that since such molecular states can only appear when the ion is as close as about 0.5 Å to the atom, the unique determination of the *mean* ion charge state in a solid by the number of electrons that are bound solely in the projectile is not distorted by such molecular states.
Turning to many-electron atoms there were correlations found. In general, the probability for capturing a *particular* electron is decreased the more electrons are included in this many-particle dynamics. These correlations arise from the inter-electronic interaction which lead to mutual perturbations, thus possibly hindering some electrons from

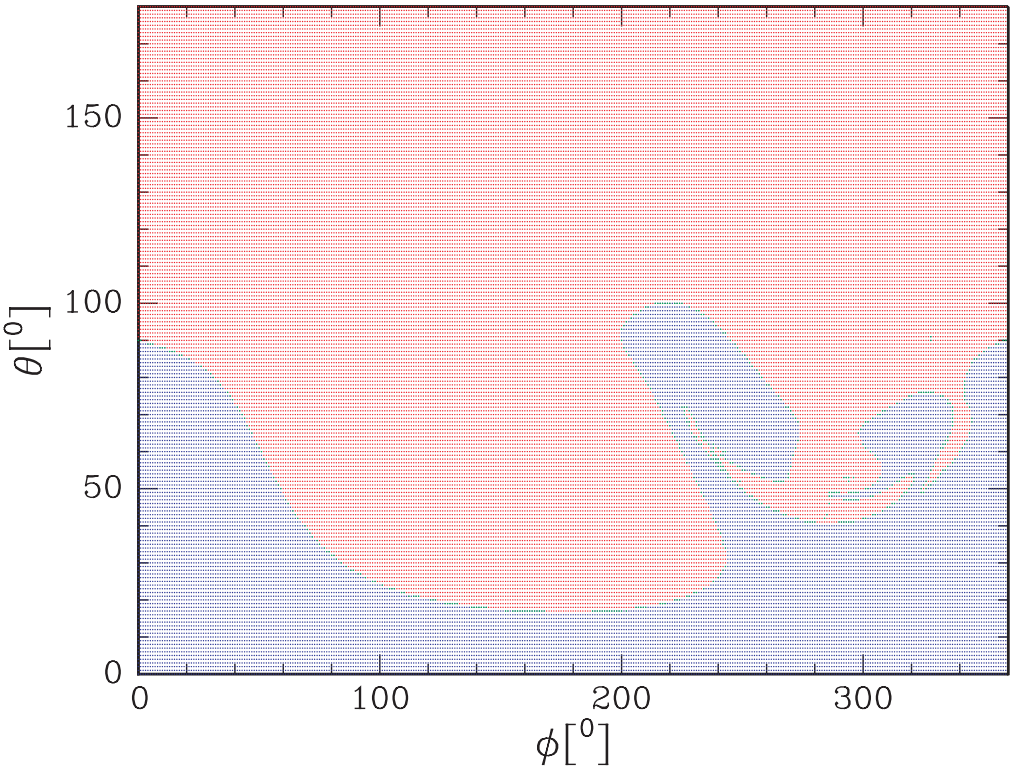

Figure 4.9: Scatter plot of the initial spherical coordinates of the electron in the one-electron-atom case: blue dots represent regions, in which the capture probability is higher then 0.8, red dots mark regions with capture probability lower than 0.1, and green dots refer to the probability interval between 0.5 and 0.9. This plot shows clearly the complexity of this three-body capturing process, as one cannot expect any simple analytical expression for describing the set of initial conditions that lead to a capture event. Note that in this plot the ion moves in a horizontal line at $\theta = 90°$.

being captured, and, furthermore, these interactions can also lead to Auger decays, hence lowering the final number of captured electrons.
Besides the mechanical electron capture (MEC) also the dielectronic recombination (DR) is entailed within nN-CTMC, because the projectile electrons interact with each other as well as with all target and free electrons. The DR has no impact parameter dependence, because in contrast to MEC the conservation of energy and momentum is satisfied by the excitation or ionization of another projectile electron. However, DR provides a capture event only in the case that the other projectile electron is not ionized, else the ion's charge state would remain unchanged. Furthermore, continuous DR processes, with simultaneous excitation only, lead to a "heating up" of the ion's internal excitation state, which finally leads to an enhanced ionization, which after all may leave the ion with the same number of electrons as before. At least at high ion velocity the simulations showed a clear impact parameter dependence, so there DR is ruled out. On the other hand, DR becomes more effective with an increasing number

of bound projectile electrons, that is, at lower ion velocity. But even there the main reason for ruling out DR is the fact that all captured electrons in the simulation were L electrons, whereas the capture of free electrons is negligible, thus it is indeed MEC which is the dominant capture process.
In summary, in accordance with other works as mentioned above, even the studied three-body dynamics exhibits quite a complex behavior with a large number of different features. It is concluded that these findings clearly point out that one may not expect a simple explanation, for instance, in form of an analytical expression from which one could then easily deduce the effective impact parameter region for electron capture, and finally the transition velocities.

4.4.4.3 Light Ion and $\langle 110 \rangle$ Channel

The body of simulated data is large only for one special case, namely the experimental case of Y ions transmitted along the $\langle 100 \rangle$ axis of a thin Si crystal. These simulations yielded signatures of cooling and heating, and even an explanation including the fast transition between these two regimes. This result is quite remarkable, because no existing theory is able to give the same insights and/or correct predictions about the experimental results. Still some experimental findings are yet open to be studied by simulations. One of them is the found disappearance of heating when the ion's nuclear charge is somewhat smaller than the one of the crystal. Due to the immense computation power necessary for yielding statistically significant results, only the above case could be fully simulated. However, the calculations of adiabatic charge states can be performed much faster than full channeling simulations, thus also the case of S ions along the two strings of Si atoms was simulated. The result was that in case of such a light ion, there is no transition from the cooling-like adiabatic charge states to heating-like ones, and even at very low velocity the charge state in the middle of the channel stays above the value at the channel boundary. Therefore, assuming that the "hysteresis" picture given above is correct, then in case of S ions one would indeed not expect the appearance of heating, which is in accordance with the experiments. The explanation for that may be given in terms of the weakness of the interaction between light ions and the string atoms. In case of weaker interactions due to lower nuclear charges, the impact parameter region for effective electron capture does not extend until the middle of the channel, and therefore cooling-like adiabatic charge states result.
Another yet to be simulated case is the disappearance of heating along the Si $\langle 110 \rangle$ axis. A very strong evidence for the disappearance was found in simulations of the impact parameter dependence of the adiabatic charge states in case of this axis. It was found that for Y ions at $\langle 100 \rangle$-heating velocities the effective impact parameter region for electron capture turned out to be smaller than the half-width of the $\langle 110 \rangle$ channel. Therefore, even at such low velocity the mean charge state of best channeled ions is higher than at the channel boundary, thus yielding a cooling-like situation, which may explain the experimentally found disappearance of any transition behavior along this axis.

4.4.5 Violation of Reversibility

The simulation results presented above show for the first time impact parameter dependent charge states of heavy ions in channeling. The asymmetry of the ion charge in respect to different directions in transverse motion ("hysteresis") is equivalent to a corresponding asymmetry in the channeling potential, because charges are the source of the potential. Thus, in case of cooling, the ion approaches the string with a higher charge state and, therefore, within a stronger potential than when leaving the string. After one such cycle the ion has lost transverse energy and this loss is *irreversible*, because electron loss and capture are not each other's time reversal, since the transition amplitudes for both processes are not obtained by simply interchanging initial and final states, as discussed in section 4.2. While this asymmetry extends over the entire impact parameter region in case of cooling, in heating only the small region around string crossings provides such an asymmetry. But one must keep in mind, that the channeling potential is much steeper around the strings than further out in the channel. Thus, even a small impact parameter region can have strong effects.
The hysteresis behavior is in agreement with the experimental finding of the extension of the angular flux redistributions beyond the critical angle for channeling. The difference in the hysteresis behavior of channeled and non-channeled ions is only the fact that the first are confined to certain impact parameters, thus their hysteresis curves do not extend over the entire impact parameter region. Hence, both channeled *and* non-channeled ions experience a hysteresis behavior of their impact parameter dependent charge states, and thus both their transverse energies are irreversibly changed. Therefore, both groups of ions are affected, which means that one may expect that cooling and heating flux redistributions extend over the critical angle of channeling.
The findings of the simulations presented in the sections above are interpreted as clear signatures of cooling and heating. Of course, there still remains the question of whether these results are able to also *quantitatively* reproduce the experimental yields, that is, whether or not they are able to lead to a *strong* violation of the rule of reversibility. Clearly one must keep in mind that a direct simulation of redistributions of the angular flux are practically impossible due to the necessary computation time. Thus, it is only possible to deduce an estimate for the flux redistribution. This is done in the following by the use of a simple two-levels model in first approximation. The upper level 1 represents non-channeled ions, while the lower level 2 stands for channeled ions. Since only ions in a very narrow region around the critical angle are discussed, the corresponding accessible areas have about the same size, thus both levels are assumed to be equally populated in case of isotropic beams. Be p_2 the probability per step dz in the depth z of the crystal for the transition from level 2 to level 1, and p_1 the probability for the reversed transition, one can set up the following rate equations under the assumption of a constant number of ions:

$$\begin{aligned} N &= N_1 + N_2 = const \\ \frac{d}{dz}N_1 &= -p_1 N_1 + p_2 N_2 \\ \frac{d}{dz}N_2 &= -p_2 N_2 + p_1 N_1 \end{aligned} \tag{4.9}$$

These equations are solved by

$$N_1(z) = \frac{N \cdot p_2}{p_1 + p_2} \left[1 - e^{-(p_1+p_2)z}\right] + \frac{1}{2} N \cdot e^{-(p_1+p_2)z}, \tag{4.10}$$

with the initial condition $N_1(0) = N_2(0) = N/2$, representative for an equal population of both levels due to an isotropic incoming beam. Thus, one actually expects a saturation behavior. However, the experiments showed a linear increase of $\chi(0) \sim \frac{N_1(z)}{N_1(0)}$ in case of the heavier ions up from Ti (see section 3.1.2.5). In other words, z is in this case much smaller than the thickness necessary for saturation and $N_1(z)$ is in the region of linear increase. Therefore, $(p_1 + p_2)z \ll 1$, and thus with

$$N_1(z) \approx \frac{N \cdot p_2}{p_1 + p_2} (p_1 + p_2)z + \frac{1}{2} N \cdot [1 - (p_1 + p_2)z] \tag{4.11}$$

one finally gets

$$\chi(0) \sim \frac{N_1(z)}{N_1(0)} = z(p_2 - p_1) + 1 \tag{4.12}$$

The experimental result gave $\chi(0) = 1.7$ for $z = 3\mu$m. Hence, $p_2 - p_1 = 0.2/\mu$m= $0.02/1000$Å. The length for half an oscillation, that is, from one string encounter to the next one, is in the order of 1000 Å. Therefore, a difference in the de- and rechanneling probabilities of about 0.02 per string encounter is already sufficient to reproduce the observed redistributions. According to Tab. 4.4 the simulated differences are even larger. However, one must keep in mind, that the simulated values only refer to the groups of ions moving close to the critical angle. One can expect that the *mean* de- and rechanneling probabilities averaged over all angles to be smaller than the simulated ones around the critical angle. Furthermore, the $\chi(0)$ measure refers to the enhancement of the best channeled ions, which certainly depends on the flux of ions with larger angles. The main goal here was to verify that the simulations give reasonable results in respect to the order of magnitude for flux redistributions in accordance with the experimental findings. It would have been certainly a negative finding, if the probabilities were too small. Furthermore, the above estimates are in very good agreement with the differences in the transition probabilities showing the violation of the detailed balance as given in Tab. 4.5.

4.4.6 Multiple Charge Exchange and Target Ionization

Besides details about the impact parameter dependence of the ion charge state the simulations presented also clear evidence for the occurrence of *multiple* charge exchange per *atomic* collision, which is quite in agreement with nCTMC calculations [10]. It was seen that during the collision with one atom several electrons can be retyped. They are captured into highly excited states, which was determined by their binding radii and energies as compared to Hartree-Fock values for the ion ground state. The consequence thereof is a high probability for electron loss in the subsequent collision. The great majority of retyped electrons are the Si L-electrons, in accordance to the expectation from any charge exchange theory, because their orbital velocity is closest to the ion velocity (see Tab. 4.1). Furthermore, especially in case of heating there occur *equally effective* interactions between the ion and *several* atoms (for instance, as mentioned above, the ion can capture electrons even from the string that is further away). This point is important as it contradicts the assumption of the first estimates of the charge exchange model, where only a few charge exchange events per *string* collisions were assumed (see 4.2). The appearance of an effective number of charge exchanges per atomic collision tends to reduce any asymmetry effects, just because in such a case the ion could instantaneously at each impact parameter take on the corresponding adiabatic charge state [45]. The simulations presented here clearly show that the key feature of charge exchange is that, if the ion velocity is not too high, the actual charge state at each impact parameter does not reach its adiabatic counterpart, and from this an asymmetry in terms of a "*hysteresis*" in the charge states between string approaching and leaving arises, as shown in Fig. 4.6. It is interesting to note that despite the number of several charge exchanges per *atomic* collision still a hysteresis behavior in the temporal development of the ion's charge states are seen in the simulations. However, this can be understood by taking into account that a charge state equilibrium, such as in the adiabatic case, does not just mean that the numbers of electron capture and loss events are equal, but that there must also be an equilibrium state of excitation. In fact, the simulations showed that also the mean binding energies averaged over all bound projectile electrons, resembling the ion's internal (excitation) state, yielded a hysteresis, but this one was independent on cooling and heating, in contrast to the charge state hysteresis. Nevertheless, this finding may help to understand why a charge state hysteresis is still possible, even if the number of electron capture and loss processes are very high per atomic collision. It seems to take some time in order to reach both an equilibrium charge and an equilibrium internal excitation state. The more charge exchange events, the more perturbation of the ion's internal electronic state, and thus the longer is the time for reaching an equilibrium state.

Besides multiple charge exchange, the simulations also showed multiple target ionization. Such a process changes significantly the ion-crystal potential, because target ionization reduces the screening of the target nuclei. In accordance with single ion-atom nCTMC results [10] it was found that the ion-atom scattering is far away from a simple Rutherford scattering. The reason is the dynamical character of the target screening,

which leads to different scattering potentials before and after a single collision. Target ionization takes effectively place at the point of closest approach between projectile and target. Therefore, the target atom is ionized when the ion already passed the atom, thus on this leaving part the projectile-target potential is stronger than on the approaching part, because target screening is reduced due to target ionization. This finding alone cannot directly add to the explanation for cooling and heating, but it is another clear signature of the complex dynamics of this many-body system.

Chapter 5

Discussion and Conclusion

The simulations presented above have shown that the effect of cooling and heating can be reproduced by a classical many-body treatment of channeling. This was done with the simplest possible model for channeling, namely the motion of an ion along two strings of crystal atoms at a fixed distance between the plane of ion motion and the plane spanned by the two strings. Within such a model channeled vs. non-channeled motion can be easily defined by "motion reflected by a string" vs. "motion crossing a string". It is then possible to calculate mean de- and rechanneling probabilities from a large enough statistical ensemble. Due to the great demand of necessary computation power full channeling simulations were only possible for the case of Y ions at two different energies, according to the experimental cooling and heating regime, along the Si $\langle 100 \rangle$ axial direction.
The simulations yielded a hysteresis in the impact parameter dependent ion charge states responsible for the violation of the rule of reversibility in terms of different de- and rechanneling probabilities of ions close to the critical angle for channeling. Since the simulations did not include nuclear multiple scattering in terms of thermal vibrations of the target atomic nuclei, which is most likely negligible due to the value of the closest possible distance of approach of 0.3 Å, taking into account that the mean thermal vibration amplitude is 0.08 Å, the found violation of reversibility is clearly an effect of the *electronic* interaction alone. Furthermore, the nN-CTMC simulated channeling trajectories looked very much like trajectories from simple considerations according to a continuum channeling potential. Thus, it looks like that violations of the rule of reversibility manifest themselves in a purely *statistical* behavior, such as different de- and rechanneling probabilities, but not in drastic changes of individual trajectories. Therefore, this may be reflected by the picture of a "semi-permeable membrane", which does not change so much the absolute value of the momentum of particles, but only their direction of motion: either passage of the membrane or reflection from it. In this sense the strings build such a membrane, and its permeability is asymmetrical in favor of one direction, determined by the larger of the de- and rechanneling probability.

The explanation of cooling and heating in terms of asymmetrical charge states during the ion's approaching of a string and leaving a string could not be reduced down to

simple analytical expressions. Whereas the cooling case can be expected from any impact parameter dependent estimate for electron capture, the found results by the simulations in the heating case yielded an unexpected feature in terms of a large impact parameter region for electron capture at lower ion velocity. Despite the fact that the simulations yielded the rapid transition from the cooling charge state-hysteresis to the heating-hysteresis, no simple argument could be extracted from these detailed calculations. At this stage, the chain of explanations ends in the complexity of many-body capture processes.

All these findings refer to only one ion and one crystal species, besides preliminary simulations for one light ion and another channeling direction, which were also found to be in agreement with experiments. It was not possible within the available time to also simulate full channeling cases for other ion-crystal combinations. It would have especially been very interesting to simulate the transmission through a Pt crystal, as this case showed a behavior clearly distinct from Si and Ni crystals. However, any Pt atom carries 78 electrons, among which are about 40 electrons to be explicitly included in the simulations, because these resemble binding energies comparable with the Si L-electrons, which are the ones that are most likely captured. From this follows that detailed simulations with Pt atoms would require much more computation time, and thus they could not be performed in the available time. However, the calculations of the corresponding adiabatic charge states were found to be in agreement with the measured shifts in the charge state distributions, that is, at high ion velocity the mean channeling charge state is higher than along random direction, whereas this is reversed in case of low velocity. One may expect from this that also Pt should show heating, but this is experimentally not the case. A tentative explanation for the lack of heating despite the fact that the impact parameter dependent adiabatic charge states would allow that may be given in terms of higher ionization rates in the actual channeling motion as compared to the fixed impact parameters. The idea here is that on the transverse motion from the middle of the channel to its boundary the actual charge state of the ions lies *above* the adiabatic ones due to the large amount of target electrons which may lead to a greater ionization rate when moving from one impact parameter to the next as compared to the adiabatic case. At high ion velocity the actual charge states may again lie below the adiabatic ones, because here the charge states change mostly by electron capture, not electron loss as in the tentative explanation in case of low ion velocity. This explanation may also give an account of the experimentally found "discrepancy" between shifts in charge state distributions and the appearance of cooling/heating in Si and Ni crystals on one side, and only cooling in Pt crystals on the other side. This means that there need not necessarily be a direct correlation between positive/negative shifts and cooling/heating, if the latter is determined not only by the impact parameter dependent adiabatic charge states, but also by the direction of the cycle of the actual charge states around the adiabatic ones. Thus, at low ion velocity, it may be possible that in crystals with a high electron density the actual charge states are above the adiabatic ones, but below when they are in crystals with low electron density.

From the experiments and the simulations it follows that an understanding of the behavior of ions in a Pt crystal is still far away. Both experiment and simulation yielded a shift of the channeling charge states to lower values than along random direction for lower ion velocities, but experimentally only cooling was observed. While for the present understanding of cooling and heating there is a correlation between the impact parameter charge state hysteresis and the appearance of cooling/heating, the Pt case prevents this picture from being general. It is thus concluded that the Pt crystal may require an additional argument for cooling and heating besides a hysteresis behavior in comparison to the corresponding adiabatic charge states.
The experimental approach to a better understanding was sought in the tilting experiment (see section 3.2.2.2). The basic idea for saving a strict correlation between impact parameter dependent charge states and cooling/heating is to acknowledge the possibility that at different impact parameters different conditions for cooling or heating may be realized. The flux redistribution measurements showed strong cooling of channeled ions with low exit angles relative to a crystal direction, but embedded in a region of flux reduction. For such a "depletion zone" there are two possibilities: either cooling at low angles is so strong that the supply from larger angles is too weak, so that a depletion arises, or the flux reduction is due to heating condition in the corresponding impact parameter region. If cooling occurs at low exit angles only, the corresponding charge state must not necessarily be above the random charge state. It would be sufficient that within the cooling impact parameter region the channeling charge state is higher at zero exit angles as compared to the largest exit angle of this restricted impact parameter region. Therefore, a negative slope of the mean channeling charge state vs. tilting angle at zero tilting would be expected in order to save the idea of a strict correlation between (shifts of) channeling charge states and appearance of cooling/heating. However, the experimental data (Fig. 3.21) could not yield a sufficient negative slope within the error bars.
Summing up, the measurements with Pt crystals show quite different features as compared to Si and Ni crystals. In such a high-Z crystal it is possible that the absence of cooling/heating around the critical angle may reflect the strong multiple scattering on target nuclei and electrons present there, and, furthermore, the dependence on the ion charge state of the deflection in a close ion-atom collision may be considerably weaker in Pt crystals than in low-Z crystals due to the presence of many target electrons screening the ion charge. It may thus be concluded that channeling trajectories in Pt crystals may not depend on the ion's charge state alone, but may require some additional mechanism that is not necessary for understanding cooling and heating in lower Z crystals.

Chapter 6

Outlook

There are still open questions for the understanding of cooling/heating. One is the distinct behavior of ions in Pt crystals, where both experiments and preliminary simulations could not provide an explanation. Thus, for the future full channeling simulations must be performed for the case of Pt crystals, that is, the detailed simulations of channeling along two strings of Pt atoms. Besides that, further simulations must be done for light ions in order to confirm the disappearance of any transition to heating, as seen by experiments and suggested by preliminary calculations. Of course, in order to reproduce the scaling of the transition energies further calculation with different ions besides Y ions must be performed.
Due to the detailed study of three-body capture processes the expectation for any simple analytical expressions were clearly attenuated. A much extended further study of the relevant parameters may leave this situation basically unchanged, but could help finding numerical, "semi-empirical", regularities between ion charge state, velocity, impact parameter and electron capture probabilities.
On the experimental side the body of data is still so large that the theoretical approaches for an understanding of the found results could not catch up yet. Moreover, many important parameters are experimentally inaccessible. At this stage it seems that no further experiments can help to clarify the present complex results.

The found effect of cooling and heating gains a great attention in the community of ion-solid interactions, because it allows new insights into the features of the impact parameter dependent interaction of swift heavy ions in crystals [24]. The advantage of the nN-CTMC simulations is their access to otherwise inaccessible parameters, such as impact parameter dependent charge states or excitation states. Furthermore, the dynamical description of the strong ion-solid interaction is another advantage of these simulations as compared to other theoretical approaches. The results found for cooling and heating can be easily extended to the much broader area of ion-solid interaction, for instance charge state dependent energy loss. In this sense cooling and heating is not just a side issue but strongly linked to current scientific activities.

Bibliography

[1] J. Lindhard, Medd. K. Dan. Vidensk. Selsk. **34**, No. 14 (1965).

[2] J.S. Forster, in *Relativistic Channeling*, edited by R.A. Carrigan, Jr. and J.A. Ellison (Plenum, New York, 1987).

[3] W. Assmann, H. Huber, S.A. Karamian, F. Grüner, H.D. Mieskes, J.U. Andersen, M. Posselt, and B. Schmidt, Phys. Rev. Lett. **83**, 1759 (1999).

[4] Y. Quere and H. Cuve, J. of Appl. Phys. **39**, 4012 (1968).

[5] G. Dearnaly, I.V. Mitchell, R.S. Nelson, B.W. Farmery, and M.W. Thompson, Phil. Mag. **18**, 985 (1968).

[6] S.A. Karamian, Nucl. Instrum. Methods Phys. Res. B **51**, 354 (1990).

[7] M. Posselt, Radiat. Eff. Defects Solids **130-131**, 87 (1994).

[8] N. Bohr and J. Lindhard, Medd. K. Dan. Vidensk. Selsk. **28**, No. 7 (1954).

[9] R. Abrines and I.C. Percival, Proc. Phys. Soc. **88**, 861 (1966).

[10] R.E. Olson, J. Ullrich, and H. Schmidt-Böcking, Phys. Rev. A **39**, 5572 (1989).

[11] H. Lutz and R. Sizmann, Phys. Letts., **5**, 113 (1963).

[12] D.S. Gemmell, Rev. Mod. Phys. **46**, 129 (1974).

[13] J. Lindhard and V. Nielsen, Medd. K. Dan. Vidensk. Selsk. **38**, No. 9 (1971).

[14] E. Bonderup, H. Esbensen, J.U. Andersen, and H.E. Schiøtt, Rad. Eff. **12**, 261 (1972).

[15] H. Huber, PhD thesis, Sektion Physik, Ludwig-Maximilians Universität München (1998).

[16] B. Schmidt, J. von Borany, U. Todt, and A. Erlebach, Sensors and Actuators A **41-42**, 689 (1994).

[17] F. Grüner, Diploma thesis, Sektion Physik, Ludwig-Maximilians Universität München (2000).

[18] R.L. Fleischer, P.B. Price, and R.M. Walker, in *Nuclear Tracks in Solids* (University of California Press, 1975).

[19] W. Günther, Fachbereich Physik. Universität Siegen, personal communication.

[20] G. Rusch, E. Winkel, A. Noll, and W. Heinrich, Nucl. Tracks Radiat. Meas. **19**, 261 (1991).

[21] F. Grüner, M. Schubert, W. Assmann, F. Bell, S. Karamian, and J.U. Andersen, Nucl. Instrum. Methods Phys. Res. B **193**, 165 (2002).

[22] F. Grüner, W. Assmann, F. Bell, M. Schubert, J.U. Andersen, S. Karamain, A. Bergmaier, G. Dollinger, L. Görgens, W. Günther, and M. Toulemonde, Phys. Rev. B **68**, 174104 (2003).

[23] K. Shima, N. Kuno, M. Yamanouchi, and H. Tawara, At. Data Nucl. Data Tables **51**, 174 (1992).

[24] A. Baurichter, P. Sigmund, and A.H. Sørensen, Nucl. Instrum. Methods Phys. Res. B **195**, 224 (2002).

[25] A.B. Wittkower and H.D. Betz, Atomic Data **5**, 120 (1973).

[26] S. Datz, F.W. Martin, C.D. Moak, B.R. Appleton, and L.B. Bridwells, Radiation effects **12**, 163 (1972).

[27] H.O. Lutz, S. Datz, C.D. Moak, and T.S. Noggle, Phys. Letts. A **33**, 309 (1970).

[28] M. Schubert, Diploma thesis, Sektion Physik, Ludwig-Maximilians Universität München (2001).

[29] G. Dollinger, T. Faestermann, and P. Maier-Komor, Nucl. Instrum. Methods Phys. Res. B **64**, 422 (1992).

[30] W. Mayer, PhD thesis, Technical University München, 1985.

[31] R. Schramm and H.D. Betz, Nucl. Instrum. Methods Phys. Res. B **69**, 123 (1992).

[32] M. Schubert, F. Grüner, W. Assmann, F. Bell, A. Bergmaier, L. Goergens, G. Dollinger, and S. Karamian, Nucl. Instrum. Methods Phys. Res. B **209**, 224 (2003).

[33] T.S. Ho, D. Umberger, R.L. Day, M. Lieber, and T. Chan, Phys. Rev A **24**, 705 (1981).

[34] D. Jakubassa-Amundsen, Phys. Rev. B **65**, 174110 (2002).

[35] J.P. Rozet, Nucl. Instrum. Methods Phys. Res. B **107**, 67 (1996).

[36] F.P. Larkins, J. Phys. B: At. Mol. Phys. **5**, 571 (1972).

[37] B.R. Appleton, R.H. Ritchie, J.A. Biggerstaff, T.S. Noggle, S. Datz, C.D. Moak, H. Verbeek, and V.N. Neelavathi, Phys. Rev. B **19**, 4347 (1979).

[38] H.F.Krause and S.Datz, Adv. At. Mol. Opt. Phys. **37**, 139 (1996).

[39] P.L. Grande and G. Schiwietz, J. Phys. B: At. Mol. Opt. Phys. **28**, 425 (1995).

[40] V.J. Montemayor and G. Schiwietz, Phys. Rev. A **40**, 6223 (1989).

[41] C.C. Lu, T.A. Carlson, F.B. Malik, T.C. Tucker, and C.W. Nestor, Jr., Atomic Data **3**,1 (1971).

[42] N. Bohr and J. Lindhard, Medd. K. Dan. Vidensk. Selsk. **28**, No. 7 (1954).

[43] C.M. Frey, G. Dollinger, A. Bergmaier, T. Faestermann, and P. Maier-Komor, Nucl. Instrum. Methods Phys. Res. B **107**, 31 (1996).

[44] H. Varvoglis, K. Katsonis, M. Savopulos, and G. Maynard, Physica Scripta. **62**, 1 (2001).

[45] J.U. Andersen, F. Grüner, V.A. Ryabov, and A. Uguzzoni, Nucl. Instrum. Methods Phys. Res. B **193**, 118 (2002).

Acknowledgement

- First of all I want to thank Dr. Walter Assmann for bringing me into the field of cooling and heating, and for supporting me strongly from the very beginning. This included to send me to various conferences where I could meet and discuss with many international experts. It was Walter's experimental expertise that enabled us to perform the systematic study of this newly discovered effect. Very often Nature "teased" us by unexpected answers, but with more and more beam times, preferably on weekends and holidays, we came closer and closer to a bigger picture of cooling and heating. And it was him who managed to buy the computer cluster, without which the simulations could have not been performed within the available time.

- I am deeply grateful for the fruitful support from Prof. Dr. Friedhelm Bell. Thanks to his critical and at the same time constructive remarks I was able to steadily proceed forward in the development of nN-CTMC. He strongly encouraged me from my very first steps in extending CTMC. During innumerable discussions we moved deeper and deeper into a better understanding of the puzzle posed by transverse cooling and heating.

- I also thank Prof. Dr. Dietrich Habs for his friendly and supportive admission to his institute. Despite the fact that the term "cooling" may have at first sight made him think rather of laser cooling than "*transverse* cooling and heating", I was invited to give several talks in his group seminars, where cooling and heating in ion channeling was constructively discussed.

- For his patient explanations in the theory of charge exchange I am thankful to Prof. Dr. Jens-Ulrik Andersen from the "Aarhus Center of Atomic Physics" at the University of Aarhus, Denmark. During several visits to him the world of charge exchange, and more generally, ion-solid interactions, has become more understandable to me.

- Special thank goes to Dr. Günther Dollinger from the Technical University of Munich, because without his hint I would have not become aware of such things as CTMC. He was the first who pointed to the possibility of creating a simulation of cooling and heating with the help of classical computer simulations.

- For helpful remarks about the power of classical simulations I am grateful to Dr. Gregor Schiwietz, Prof. Dr. Pedro Grande and Dr. Gilles Maynard. All three of them encouraged me to extend CTMC to what is now called nN-CTMC. It is one thing to read about the possibility of applying classical methods, but it is something quite different when talking directly to the experts in such a field.

- I am highly indebted to Dr. Sarkis Karamian - for a very simple reason: without his early measurements there just would be no "cooling and heating". Of course, this is not the only point I am thankful about. In annual guest visits to us we have developed a very fruitful cooperation. We performed many experiments together and had long discussions about them. Besides the scientific merits I must mention that, thanks to him, I got for the first time in my life real Russian caviar to eat.

- I am also indebted to Bernd Schmidt from *Forschungszentrum Rossendorf* for producing the Si crystals, and to Jacques Chevalier from the University of Aarhus for producing the thin Ni and Pt crystals. Surely, without such crystal, not a single experiment could have taken place.

- I thank Prof. Dr. Peter Sigmund for inviting me to several opportunities for various discussions of energy loss and charge states of ions in solids. Most intensive talks took place during a few days at his summer house, where we have discussed relations between cooling and heating on one side, and energy loss on the other side. I was also given the possibility to present our results during the STOP01 conference organized by him. In a panel discussion experts expressed the opinion that cooling and heating is a quite interesting topic for the community of ion-solid interactions.

- *Dankeschön* to Dr. Christine Trautmann and *merci beaucoup* to Dr. Marcel Toulemonde: in several beam times we have undertaken measurements, which were in fact not directly related to cooling and heating, but still provided me with better insights into the field of ion-solid interactions. This has caused to open my view to a much greater applicability of nN-CTMC simulations. Marcel has also strongly supported our group during experiments at the GANIL accelerator in Caen, France, where we could measure 1 GeV Pb ions. I am also grateful for his introducing me to other experts on many occasions during international conferences.

- I certainly want to thank Mario Schubert who was the diploma student enabling our group to perform the measurements of charge state distributions. He programmed and installed the goniometer in order to perfectly align our crystals. In long beam nights we finally found out that Pt crystals are indeed quite different from what we have expected. Besides Mario's many experimental contributions I thank him for his great effort in maintaining our computer cluster called "matrix".

- In context of the charge state measurements our group is very grateful to Dr. Andreas Bergmaier and Dr. Lutz Görgens for their great support during beam times.

- I also want to thank Werner Günther from the *Fachbereich Physik* of the University of Siegen, Germany, for his very patient support of etching and analyzing our track detectors. Several experiments, especially with alphas and Pb ions, could have been not performed with this simple method of detecting low and high energy ions.

- Of course, special thank goes to all operators of the Tandem accelerator - without them I could have measured not a single ion.

- I also thank the computer group of the Tandem lab, especially for finding out more and more computers on which I could let my simulations run - before we finally got the cluster.

- I am thankful to all colleagues at the Tandem lab who suffered from my "abuse" of their computers by my highly time consuming calculations. Surely a lot of computer crashes were caused by me - until our group finally became a happy user of our own "matrix".

- Last, but certainly not least, I thank Kerstin Korge for giving me the biggest support in all matters over and above physics.

- I am deeply indebted to my parents for their backing me all the way from Kindergarten (and supposedly even much earlier) up to now.

This work was financially supported by the *Deutsche Forschungsgemeinschaft* under treaty AS 102/3-1,2,3.